Available online at **www.joac.info**

ISSN: 2278-1862

Journal of Applicable Chemistry

2024, 13 (2): 211-188

(International Peer Reviewed Journal)

New Chemistry News

$^{-}N=C=N^{-}$

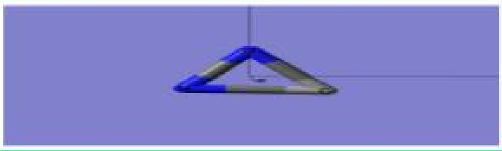

New News of Chem (NNC)

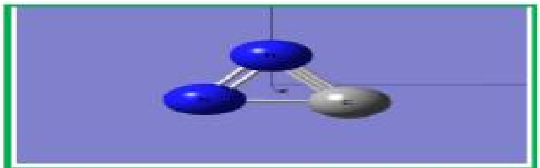

ChemNewsNew (CNN)

...CNN – 60 b...*I a m ...*

...Intelligence Augmented Medicine...

Pulmonology

Fits (Figure Image Table Script ...)Base

Information Source	sciencedirect.com;ACS.org ;	
S. Narasinga Rao M D Associate Professor, Emergency Medicine dept., Andhra Medical College, King George Hospital Visakhapatnam, A.P., India	K. SomasekharaRao, Ph D Dept. of Chemistry, Acharya Nagarjuna Univ., Dr. M.R.Appa Rao Campus, Nuzvid-521 201, India	R. Sambasiva Rao, Ph D Dept. of Chemistry, Andhra University, Visakhapatnam 530 003, India
snrnaveen007@gmail.com (+91 9848136704)	sr_kaza1947@yahoo.com (+91 98 48 94 26 18)	rsr.chem@gmail.com (+91 99 85 86 01 82)

Conspectus: The subdisciplines of “I am:Intelligence Augmented Medicine”) are Pulmonology, Cardiology, Neurology, Gynaecology,Venereology,Urology. Hepatology, Ophthalmology, Dermatology, Oncology and so on. In the current news item, the diagnosis and treatment of pulmonary diseases using AI in clinical front are considered. The ailments covered under Pulmonologyare Covid-19, Pneumonia, TB, pulmonary nodules/ cancer /edema, ARDS, pulmonary artery hyper tension (PAht), focussing on AI assisted protocols in the diagnosis/prognosis/ intervention procedures. The medical instruments like x-ray, CT, Contrast-enhanced-CT, MRI (LGE; SPECT), CT-pulmonary-Angina generate data of high information content.

This news article “Fits ([Figure, Fact, False],[Image; Information],[Table;Tensor;Truth],[Script ;Sound; Science]…) Base” is a passive information report containing numerical data, figurative information, digital images, scripts of knowledge/conclusions etc. In our laboratory, an active form of FitsB is under feasibility study for search, distillation of knowledge, generation of intelligent sparkles in Medicine, Speciation, kinetics and environment.

The earlier News reports (CNNs)in the series dealt with AIM (Artificial Intelligence in Medicine) with methods and applications. The Future-of-state-of-knowledge of dealing with pulmonary diseases encompass right combination of AI output and expertise of Pulmonologist.

Keywords: Artificial intelligence (AI); Medical diagnosis; Pulmonology;
CNN : [C [Computations; Computer; Chemistry] NN [New News; News New; Neural Nets; Nature News; News of Nature;]]

Covid-19 disease

The number refers to ref.Number in CNN-60(a)

09

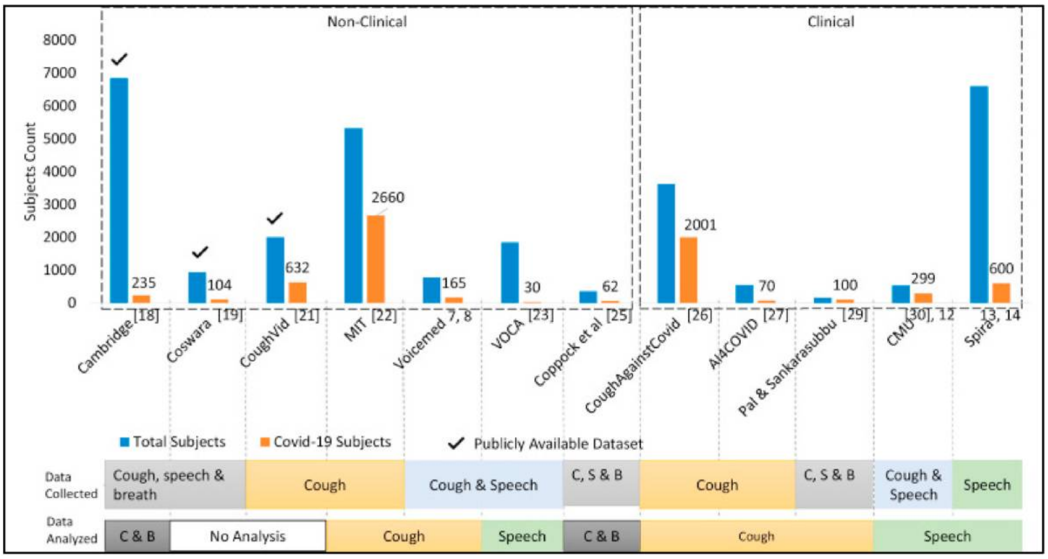

Summary of collected and analyzed cough, speech, and breathing data

09

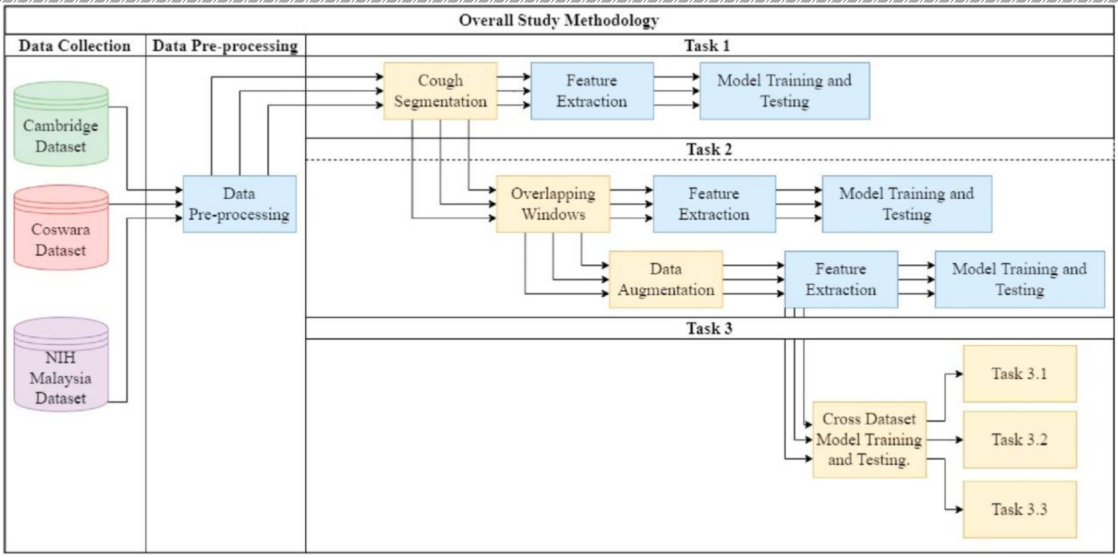

Overall methods used in the study

09-

Overall process flow for data pre-processing

09

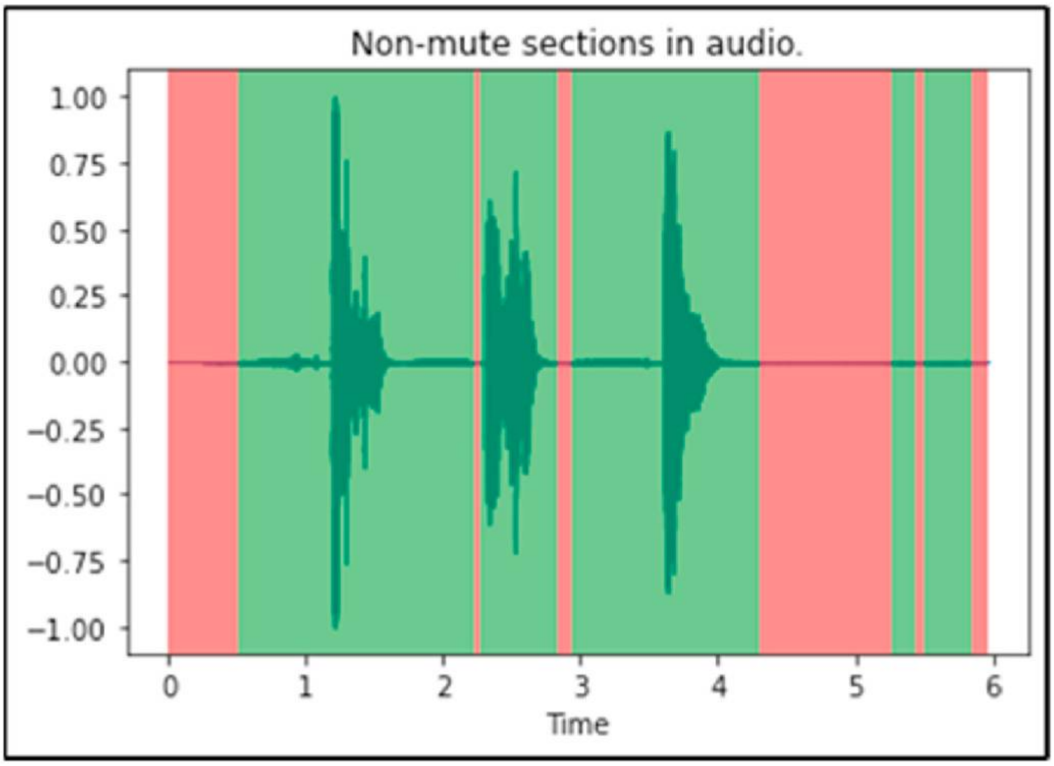

Sample of "non-mute" sections in cough waveforms

09

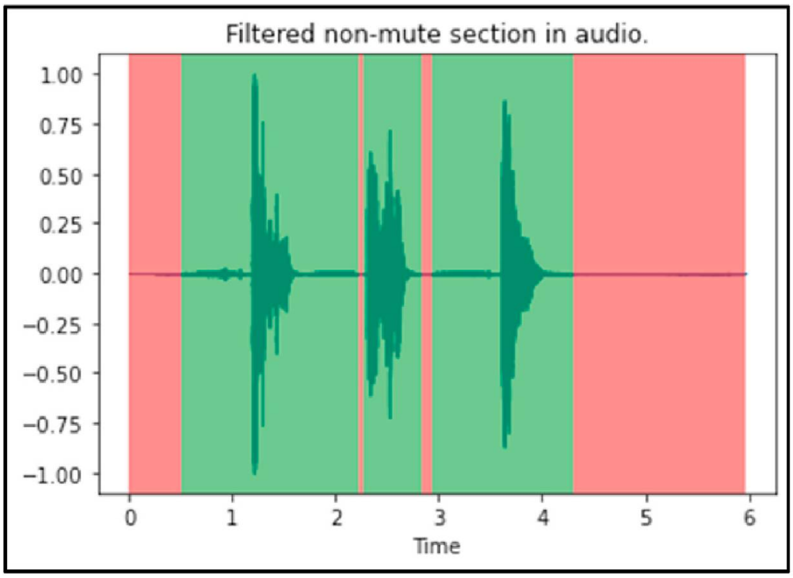

Sample of filtered “non-mute “section in the cough waveform

09

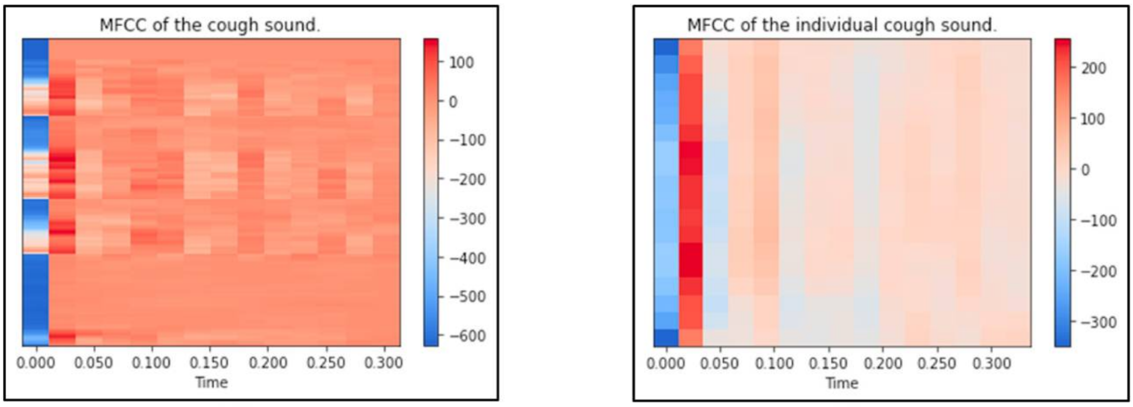

(A) (B)

MFCC spectrogram representation of the cough sound (A) and individual cough sound (B).

09

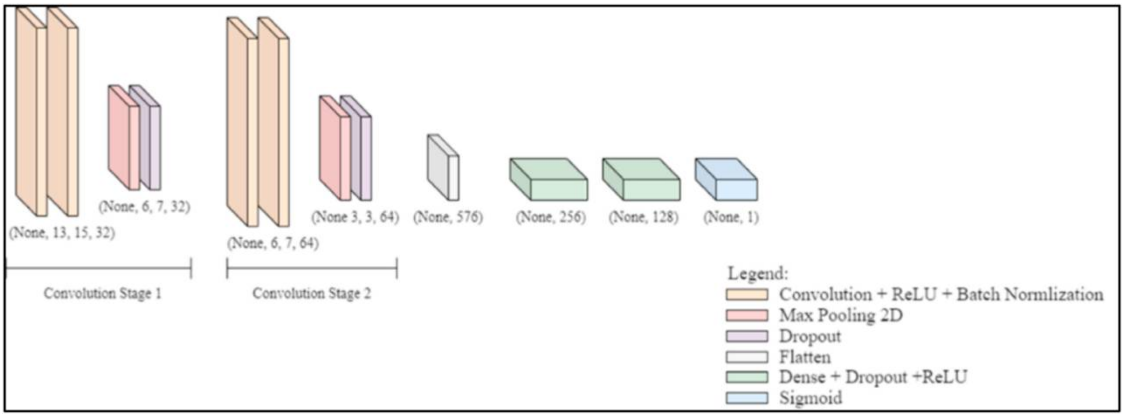

Model architecture of the Mini VGGnet

09

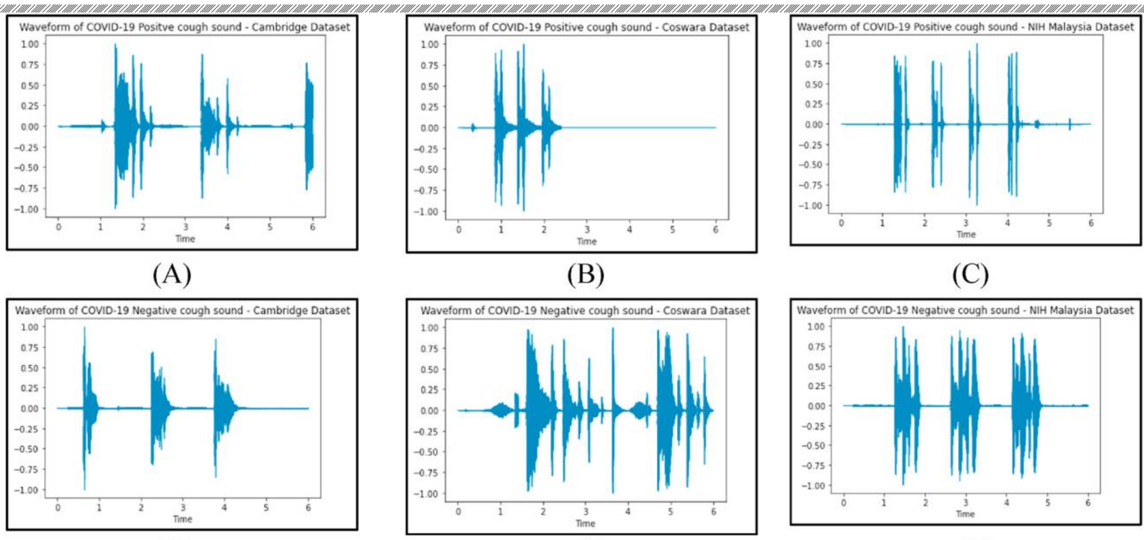

(D) (E) (F)

Sample waveforms of COVID-19 Positive and Negative Cough Sounds

✓ Cambridge Dataset (A and D), Coswara Dataset (B and E), NIH Malaysia Dataset (C to F)

09

(A) (B)

Sample waveforms of individual cough sounds,

✓ Three-phase (A) and two phase (B).

27

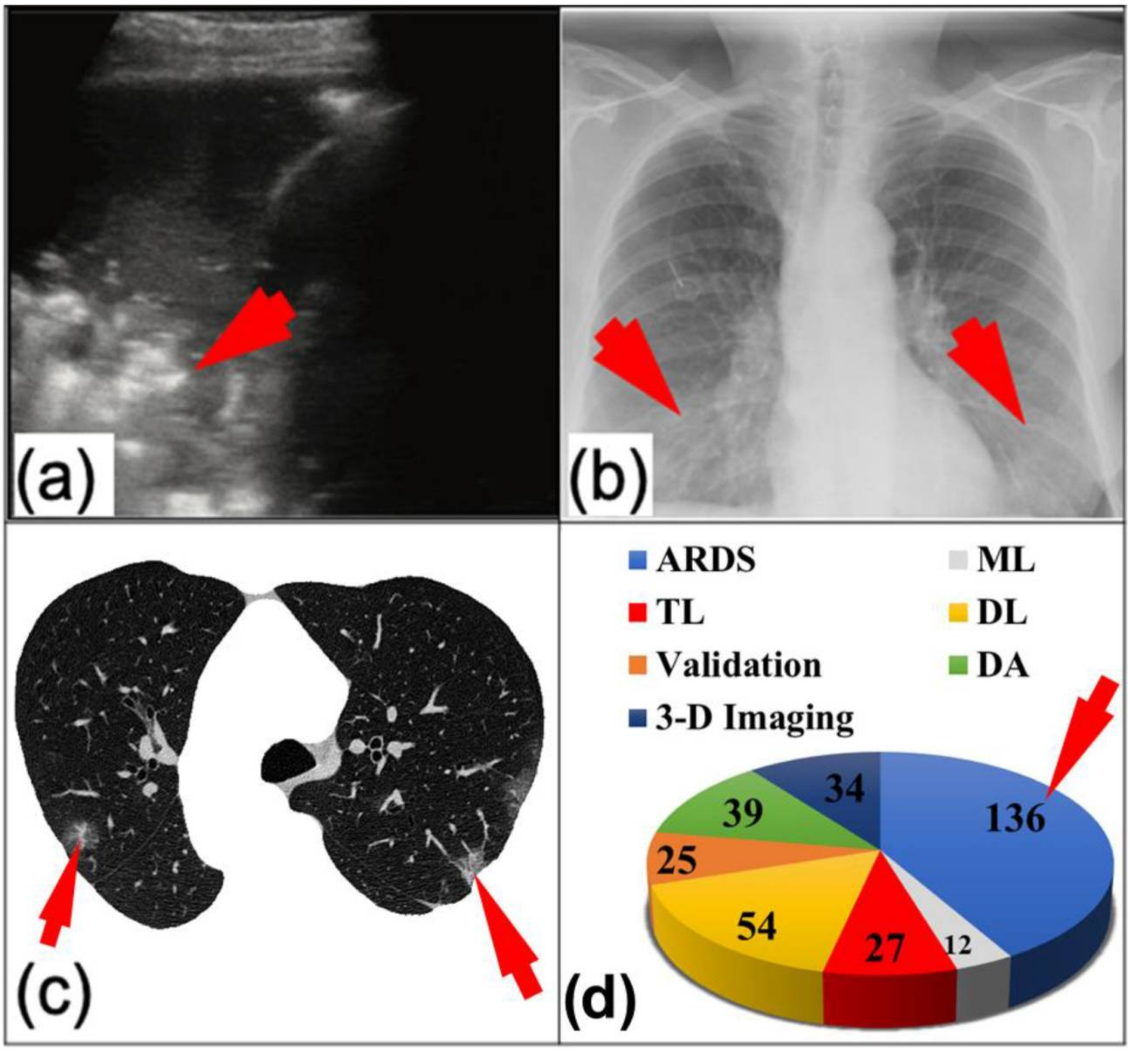

Images of COVID-19 infection:
(a) lung ultrasound (hyper-echoic region of the COVID-19 lung),
(b) chest X-rays (the infected region in the lung), and
(c) lungCT (segmented lung region; courtesy of Luca Saba, University of Cagliari, Italy).
(d) The number of COVID-19 studies involving ARDS, ML, TL, DL, validation, data acquisition (DA), and 3-D imaging

27

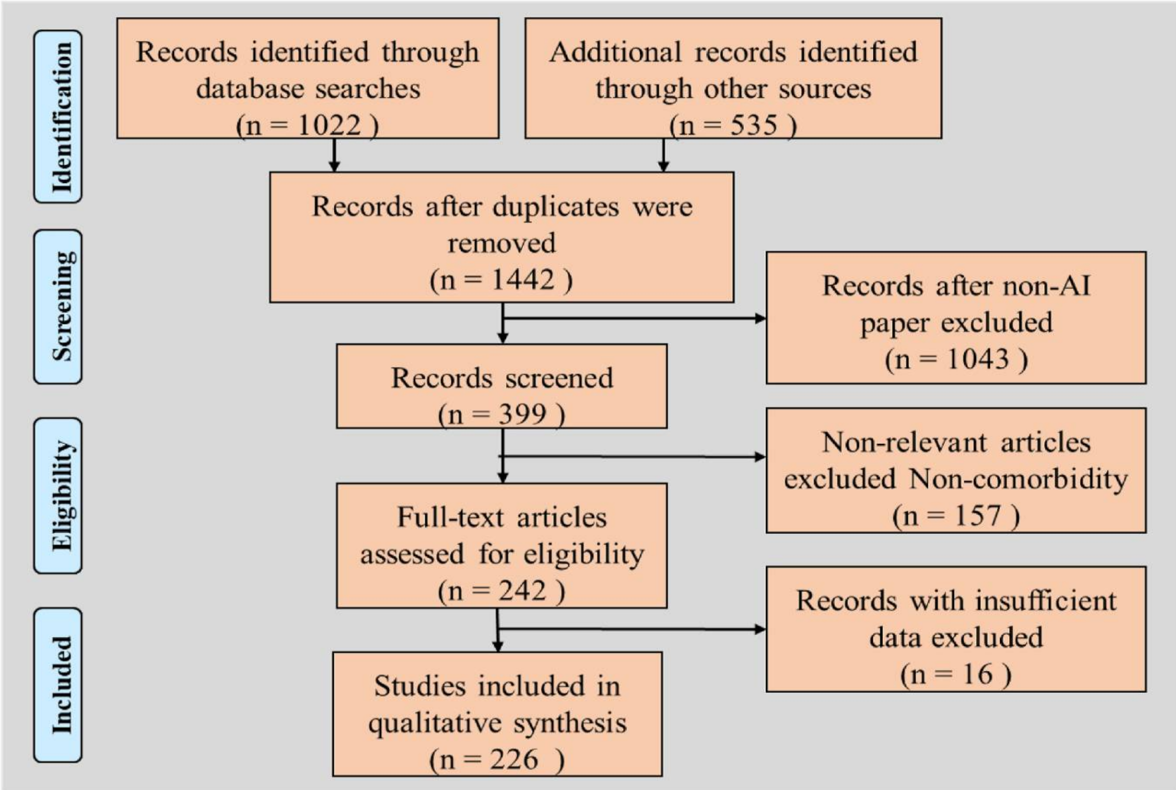

Flowchart showing research strategy

27

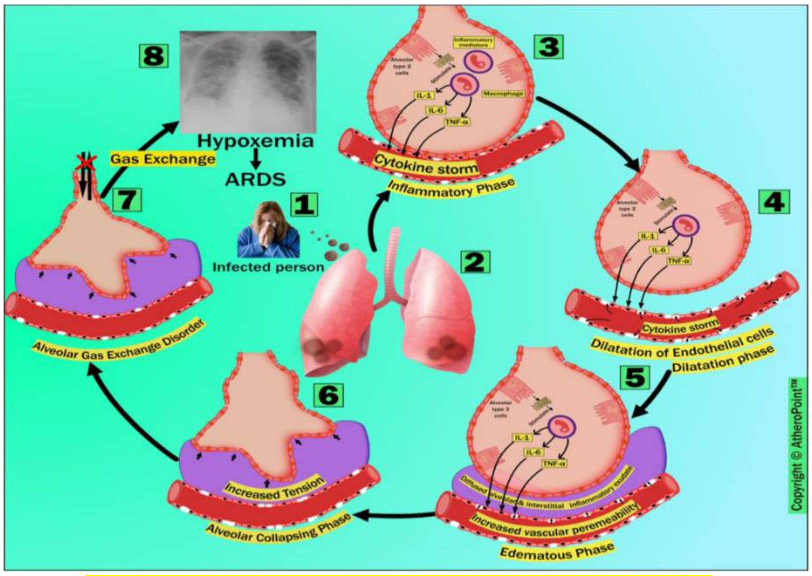

Pathophysiology of ARDS after COVID-19 infection, which consists of six phases: (i) inflammatory phase, (ii) dilatation phase, (iii) edematous phase, (iv) alveolar collapsing phase, (v) gas-exchange disorder, and (vi) hypoxemia. (Courtesy of AtheroPoint™, Roseville, CA, USA;)

27

Clustering of multimodality artificial intelligence architectures and their salient features.

SoT	Reference	Modality	Imaging	Highlight/Objective	Architecture Description
SoT-1	[147–153, 229]	CT [229]: [147, 148] X-ray [149]: [151] LUS [150]:	3-D [229]: [147,148] 2-D [149]: [150, 151]	Multiview fusion [229], Multi-view pyramid network with attention [147], training using human in loop [148], video-based real time prediction [150], end-to-end DL architecture for semi quantitative prediction COVID- 19 severity [151]	Resnet50 [229], Custom CNN with attentioı [147], VB-Net [148], commercial deep learning system by Lunit Inc [149], Spatial Transformer Net- work [150], ensemble of multiple networks (Backbone – ResNet, VGG DenseNet, Inception; Segmentation- UNet, UNet++; Alignment- Spatial Transformer Network; Scoring Head-Feature Pyramid Network; Custom Network) [151]
SoT-2	[152,153]	CT [152]: [153] X-ray: LUS:	3-D [153]: 2-D [152]:	Biomarker based model [152], model for severity in 3-D lung abnormalities [153]	Resnet34 with logistic regression [152], Dense UNet [153]
SoT-3	[154–156, 171,173, 174]	CT [154] [155,171] [156,173] X-ray: [157,174] LUS: NA	3-D [154]: [173] 2-D [171]: [155–157,174]	3-D Convolution Network [154], multi-objective differential evolution based CNN [171], comparison of ten CNNs [156], weakly supervised DL model [173], truncated InceptionNet [174], modified DarkNet CNN [157]	Resnet50 [154], Custom CNN [157,171,173], DenseNet [155] (AlexNet, VGG-16 VGG-19, SqueezeNet, GoogleNet, MobileNet-V2, ResNet-18, ResNet-50, ResNet-101, and Xception) [156] InceptionNetV3 [174]
SoT-4	[157]	CT [157]: X-ray: NA LUS:	3-D [157]: 2-D: NA	ML and DL hybrid network for classification and prognosis [157]	Resnet18 with Gradient Boosting [157]

27

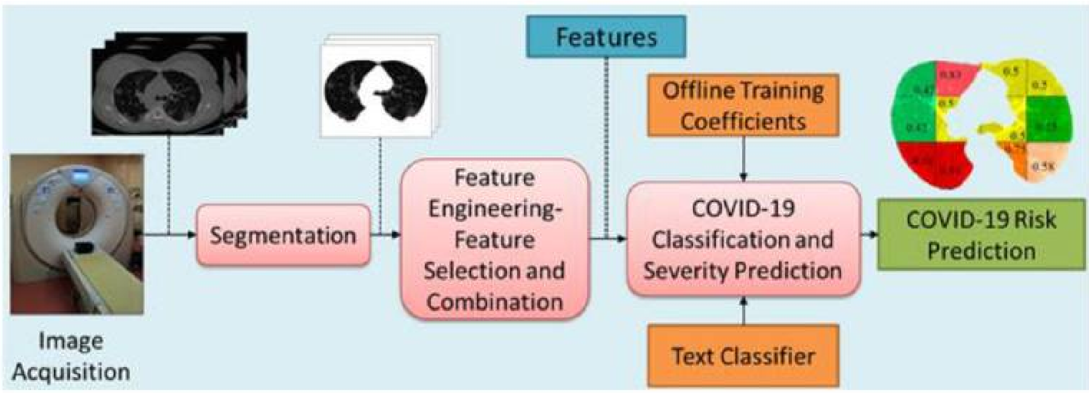

An online ML-based COVID-19 risk prediction system

27

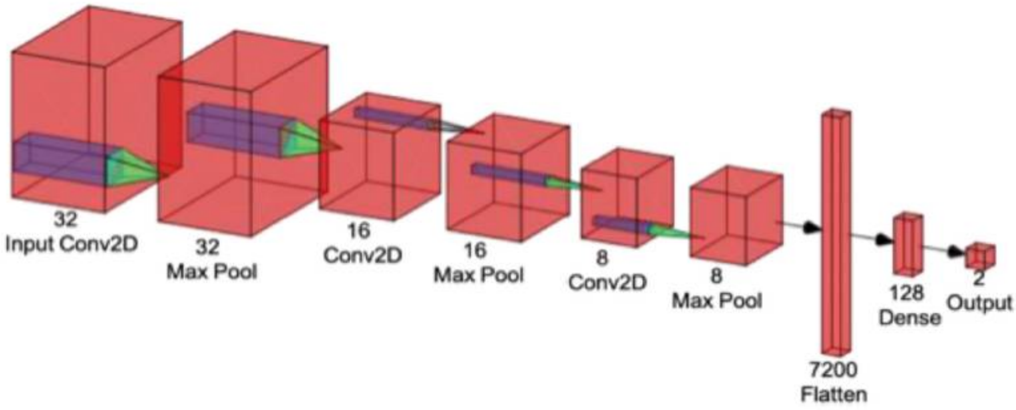

A custom CNN-based DL architecture comprising different layers

27

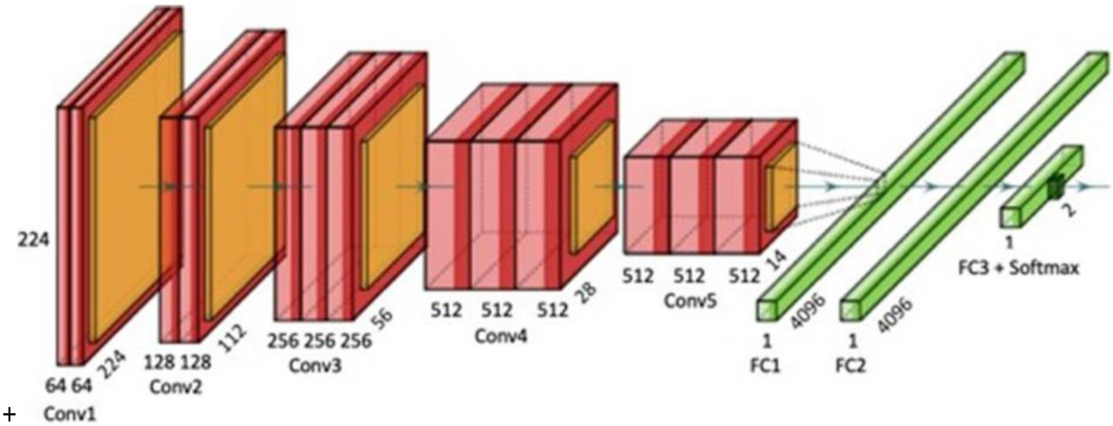

+

An example of transfer learning (TL) architecture using VGG16

27

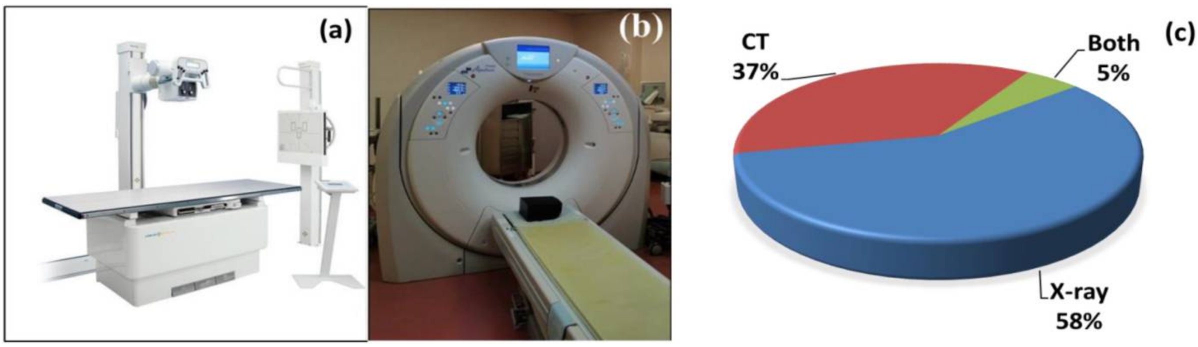

27

(a) An X-ray scanner. (b) A CT-scanner (Courtesy of Luca Saba, University of Cagliari, Italy). (c) Studies using CT vs. X-ray

27

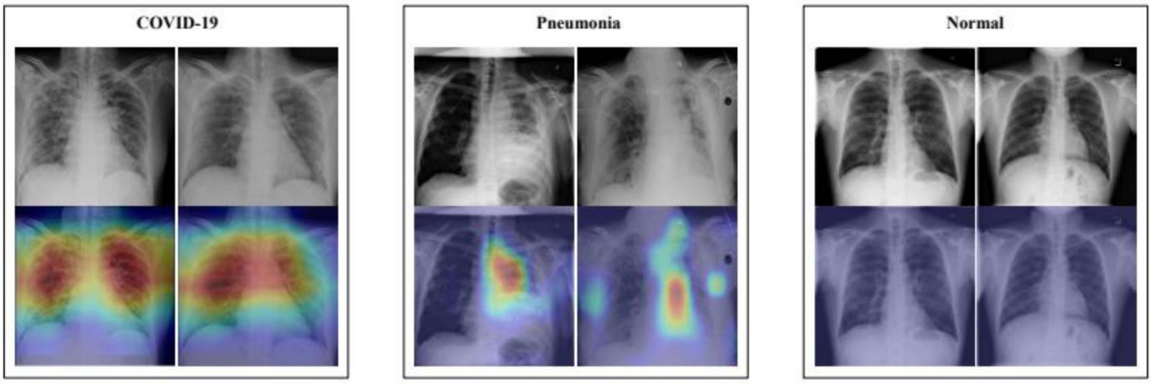

X-ray scans of COVID-19, pneumonia, and normal lungs

27

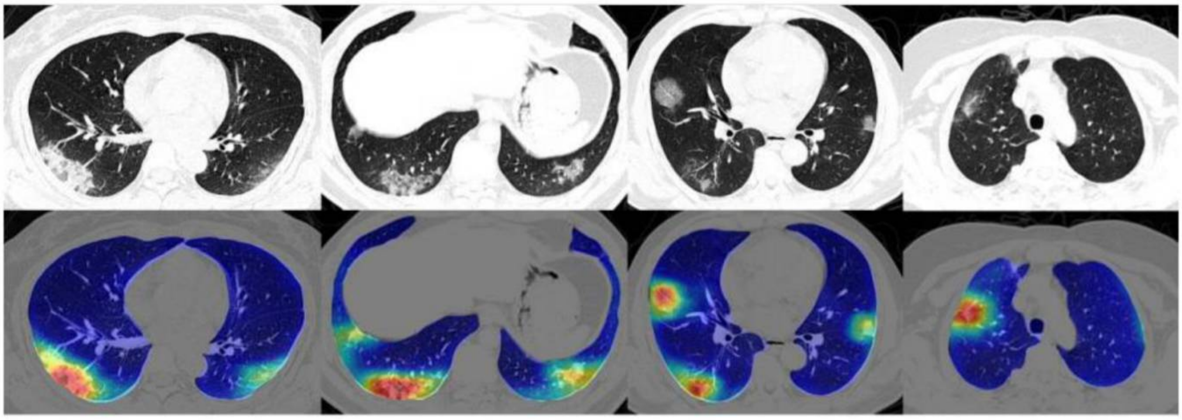

CT scans classified as positive for coronavirus abnormalities
and their corresponding color heatmaps

27

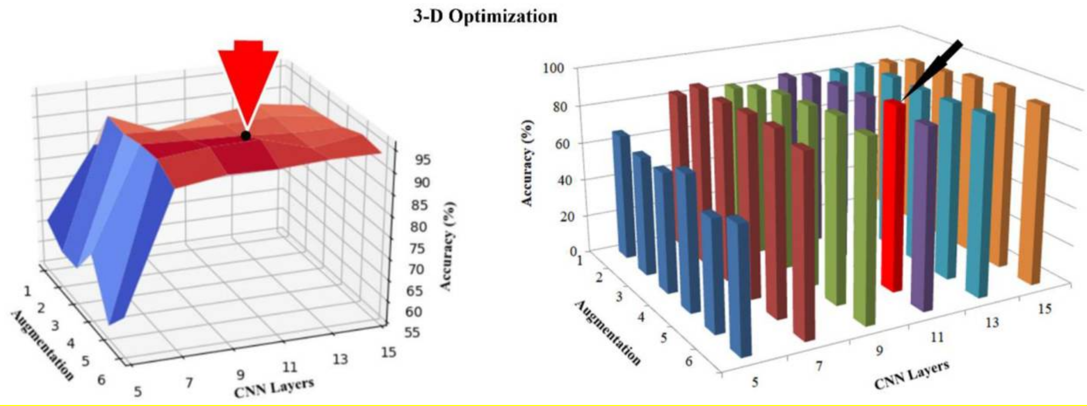

3-D graph representing the relationship between CNN layers, data augmentation, and accuracy.
(Courtesy of AtheroPoint™, Roseville, CA, USA

27

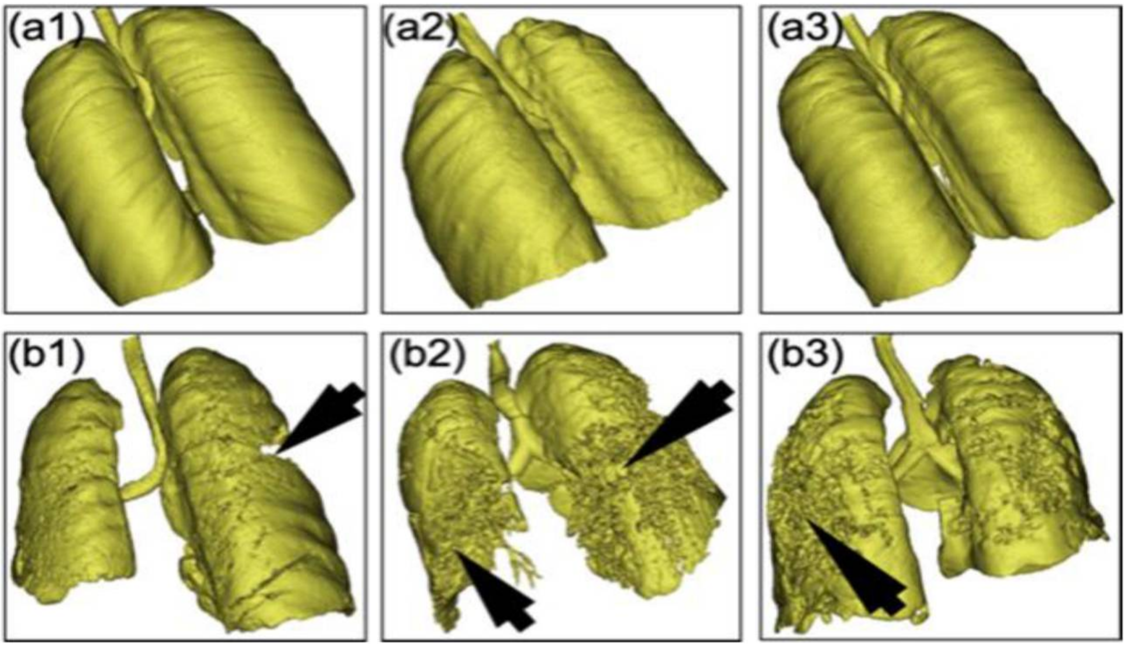

- Three lungs with non-COVID-19 pneumonia (a1, a2, and a3).
- Three lungs with COVID-19 pneumonia with different COVID-19 severities (b1, b2, and b3).

27

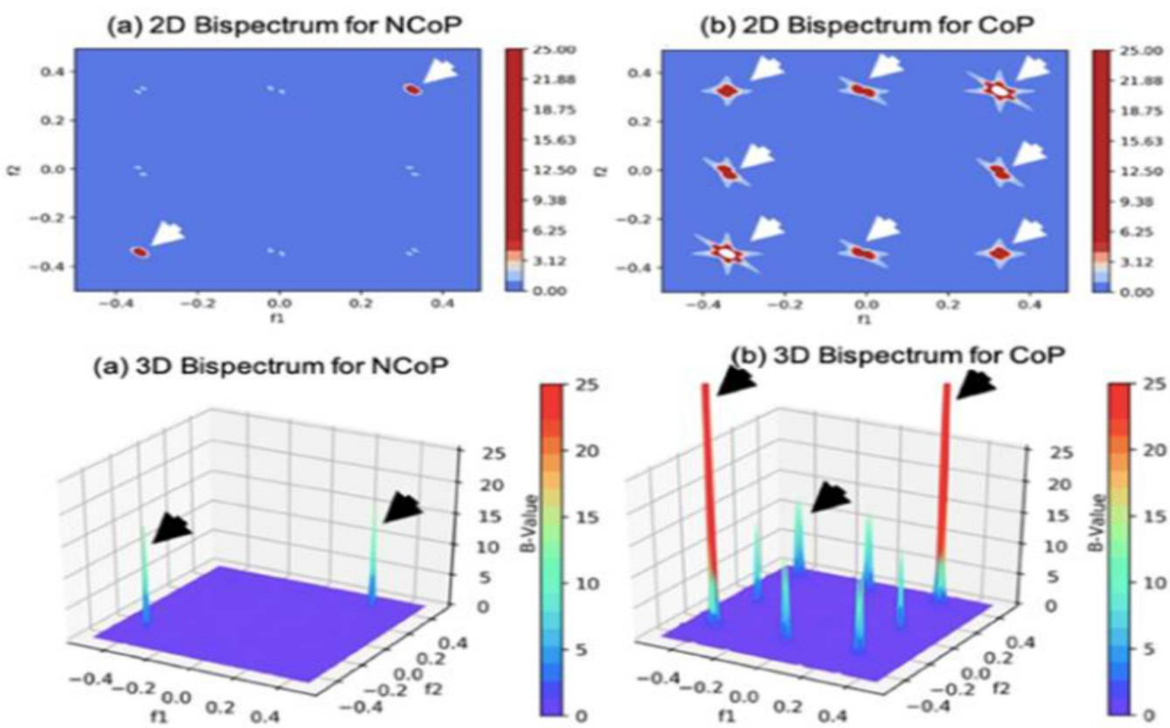

Bispectrum analysis of

- non-COVID-19 pneumonia (NCoP) and
- COVID-19 pneumonia (CoP).

32

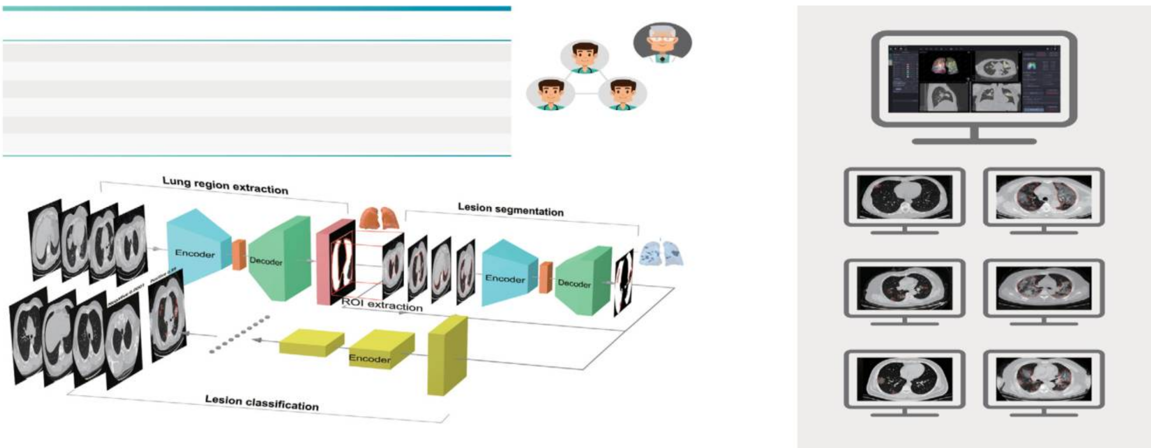

Framework of system

32

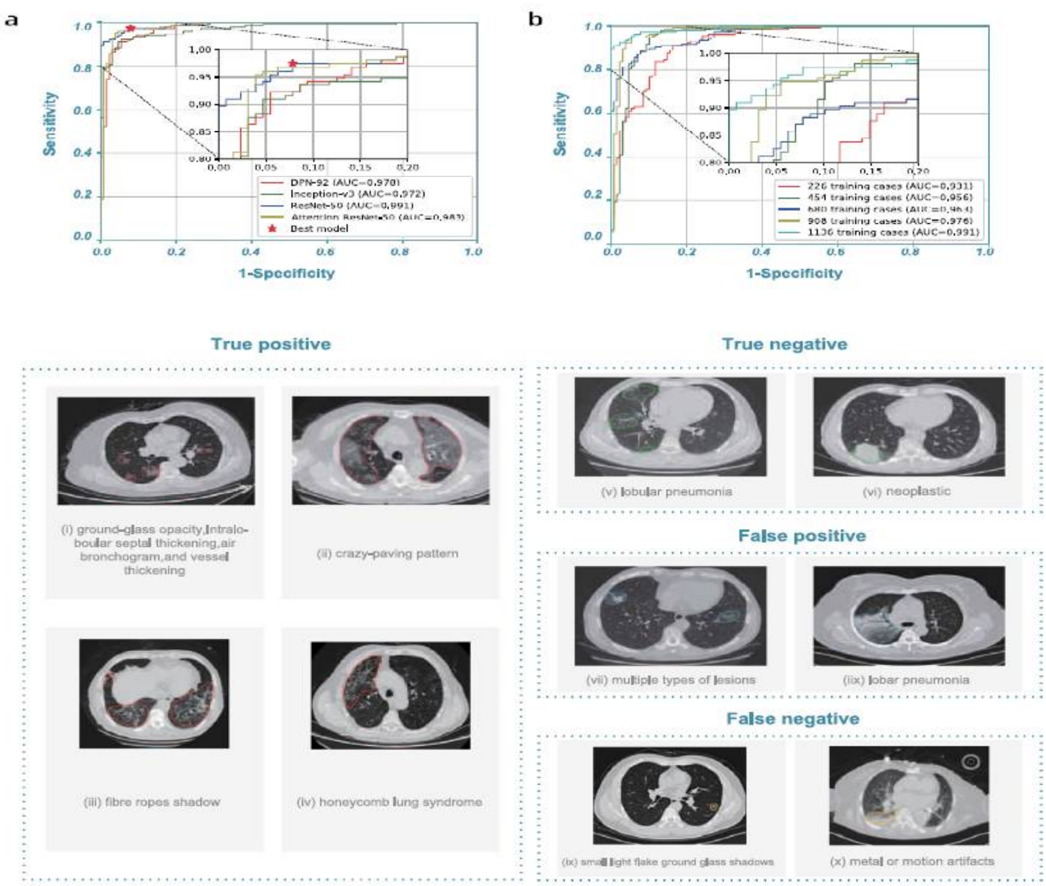

Model performance and highlights of model predictions.

- a, Receiver operating characteristic (ROC) curves of DPN-92, Inception-v3, ResNet-50, and Attention ResNet-50 with 3D U-Net++, respectively.
- b, ROC curves of 3D U-Net++ - ResNet-50 trained with different numbers of training cases.
- c, Typical predictions of the segmentation model.

32

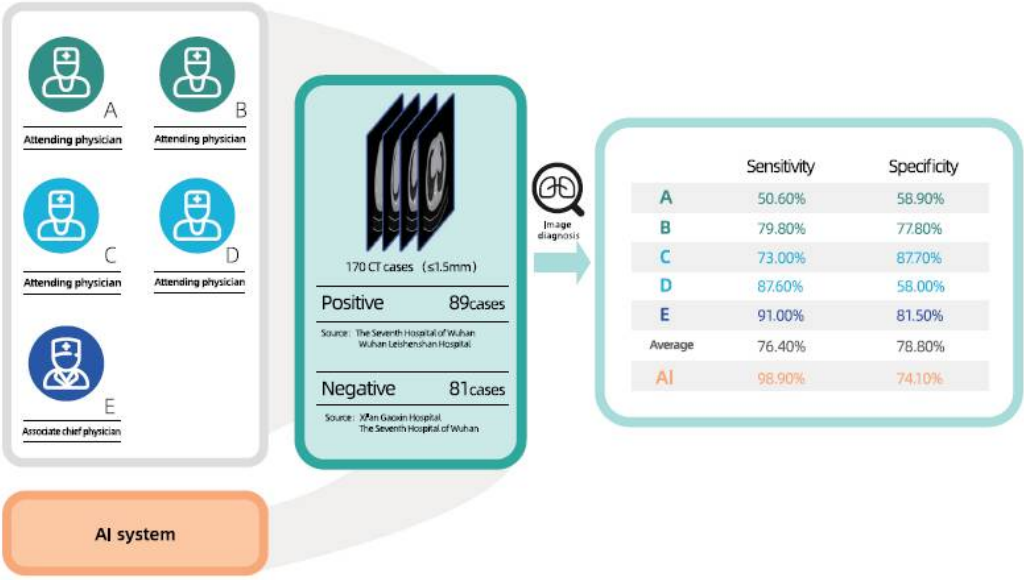

s

Illustration of the reader study.

- ✓ Five qualified physicians participated in this reader study.
- ✓ A total of 170 cases (89 were positive) were randomly selected from the test set

32

Demonstration of the deployment workstation

TB

01

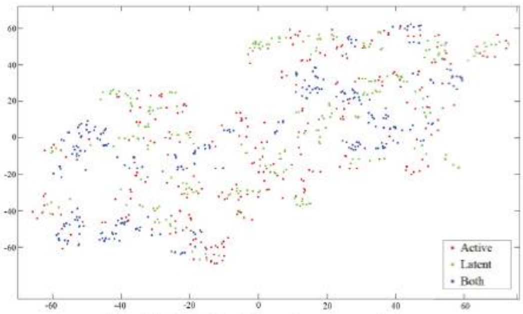

(a) t-SNE with Euclidean distance applied to the original data distribution.

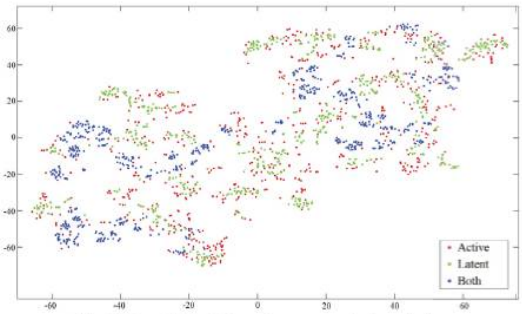

(b) t-SNE with Euclidean distance applied to the data augmented by SMOTE.

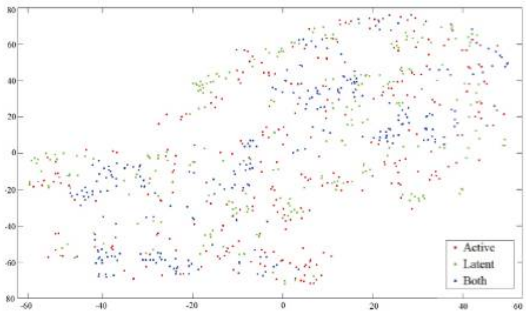

(c) t-SNE with Chebyshev distance applied to the original data distribution.

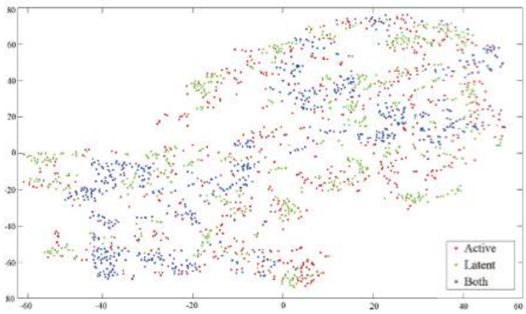

(d) t-SNE with Chebyshev distance applied to the data augmented by SMOTE.

t-SNE plots of the samples for classifying the TB stage (Active, Latent, Both) showing the distribution and dispersion of the samples between classes.

- ✓ In (a) and (c) resulting plots on original samples by Euclidean and Chebyshev distances, respectively.
- ✓ In (b) and (d) resulting plots with synthetic samples generated by SMOTE resampling.
- ✓ Each original sample corresponds to a TBX11k image represented as a feature vector generated by BPPC. Synthetic samples are obtained by SMOTE from original samples

01

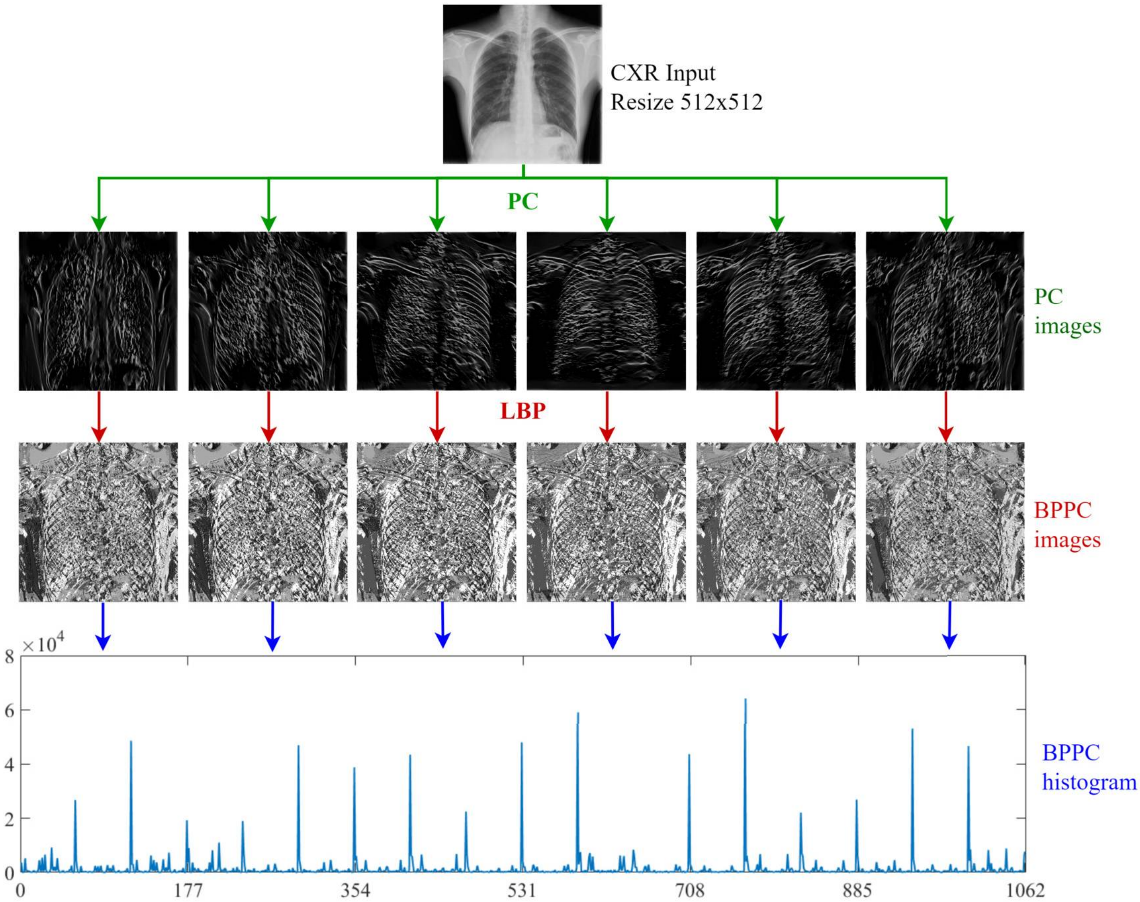

Process of extracting BPPC features from an input CXR

- ✓ Computed phase congruences (PCs) of the input image using logarithmic Gabor wavelets in six orientations (0º, 30º, 60º, 90º, 120º, 150º).
- ✓ LBP algorithm is employed on these PC images, resulting in six corresponding BPPC images.
- ✓ Each of these six BPPC images produces a 177-bin histogram.
- ✓ Six histograms are merged, creating a histogram that represents the vector of 1,062 features from the input image

01

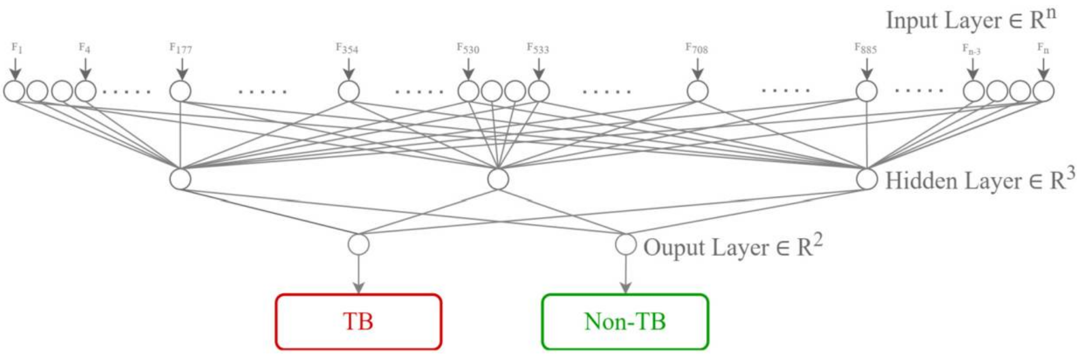

Model 1 - FFNN

- ✓ n input nodes, 1 hidden layer with 3 neurons, and the output layer to the binary classification scenario, TB versus Non-TB cases

01

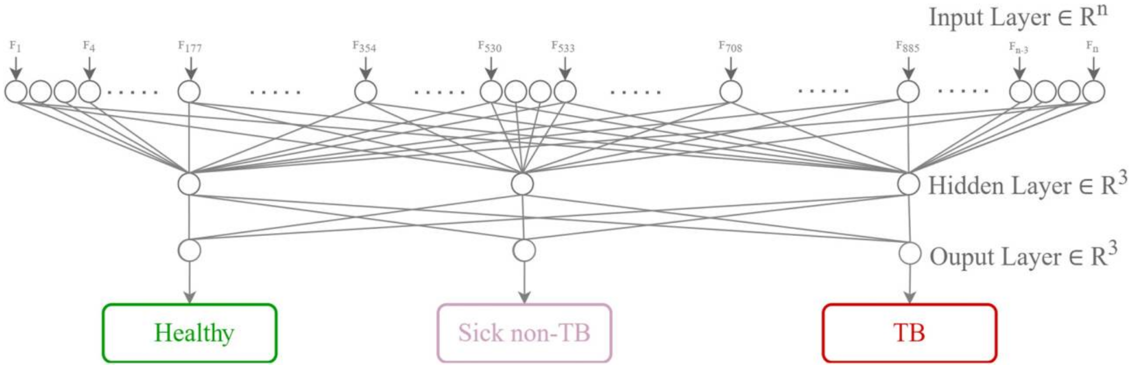

Model 2 - FFNN

✓ n input nodes, 1 hidden layer with 3 neurons, and the output layer to the multi-class classification scenario

01

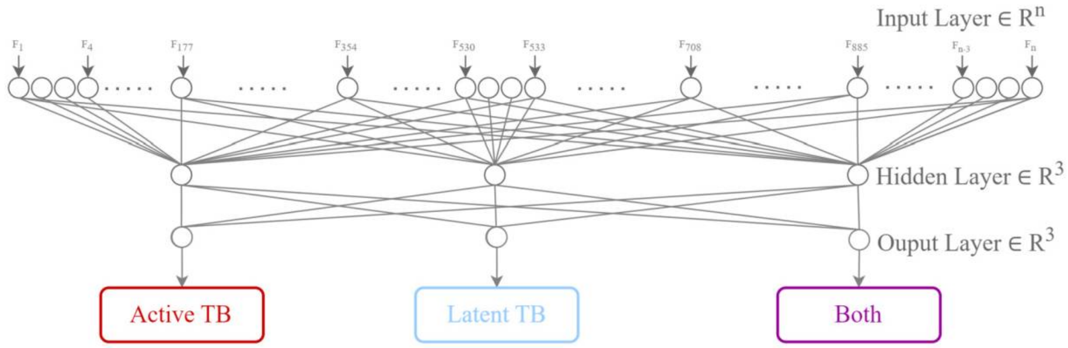

Model 3 - FFNN

✓ n input nodes, 1 hidden layer with 3 neurons, and the output layer to TB stage-classifying

01

Summary of optimized parameters used in the neural network model.

Parameter	Value	Explanation
Input	1,062 features vector	a BPPC features vector extracted from each CXR image
Learning function	Levenberq-Marquardt	used to update weight and bias values according to Levenberg-Marquardt optimization
Loss function	Mean Squared Error	measures model performance by calculating the mean squared error between estimated values and actual values
Regularization rate	$1 \times e^{-05}$	for faster model convergence while preserving data representativeness
Number of neurons	3	optimized with only 3 neurons at the hidden layer
Training process	10-CV	cross-validation to improve model generalizability and estimate performance in practice
Transfer function	Tansig	used in the hidden layer nodes to produce faster output rates
	Softmax	used in the output layer nodes to provide better correlation coefficients for the processed hidden layer output data
Validation failures	5	avoiding overfitting of the model

01

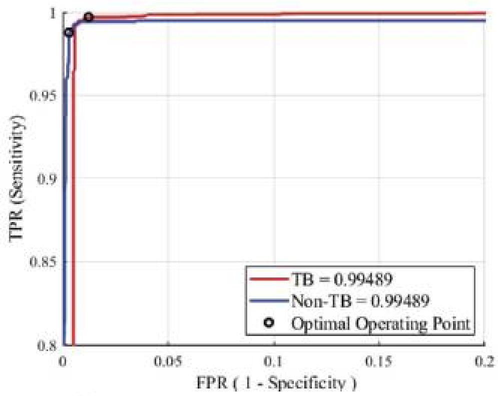

(a) ROC curve analysis on TB and Non-TB diagnosis from the original data.

(b) Sankey diagram denoting the total classification of TB and non-TB from the original data.

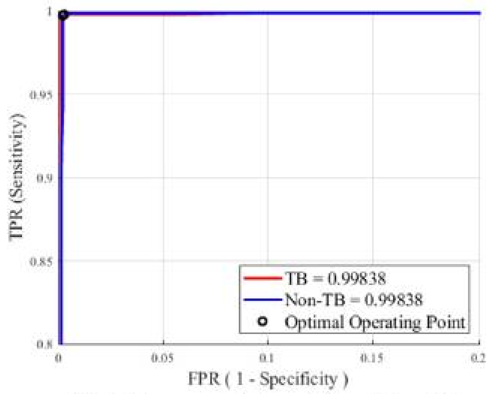

(c) ROC curve analysis on TB and Non-TB diagnosis from the augmented data.

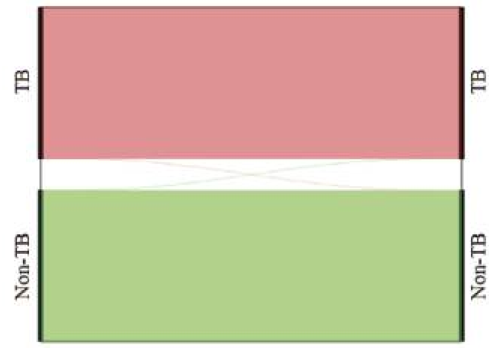

(d) Sankey diagram denoting the total classification of TB and non-TB from the augmented data.

Model 1

- ✓ In (a) and (c) Zoom of the ROC curve showing optimal operating points in the TB and Non-TB classification from the original and augmented data.
- ✓ In (b) and (d) respective Sankey diagrams denoting the total confusion matrices

01

Methodology	Dataset	Params	Partition (%) train/val/test
① Bag(GoogleNet, VggNet, ResNet)	MC SH	10^6	LOOCV 10-CV
② Ensemble GoogleNet, AlexNet	MC,SH,+	10^6	68/17/15
① FE(SetA,B,C), FS weary, MLP	MC SH	10^3	10-CV
① Custom CNN model	MC	10^6	70/20/10
③ AlexNet custom model	MC SH	10^6	5-CV
① FE(SetA,B), SVM	MC SH	10^3	≈64/36 ≈17/7
② Custom CNN model	MC SH	10^6	5-CV
② DenseNet	MC SH	10^6	SH/MC
② DenseNet121, CXR14	MC SH	10^6	CXR14/MC CXR14/SH
② ChexNet ② MetaChexNet (DFE+Metadata) ② ChexNet	MC SH MCSH	10^6	≈77/11^{SH}/N ≈77/11/11 ≈77/11/11+
② CNNs Ensemble	MC,SH,+	10^6	70/15/15
① DenseNet201	MCSH,+	10^6	5-CV
② Bayesian-CNN	MC SH	10^6	80/20
② DFE(MobileNet), Metaheuristic	SH	10^6	80/20
③ DFE(AlexNet), SVM	MC SH	10^6	-
② DFE(MobileNet), SVM	SH	10^6	5-CV
② DFE from 5 DCNNs, SVM	MC	10^6	5-CV
② VGG-16 and Bone suppression	MC SH	10^6	4-CV
③ VGG-16 Fine-tuned	SH,+	10^6	80/20
① FE(LBP), FS(MBO), KNN	MC SH MCSH	10^2	10-CV
① EfficientNetB3, DA ① InceptionRenNetV2, DA	MC SH	10^6	5-CV
① EfficientNetB3, DA	MCSH		
② ViT + EfficientNetB3	MC SH	10^6	- -

② Faster R-CNN (ResNet w/FPN)	TBX11K	10^6	≈59/16/25
③ EfficientNet-B5-FPA(KD)	TBX11K	10^6	≈94/2/4
② FE(BPPC),FFNN ② FE(BPPC),FFNN,DA(Smote)	TBX11K	10^3	10-CV

- ✓ FE: Feature extraction process, DFE: Deep feature extraction process, FS: Feature selection process, LLR: Linear Logistic Regression, DA Data augmentation.
- ✓ SetA:{IH, GM, SD, LD, HOG, LBP},
- ✓ SetB:{Tamura Texture Descriptor, CEDD and FCTH, Hu Moments, CLD and EHD, Primitive Path, Edge Frequency, Autocorrelation and Shape Features},
- ✓ SetC:{ Shape measurements as size, orientation, eccentricity, extent and centroid}. In dataset: MC: Montgomery
- ✓ SH: Shenzhen dataset (Jaeger et al., 2014), MCSH: MC and SH, and+: Others TB datasets.
- ✓ Params: Number of classification model input parameters. In partition: train/val/test or train/test percents,
- ✓ LOOCV: Leave-One-Out cross-validation, n-CV n-folds cross-validation. 1: Lung mask segmentation, 2: None segmentation and 3: Box crop segmentation

Lung Cancer disease

14

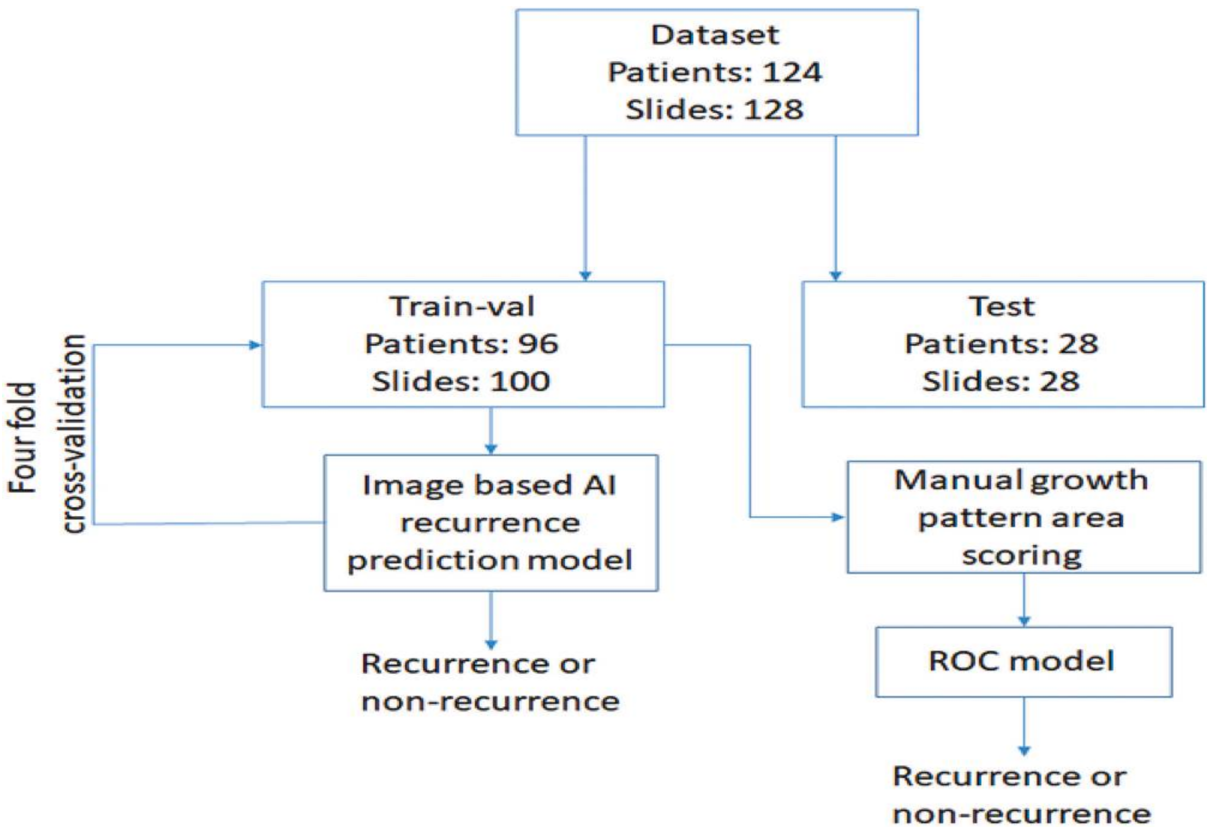

Data distribution and experimental design for both models

14

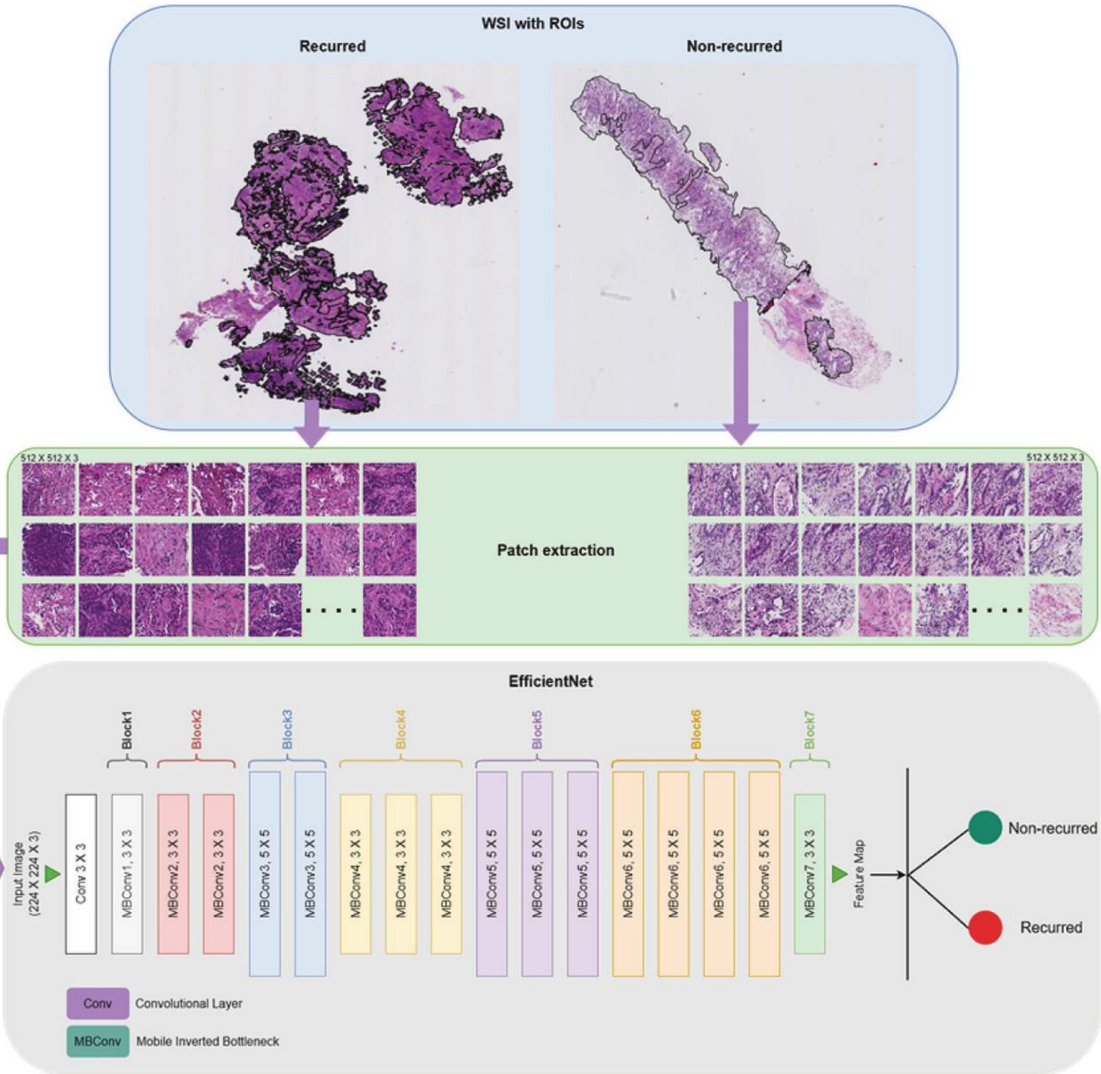

Proposed AI framework for LUAD recurrence prediction

14

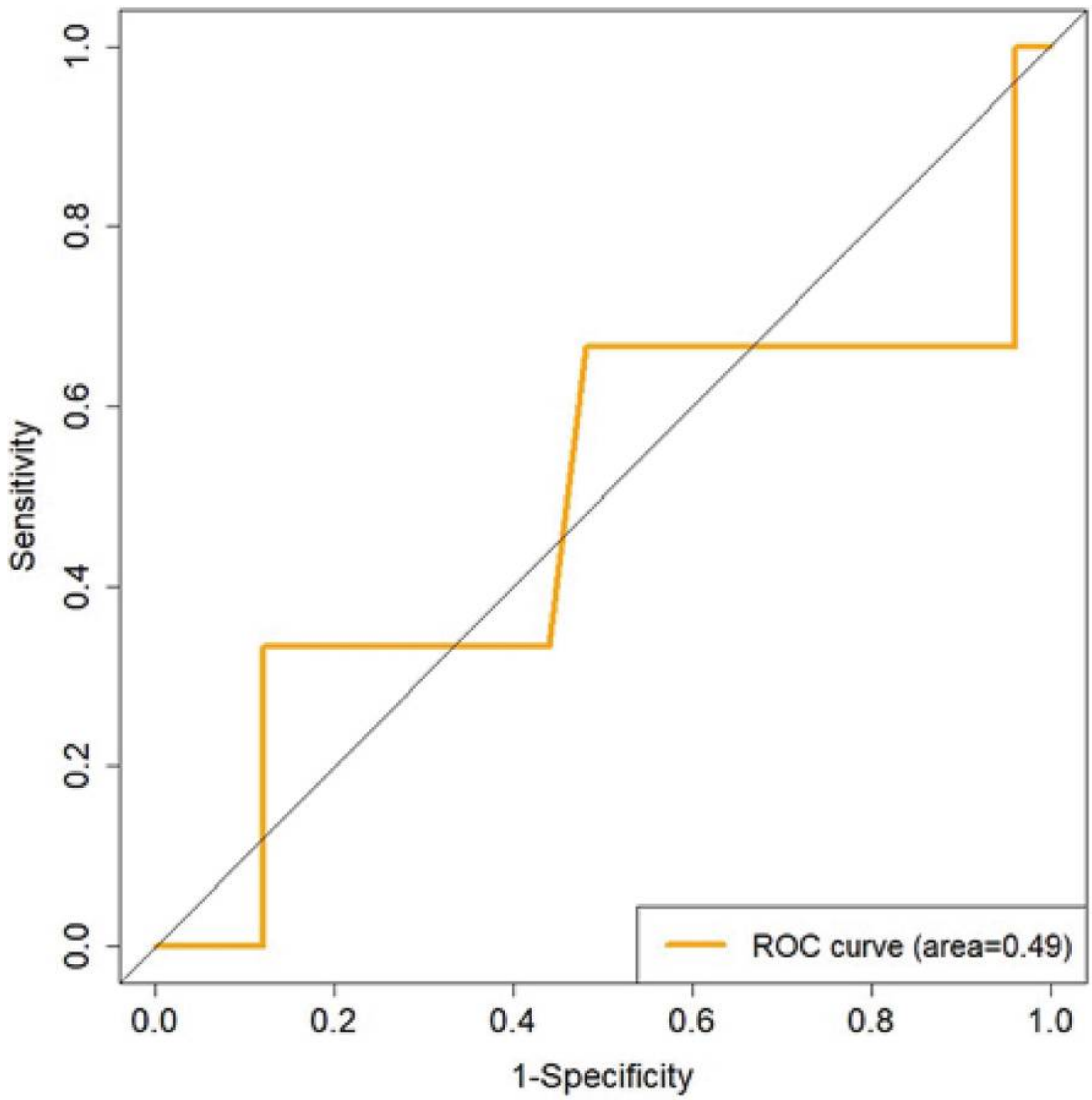

ROC curve of the statistical model

- Test set using dominant growth pattern and the dominant together with the worst growth pattern with a cut-off of 20% in predicting recurrence outcome

15

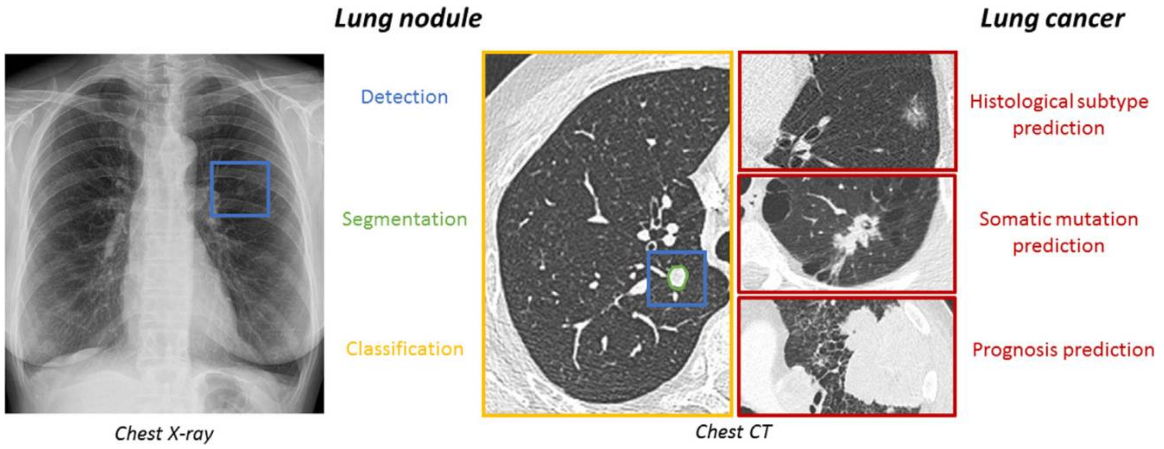

Graphical representation of deep learning applications
for lung nodule and lung cancer in chest imaging

15

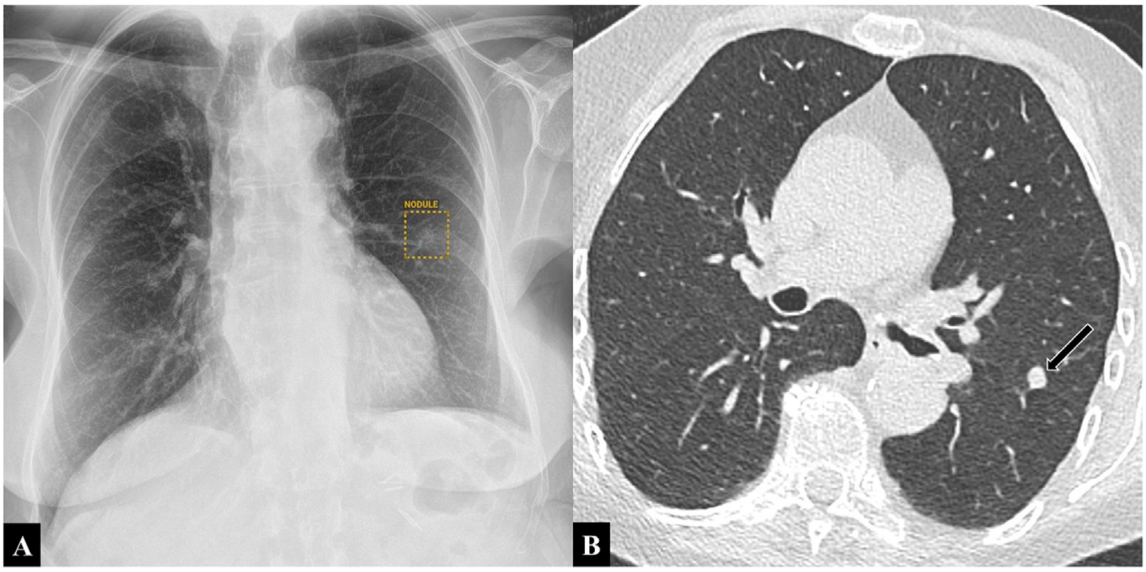

- ✓ A, commercially available deep learning based software was applied on
    - o frontal chest X-ray image and
    - o identified a faintly visible nodule in the left hemithorax (square).
- ✓ B, Corresponding chest CT image in the axial plane
    - o confirms lung nodule located in the left lower lobe (arrow).

15

- ✓ A, Chest CT image in the axial plane shows a challenging nodule in the right perihilar area (arrow).
- ✓ B, Commercially available deep-learning based software was applied on the CT volume and was able to identify the nodule. The nodule was correctly classified as Lung-RADS 4a, based on its dimension

21

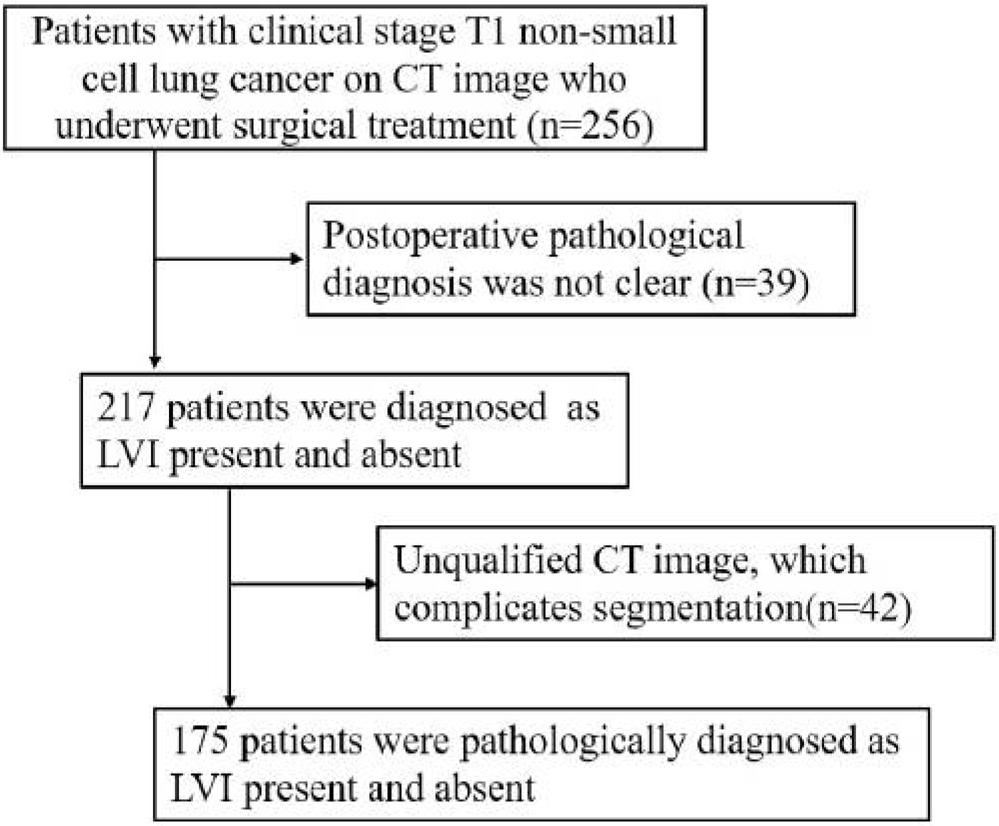

Study flowchart for recruitment of participants

21

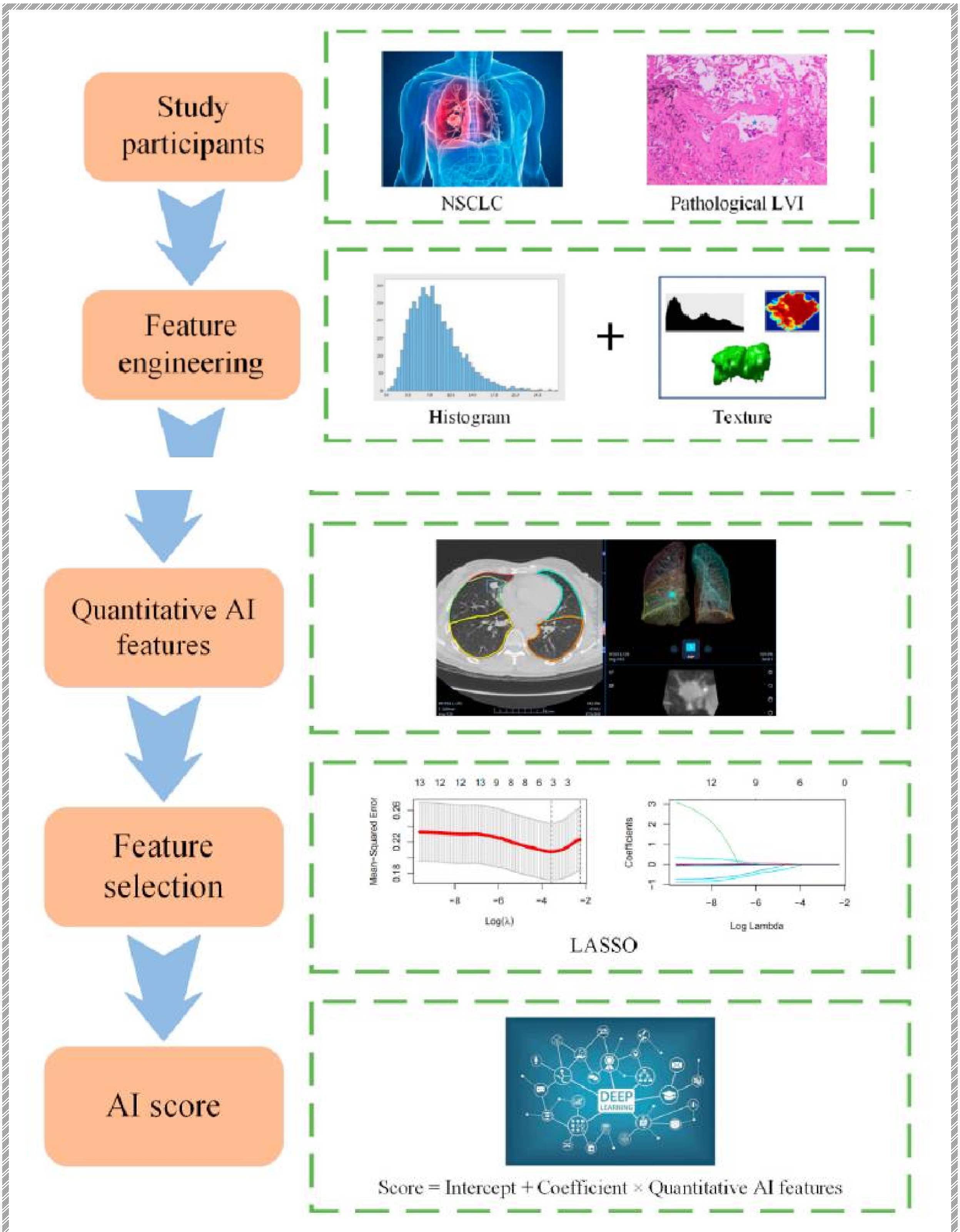

Diagram showing the procedure for obtaining the AI score

Acute respiratory distress syndrome (ARDS)

38

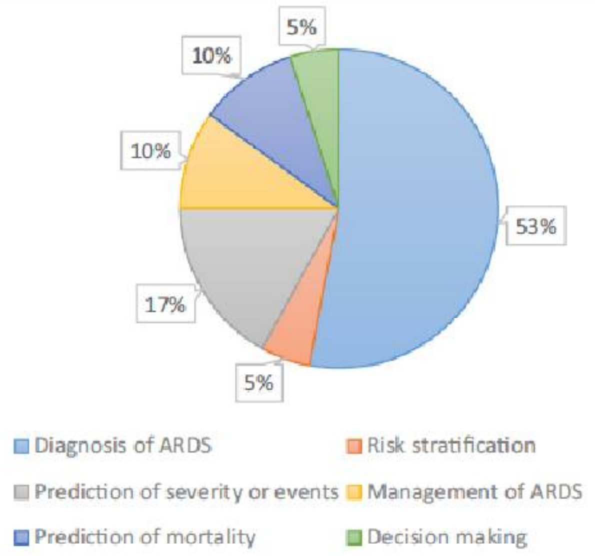

Role of AI in ARDS.

38

Characteristics of included studies.

Author, year & country	Purpose of study	Source of data	Type of data	Feature/variable selection	Classification algorithm/ model developed	Method of validation
Yang P et al., 2020, China	Identification of ARDS based on noninvasive physiological parameters	MIMIC-III Database	Demographics (age, gender, height, weight, body mass index, ethnicity); ICU information (type, length of stay, admission type, in-hospital mortality); Clinical measures (SpO2, temperature, heart rate, blood pressure, Glasgow Coma Scale; Respiratory system (respiratory rate, tidal volume, minute ventilation volume, peak pressure, plateau pressure, mean air pressure, PEEP, FiO2); Oxygenation index: P/F, S/F, Oxygenation Index, Oxygenation Saturation Index	Feature: Relief-F, Chi-squared, MIFS, Rank aggregation	Classification algorithm: L2–LR, SLP–FNN, AdaBoost, XGBoost, Traditional noninvasive classification method	10-fold cross-validation methods
Sinha P et al., 2020, USA	Develop phenotype identification in ARDS	RCT cohorts	Demographics, laboratory parameters, APCHE score, ARDS Risk factors	Variable: Random forest, bagging, LASSO (to select six most important predictor variables)	Model: Nested logistic regression models Algorithm: Parsimonious algorithms	10-fold cross-validation methods

Zeiberg D et al., 2019, USA	Automatic prediction of ARDS from EHR	EHR of a tertiary care centre	Baseline patient characteristics (e.g., age, race, and sex); Structured, time-stamped data elements (laboratory values, vital signs, medication administration records) from the six-hour window.	Varables: Baseline patient characteristics (e.g., age, race, and sex) and structured, time-stamped data elements (laboratory values, vital signs, medication administration records)	Model: L2-LR model, L1-LR model, XGBoost, EALI Score	5-fold cross validation
Afshar M et al., 2018, USA	ARDS identification	Patients records from a tertiary academic center	Radiology reports (chest radiographs and CTs)	Feature: UMLS, word n-grams	Model: NLP and machine learning model	10-fold cross-validation
Reamaroon N et al., 2017, USA	To account clinical diagnostic uncertainty while detecting ARDS	Raw data (HER) from ARDS patient cohort	Clinical features; vital signs; laboratory values	Features: vital signs and laboratory values	Model: Linear SVM	5-fold cross validation
Bernstein DB et al., 2013, USA	To identify the discordance between physicians in choice of TV and PEEP in ARDS patients	10,000 hypothetical patient scenarios	Peak airway pressure; PEEP; Arterial oxygen saturation	Variables: PAP, PEEP and arterial oxygen saturation	Algorithm: Fuzzy Logic Algorithm Monte Carlo approach	–
Ganzert S et al., 2012, Germany	To predict the nonlinear lung compliance for the individual patient	A multicentre study population of ARDS	Mechanical ventilator parameters such as maximum compliance value (Cmax); Plateau pressure value at Cmax	Feature extraction: spring-and-dashpot model	Model: Gaussian process modeling Algorithm: M5P (Reference)	–
Pearl A et al., 2009, USA	To predict complications during trauma patients' hospitalization period	National Trauma Data Bank (V6.2) data files	Patient demographic and physiological variables	Variables: Patient demographics and physiological variables	Algorithm: standard back propagation Model: ANN	–
Ganzert S et al., 2002, Germany	To compare different methods of measuring pressure-volume curves in artificially ventilated ARDS patients	Artificially ventilated ARDS patients records	Background information (age, weight, height, ventilation period, tube type, tube ID and calculated compliance) and pressure volume measurement	Features: LOW-FLOW, SCASS, SUPER-SYRINGE and SLICE.	Model: Regression model by CUBIST and C5.0	10 runs of 10-fold cross-validation
Le S et al., 2020, USA	Development and analysis of a novel application of supervised machine Learning model CDS for the detection and early prediction of ARDS.	Medical Information Mart for Intensive Care III (MIMIC-III) database	Clinical features; Organ dysfunction feature; Radiology reports	Variables: Quantitative clinical features (age, heart rate, respiratory rate, temperature, diastolic and systolic blood pressure, and SpO2); organ dysfunction feature: systolic blood pressure $<$ 90 mmHg, lactate $>$2.0 mmol/L, platelet count $<$100,000 µL, and international normalized ratio $>$ 1.5; radiology reports	Model: XGBoost gradient boosted tree model Algorithm: Machine learning algorithm	10-fold cross validation

38

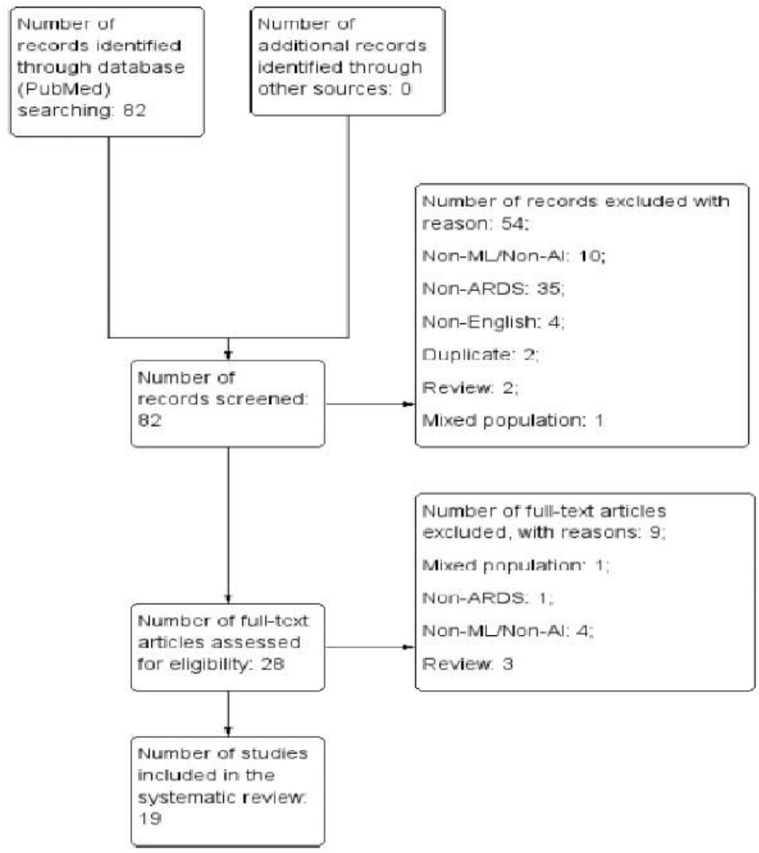

Study selection process/PRISMA flow diagram.

Lung perfusion,
Ventilation,
Lung microstructure

33

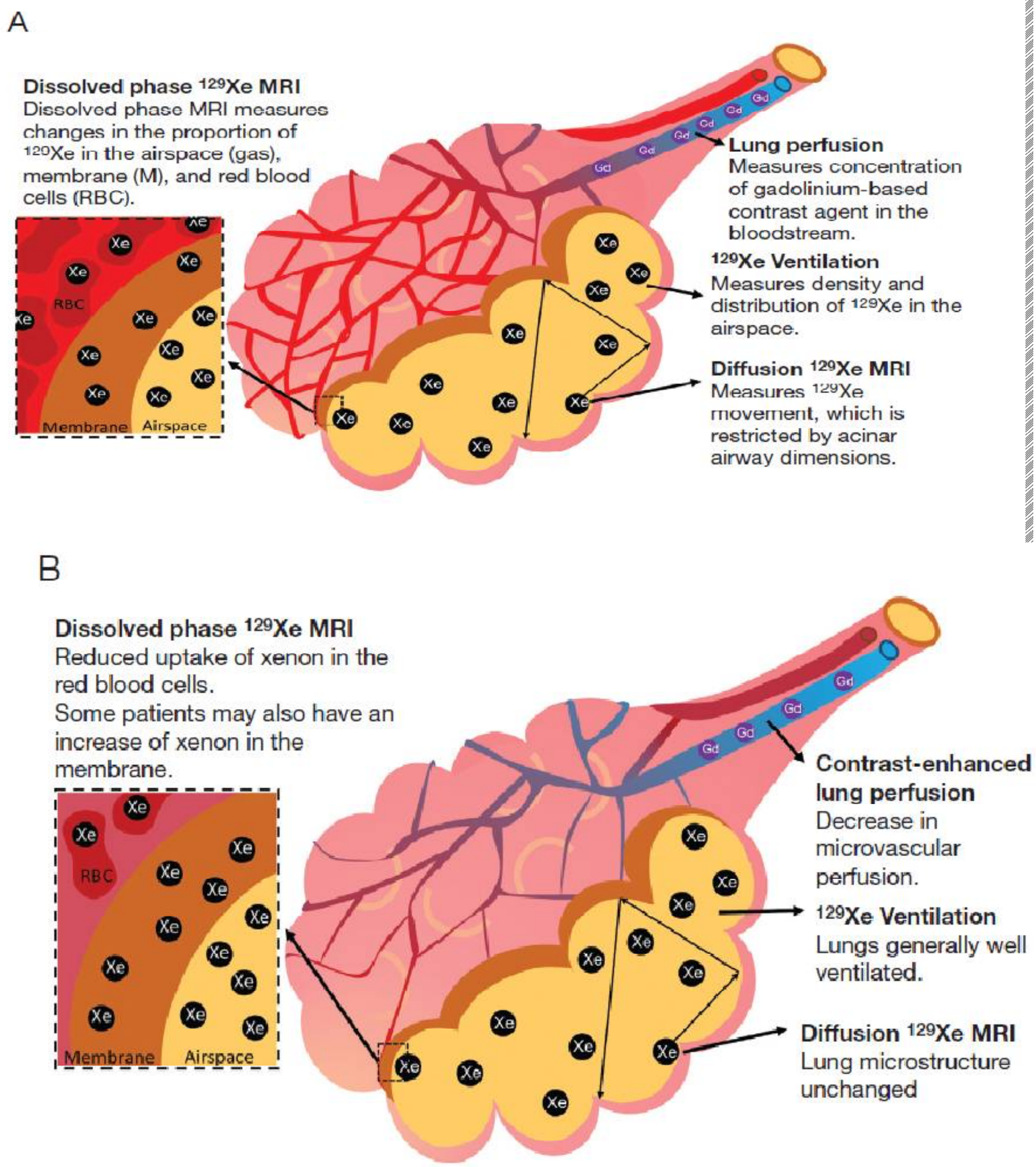

How lung MRI techniques measure lung perfusion, ventilation, lung microstructure

- ✓ A, Techniques in a healthy alveolus.

✓ B, Possible interpretation of the findings in patients who have had COVID-19, with reduced RBC:M due to damage to pulmonarymicrocirculation but preserved acinar airway dimensions. RBC:M : RBC to membrane fraction

33

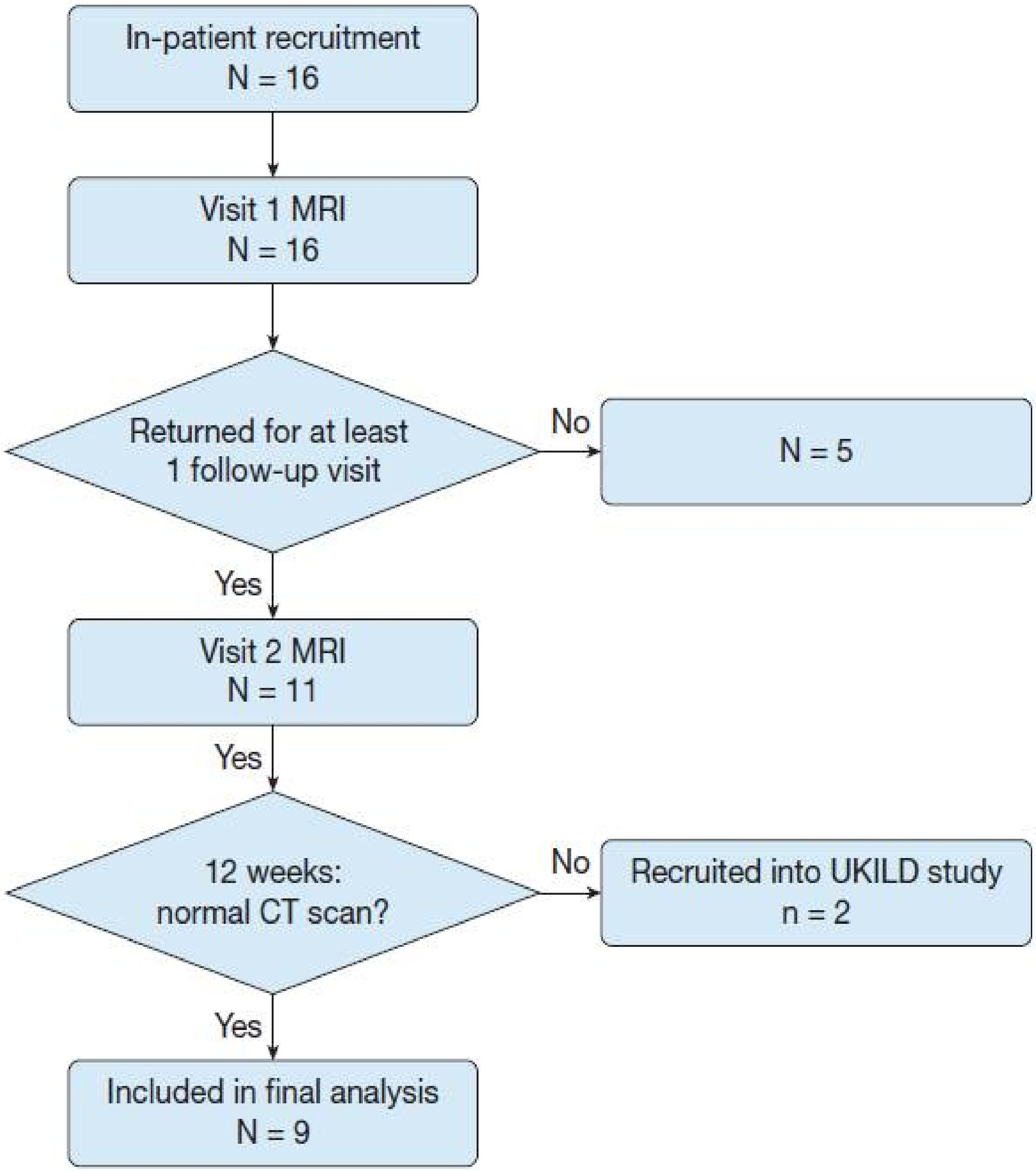

Flow chart of patient recruitment. UKILD : UK Interstitial Lung Disease Long-COVID-19 study

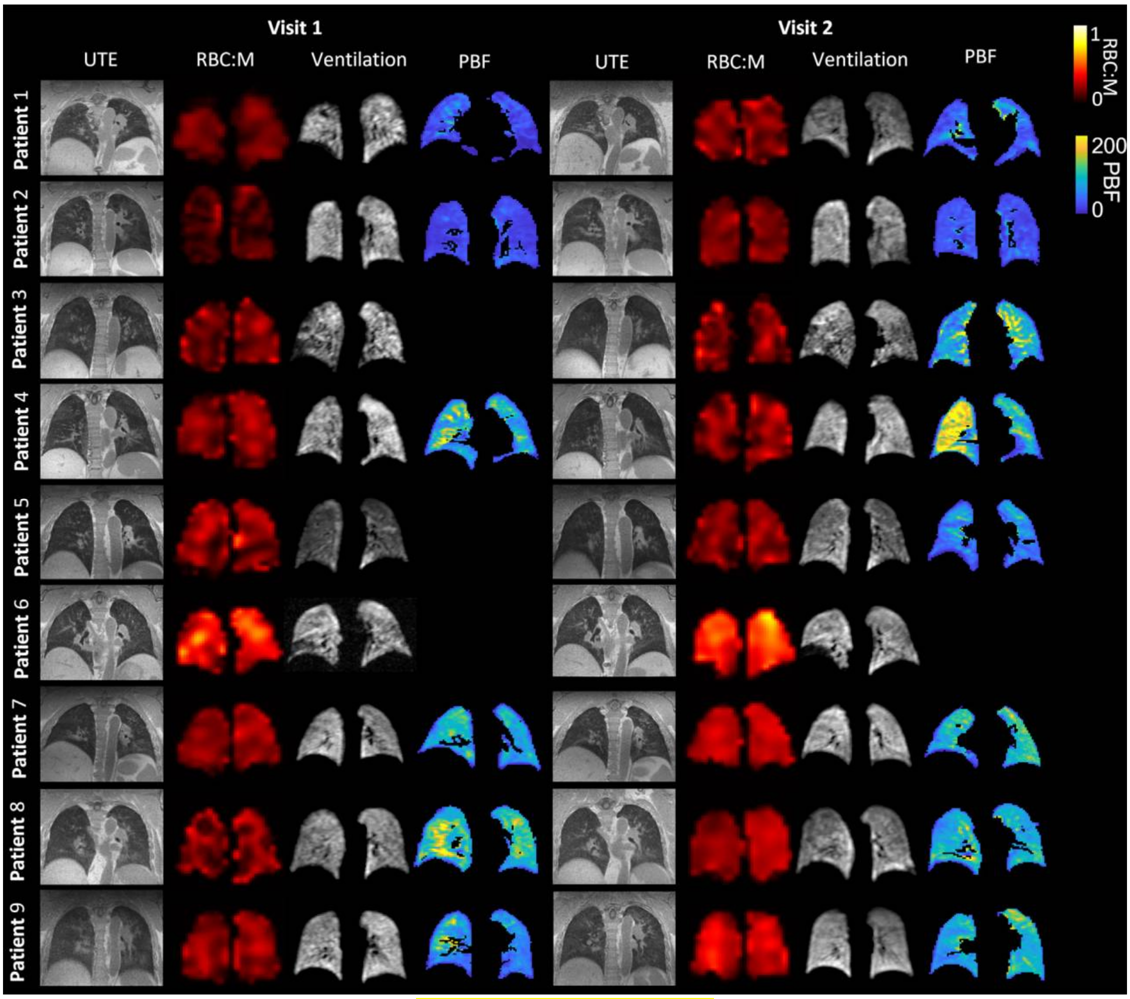

Example of UTE images,
RBC:M maps,
129Xe ventilation images, and
maps of pulmonary blood flow

- ✓ at visit 1 and visit 2, for each patient.
- ✓ The white arrow indicates a segmental perfusion defect visible at visit 1,
- ✓ which improves at visit 2.

! M : membrane;
! PBF : pulmonary blood flow;
! RBC:M : RBC to membrane fraction;
! UTE : ultra-short echo time.

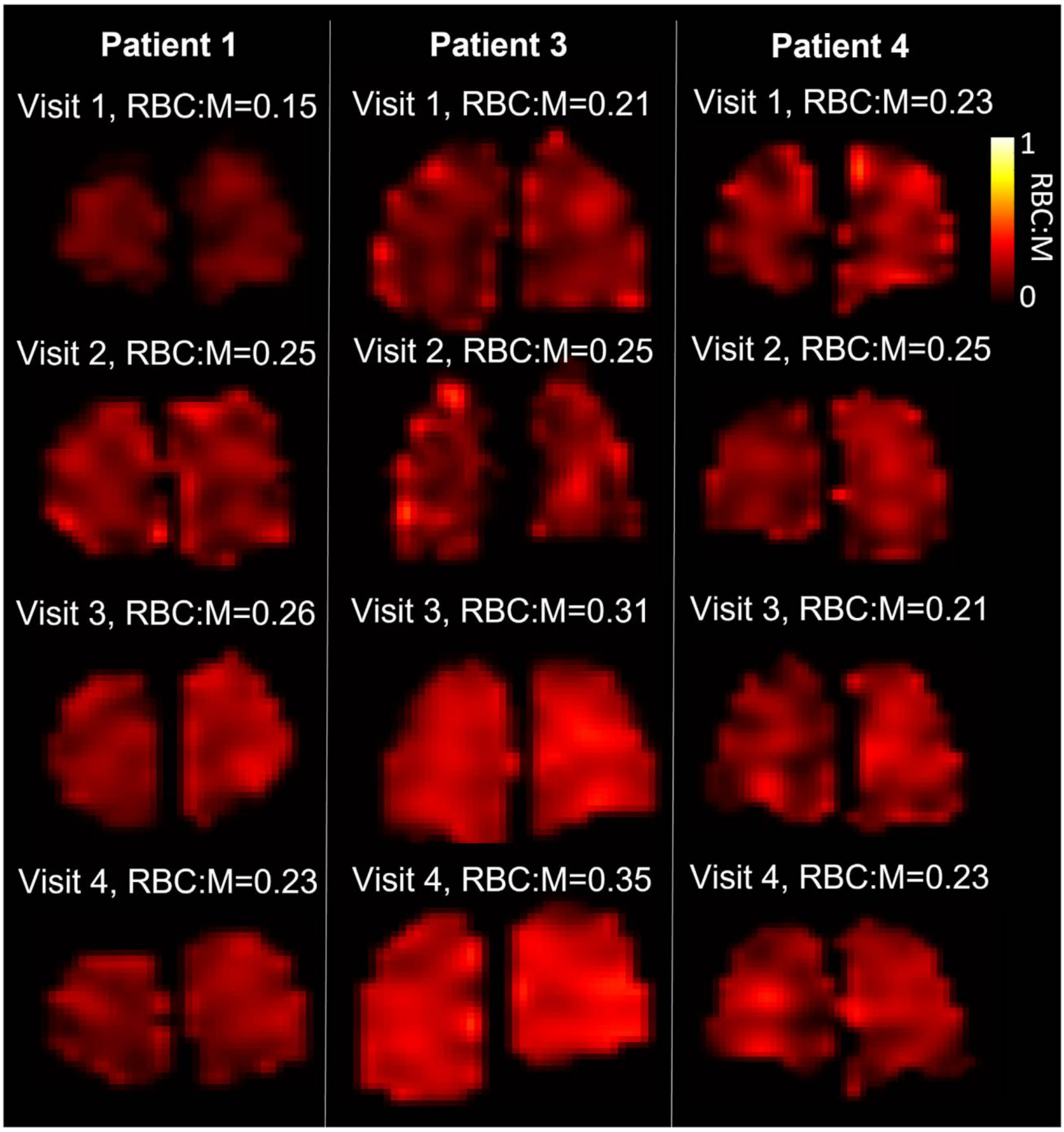

Lung RBC:M maps in three patients with four MRI visits

- ✓ at 6, 12, 25, and 51 weeks following hospital admission.
- ✓ Mean RBC:M at eachvisit is shown. M : membrane; RBC:M : RBC to membrane fraction

36

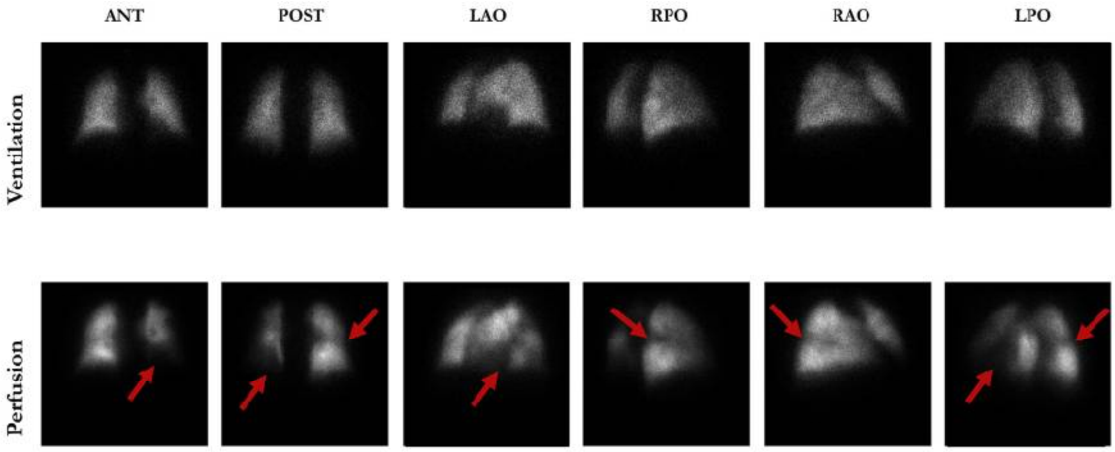

Ventilation-perfusion(V/Q)planarimagesforpulmonaryembolism(PE)detectioninsixviews.Redarrowsindicateperfusiondefects(V/Qmismatches)correspondingtoapositivediagnosisofPE.ANT,anterior;LAO,leftante-rioroblique;LPO,leftposterioroblique;POST,posterior;RAO,rightanterioroblique;RPO,rightposterioroblique.

36

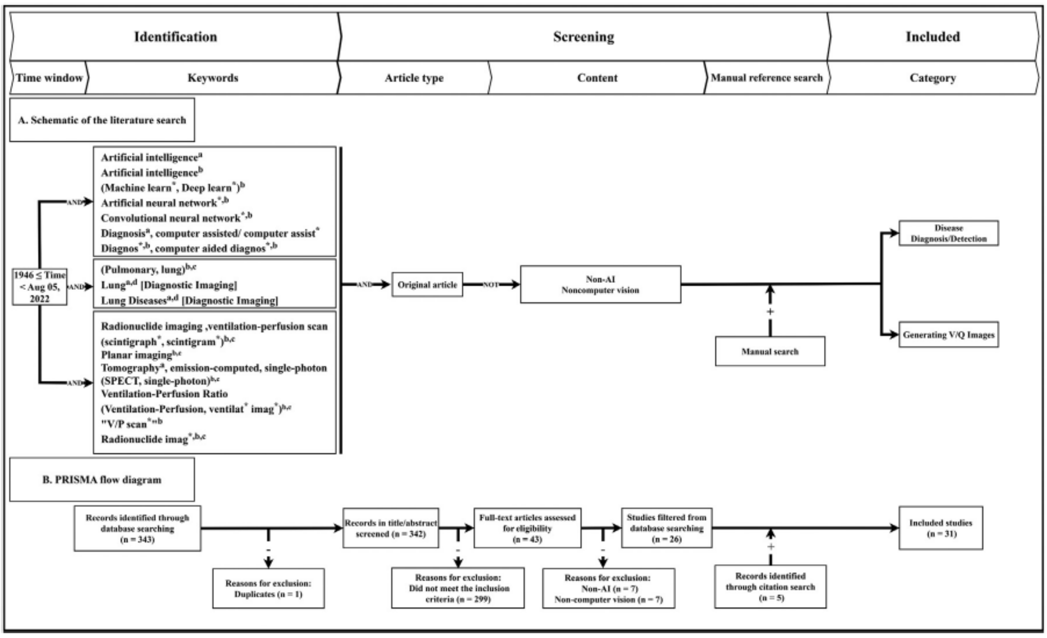

(A)Aschematicrepresentationofoursearchstrategyincludingthetimewindow,keywords,screeningcriteria,andthefinalapplicationcategory.(B)PRISMAflowdiagramofsystematicliteraturereviewprocesscorrespondingtoheadersin(A).a:MedicalSubjectHeadings(MeSH)andallSubheadingsasusedinMedline/PubMed.b:wordofphraseappearingintitlesandabstracts.c:keywordsuppliedbytheauthor.d:MeSHtopicalqualifierforDiagnosticImaging.*:wildcardforallwordsbeginningwithgivencharacters./:specificMeSHSubjectheading

37

Schematic of ECG-enabled stethoscope and AI-ECG

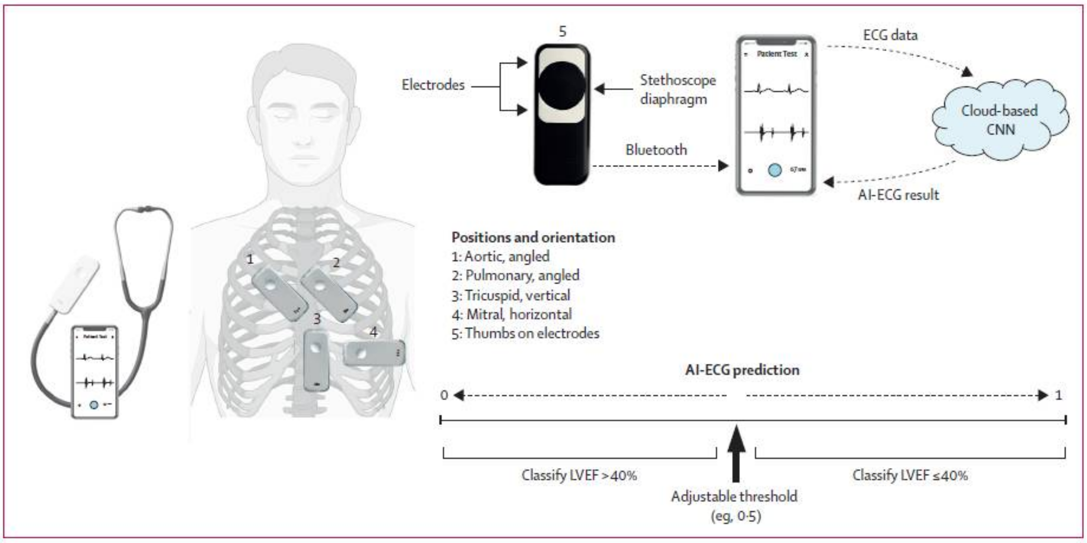

Illustration of anatomical positions for auscultation and position-specific angulation (vector) of ECG-enabled stethoscope; and flow diagram of raw ECG data to cloud-based CNN for interpretation of AI-ECG, with illustration of how raw outputs are classified according to adjustable (optimised) threshold. Anatomical images adapted from BioRender. AI=artificial intelligence. CNN=convolutional neural network. LVEF=left ventricular ejection fraction

37

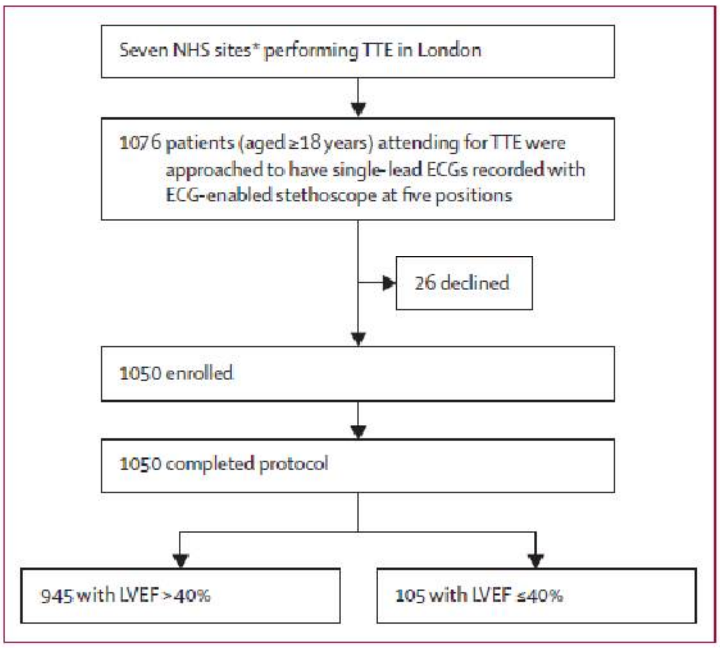

TTE=transthoracic echocardiogram. LVEF=left ventricular ejection fraction. NHS=National Health Service. *Three hospitals and four community centres

	All participants (n=1050)	LVEF >40 group (n=945)	LVEF ≤40 group (n=105)	p value
Age, years				
18–69	636 (61%)	583 (62%)	53 (50%)	0·034
≥70	414 (39%)	362 (38%)	52 (50%)	..
Mean (SD)	62 (17·4)	62 (17·5)	67 (15·3)	0·0014
Sex				
Male	535 (51%)	466 (49%)	69 (66%)	0·0015
Female	..	..	..	..
Mean TTE LVEF (SD), %	54% (10·3)	57% (5·8)	30% (8·2)	<0·0001
Ethnicity	..	..	..	0·4
Asian	199 (19%)	176 (19%)	23 (22%)	..
Black	95 (9%)	84 (9%)	11 (10%)	..
Mixed	22 (2%)	18 (12%)	<5	..
Other	116 (11%)	102 (11%)	14 (13%)	..
White	618 (59%)	565 (60%)	53 (50%)	..
Medical history				
Hypertension	395 (38%)	338 (36%)	57 (54%)	<0·0001
Myocardial infarction	102 (10%)	62 (6%)	40 (38%)	<0·0001
Atrial fibrillation	173 (16%)	146 (15%)	27 (26%)	0·011
Pacemaker	59 (6%)	43 (5%)	16 (15%)	<0·0001
Diabetes	224 (21%)	181 (19%)	43 (41%)	<0·0001
Stroke or transient ischaemic attack	100 (10%)	85 (9%)	15 (14%)	0·11
Chronic kidney disease	98 (9%)	74 (8%)	24 (23%)	<0·001
Smoking	148 (14%)	132 (14%)	16 (15%)	0·78
Excessive alcohol intake	26 (2%)	25 (2·6%)	<5	0·48
Hypercholesterolaemia	188 (18%)	159 (17%)	29 (28%)	0·0098
Pregnancy (current)	21 (2%)	21 (2%)	0	0·24
Chronic obstructive pulmonary disease	57 (5%)	48 (5%)	9 (89%)	0·20

Data are n (%) unless otherwise stated. Characteristics reported in fewer than five participants are shown as <5. p values were calculated via Student's *t* test or Pearson's χ^2 test. Ethnicity was self-reported from a list of 18 options drawn from the UK Office of National Statistics Census for England.[15] Full ethnicity breakdown is available in the appendix (p 2). TTE LVEF=transthoracic echocardiogram-derived left ventricular ejection fraction.

Baseline characteristics of study participants

03

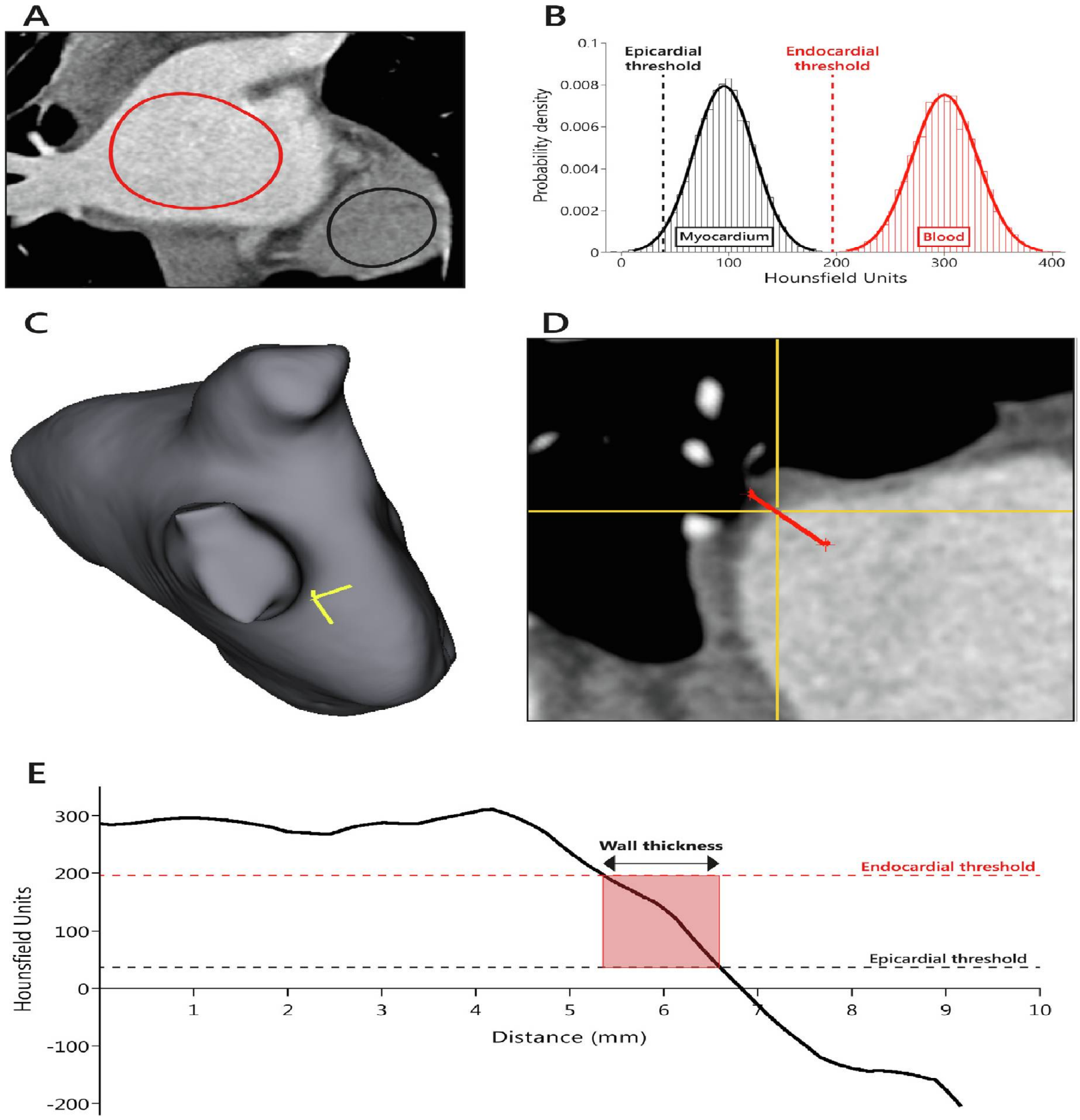

Example of wall thickness measurement.

- Panel A: Regions of interest were drawn inside the left atrium and ventricular apex.
- Panel B: Blood pool and myocardium intensity histograms were constructed from the regions of interest. The endocardial threshold value was calculated by averaging the means of the blood pool and myocardial image intensity. The epicardial threshold value was calculated as two standard deviations below the mean of the myocardial image intensity.
- Panel C: Locations for left atrial wall thickness measurement of the pulmonary vein (PV) antra were manually selected using a 3D segmentation of the left atrium. The yellow crosshair represents the location of wall thickness measurement on the anterior segment of the right inferior PV.

- ✓ Panel D: Multiplanar reformatted images were generated perpendicular to the atrial wall and the crosshair corresponds to the location chosen on the 3D segmentation (panel C). Subsequently, a line (in red) perpendicular to the atrial wall was drawn.
- ✓ Panel E:The intensity profile of the line perpendicular to the atrial wall was obtained. Atrial wall thickness was calculated using the patient-specific endocardial and epicardial thresholds.

03

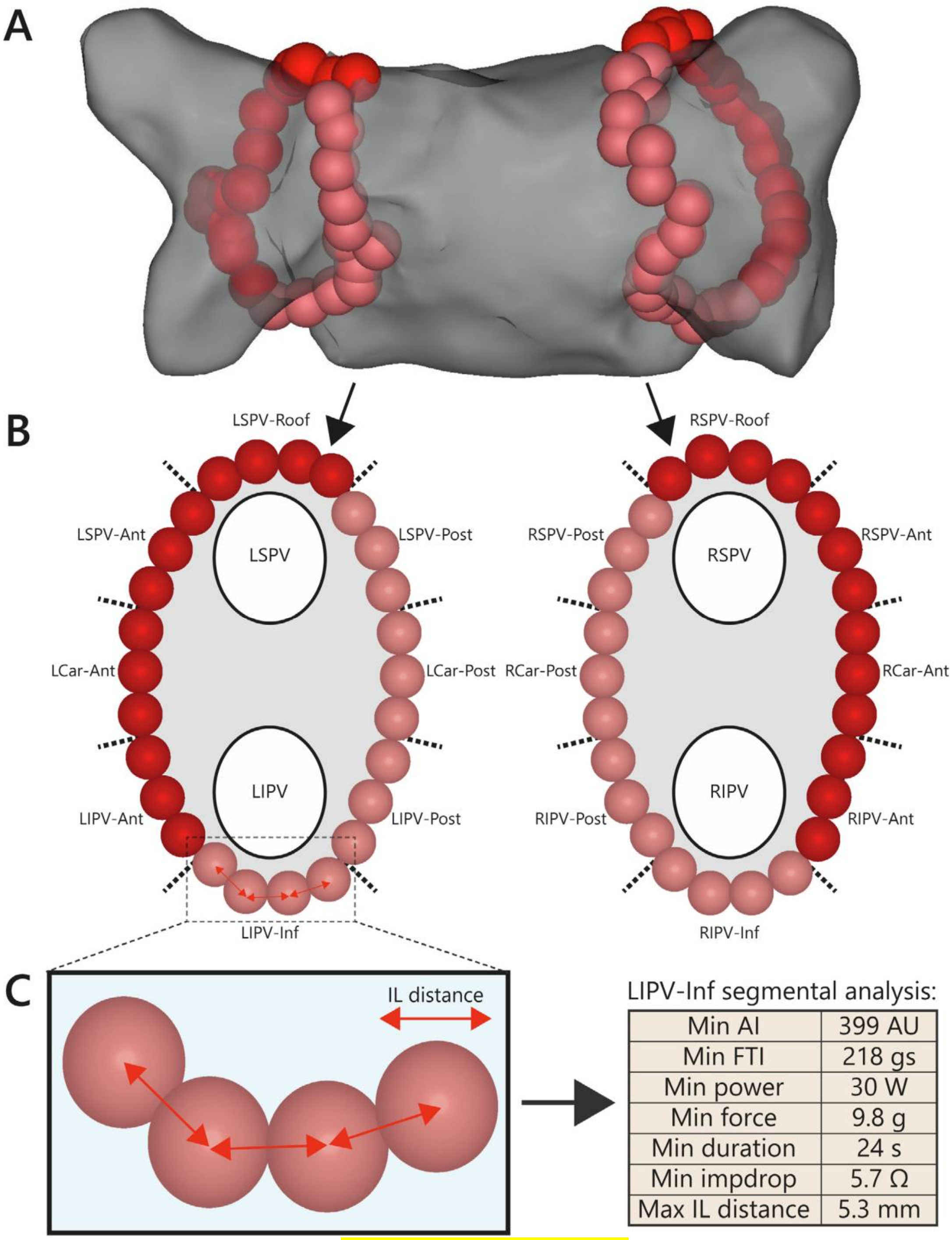

✓ Ablation procedure analysis.

- ✓ Panel A: Posteroanterior projection of a typical circumferential antral ablation approach. Ablation tags are automatically color coded based on Ablation Index (AI) values. Pink ablation tags represent AI values 380 to 499, whereas red tags represent AI values > 500.
- ✓ Panel B: Ablation tags were classified according to a 16-segment model for segmental analysis. Ablation tags belonging to additional ablation applications to treat acute pulmonary vein reconnection were excluded from analysis.
- ✓ Panel C: Minimum AI value, force–time integral (FTI), contact force (CF), ablation duration, power, impedance drop (impdrop) and maximum interlesion (IL) distance were determined for each segment.
- o Ant = anterior, AU = arbitrary units, Inf = inferior, LCar = left carina, LIPV = left inferior pulmonary vein, LSPV = left superior pulmonary vein, Post = posterior, RCar = right carina, RIPV = right inferior pulmonary vein, RSPV = right superior pulmonary vein

03

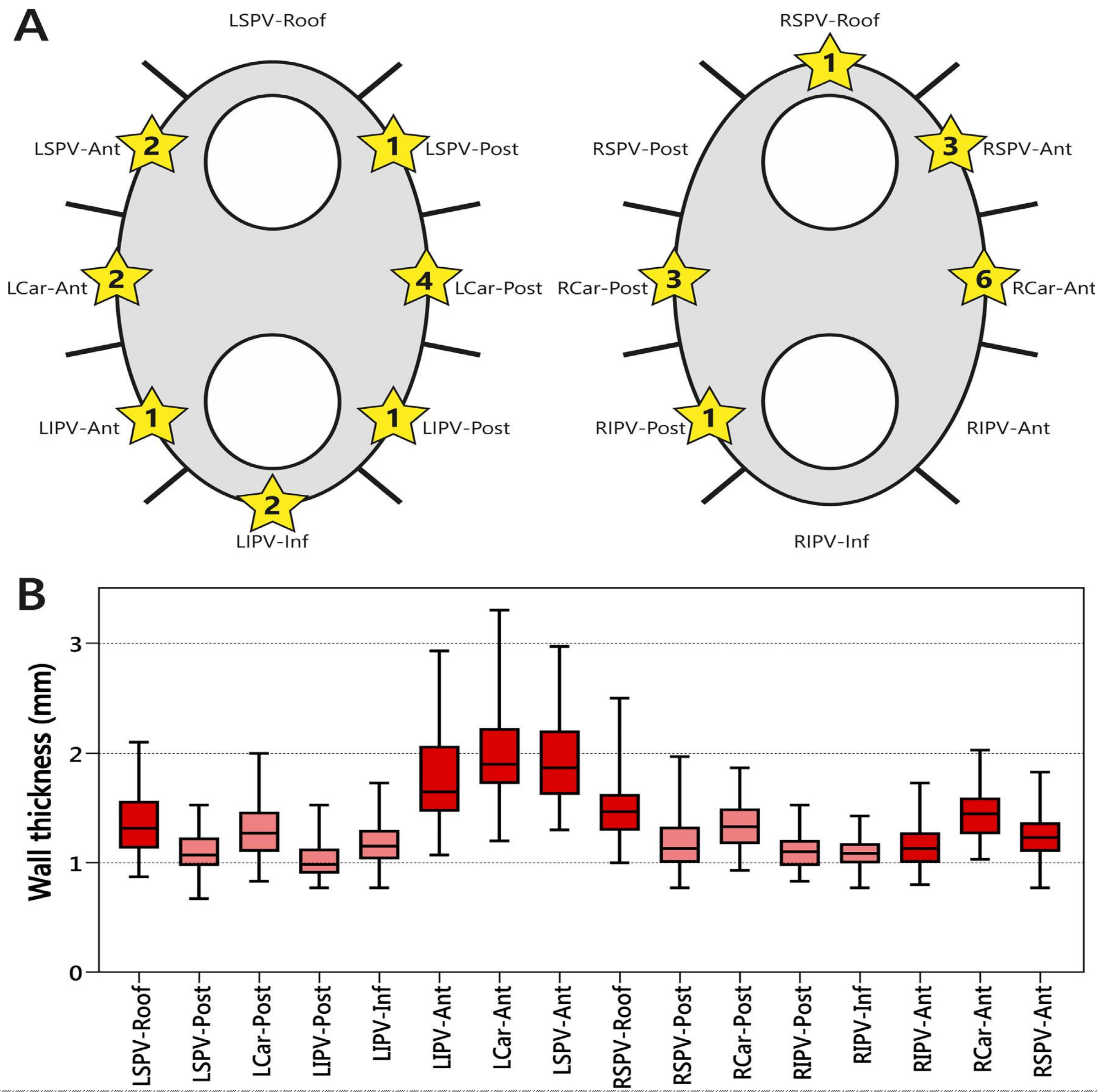

Acute reconnection and wall thickness per segment.

- ✓ Panel A: Sites of acute pulmonary vein reconnection were defined according to a 16-segment model. Numbers inside the stars indicate the total number of acute reconnections per segment.
- ✓ Panel B: Box plots showing local left atrial wall thickness per segment. Anterior/superiorsegments and posterior/inferior segments are displayed by red and pink colors, respectively.
- o Ant = anterior, Inf = inferior, LCar = left carina, LIPV = left inferior pulmonary vein,
- o LSPV = left superior pulmonary vein, Post = posterior, RCar = right carina, RIPV = right inferior pulmonary vein, RSPV = right superior pulmonary vein

Pulmonary nodule

10Expert Consensus on

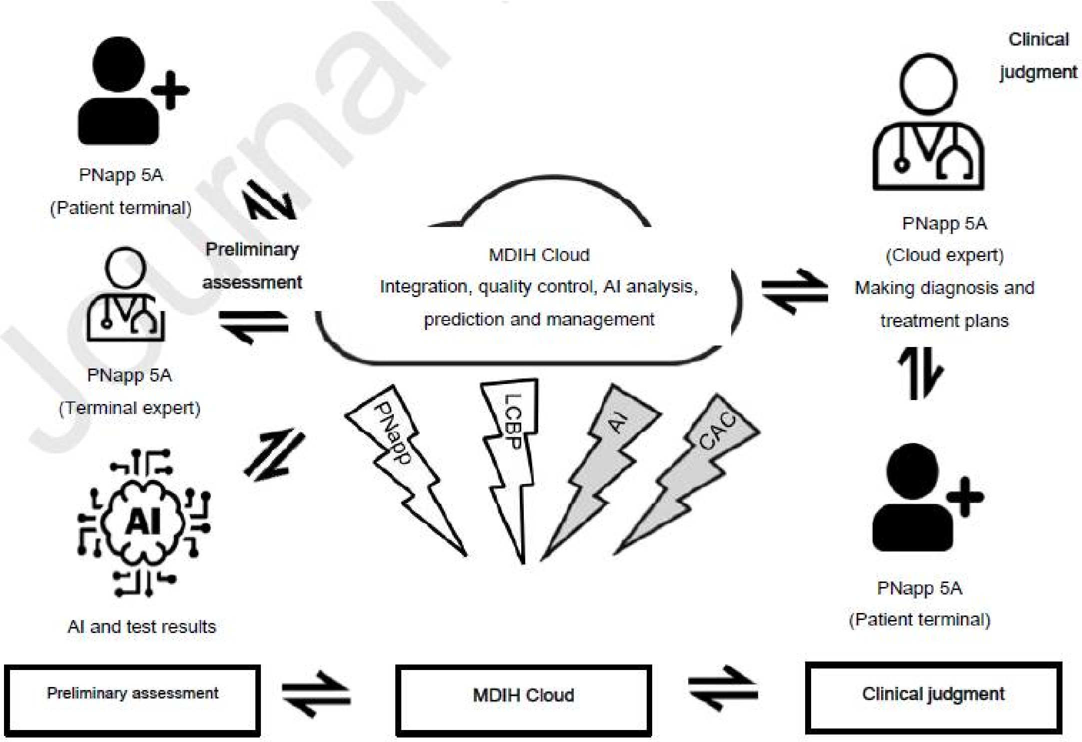

Second-read workflow:

- o Preliminary assessment and clinical judgement.
- o The communication and interaction between experts and computers can achieve assessment results with a higher accuracy.
- o MDIH: medical doctor intelligent health

10

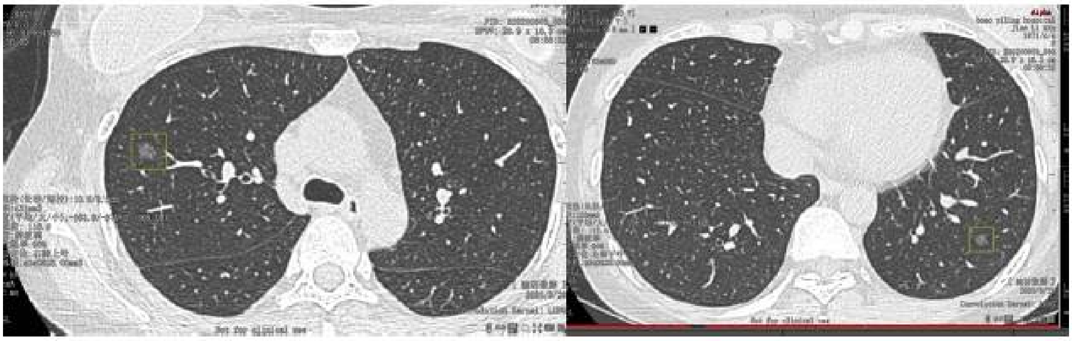

CT scan of a case with high-risk indeterminate pulmonary nodule

26

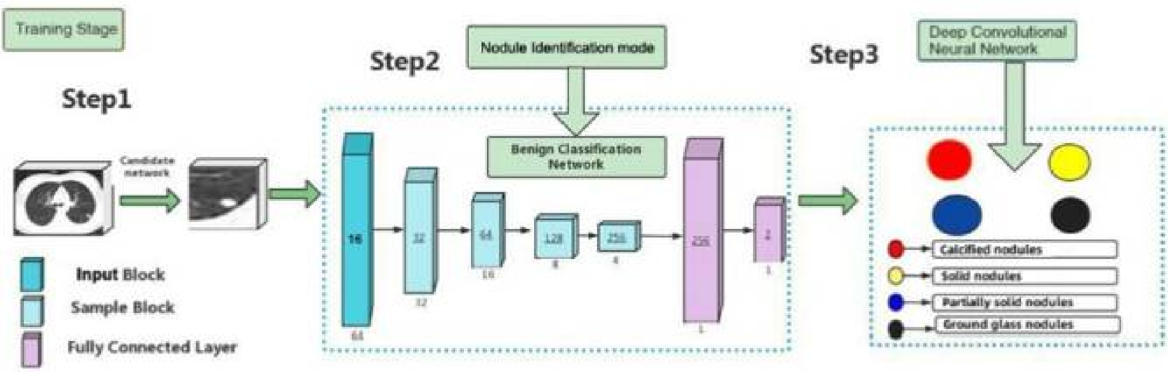

Deep convolutional neural network for assessing pulmonary nodules

26

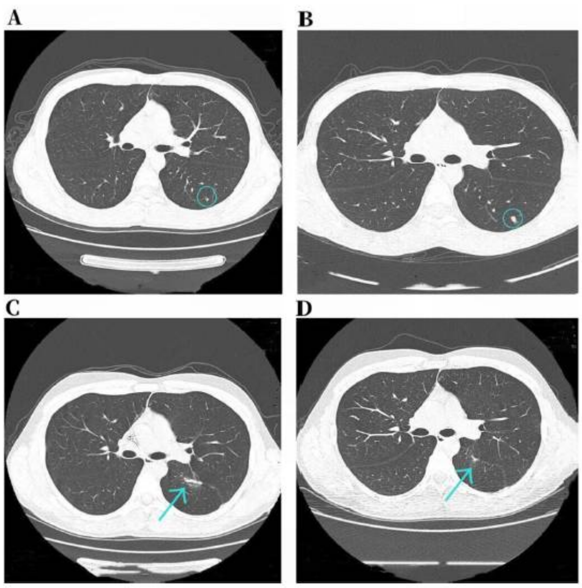

Case 1 Chest CT images (A-D).

- Artificial Intelligence-based diagnostic software showed a 3 mm calcified nodule in the Superior segment of the lower lobe (A).
- Follow up with enlarged nodules, and surgical, and postoperative follow-up images (B-D).

26

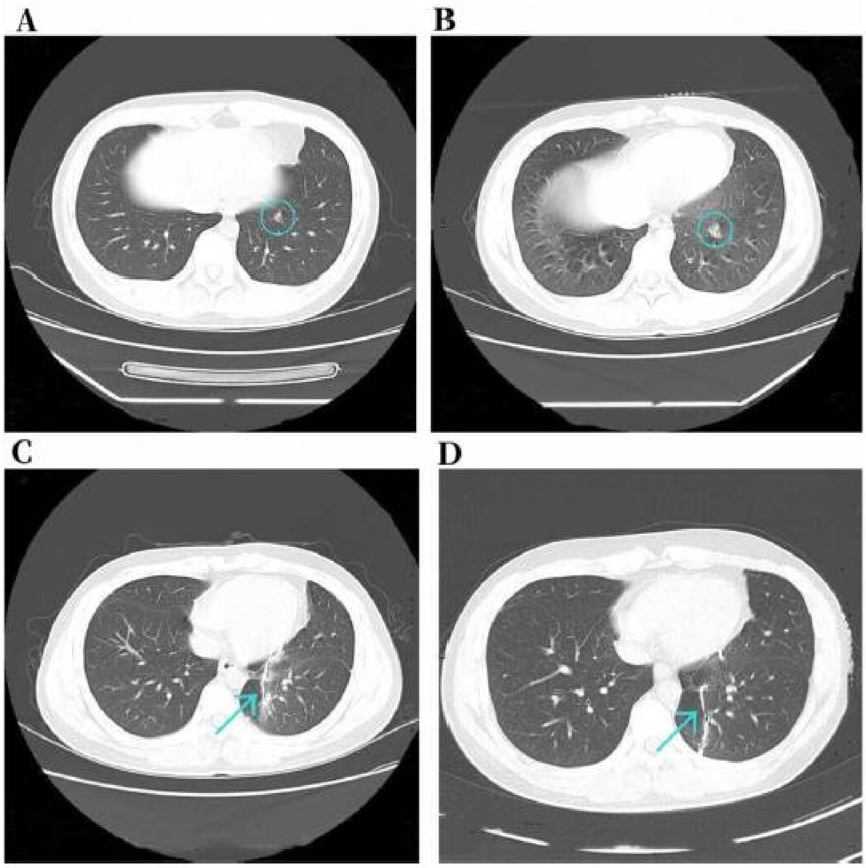

Case 2: Chest CT images (A-D).

- AI software shows a solid nodule of 4 mm in the posterior basal segment of the left lower lobe of the lung (A). single nodule is significantly enlarged on thoracoscopic surgery and postoperative follow-up images (B-D).

30

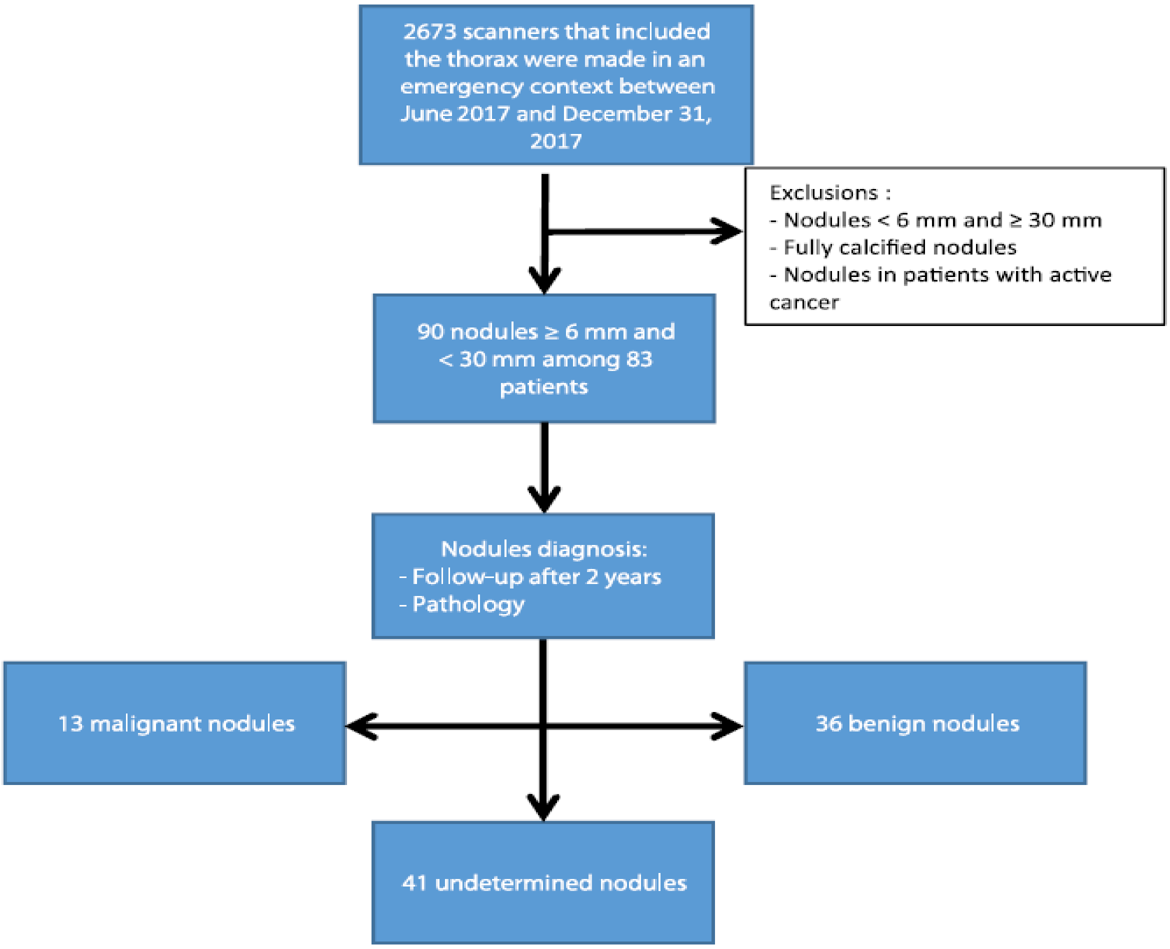

Pulmonarynodulesflowchart

30

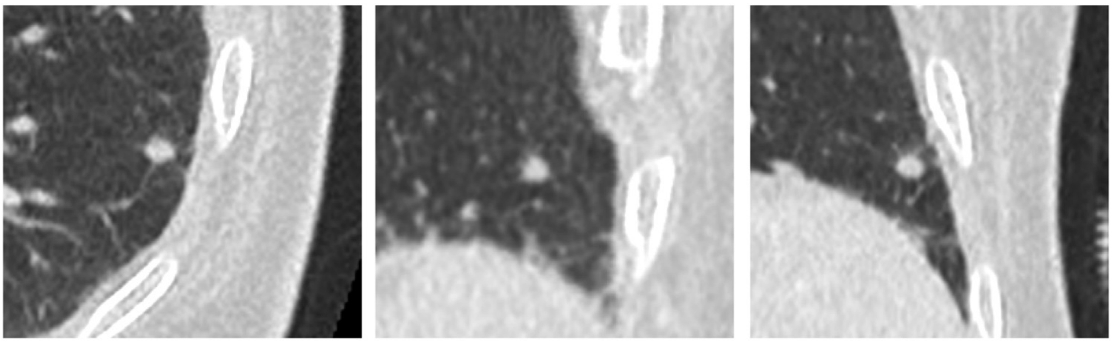

Axial Coronal Sagittal

Example of a nodule which was confirmed benign

- ✓ (stability2yearslater),which was correctly categorized as benign by AI software (AIscore=1.12) (AIscore between 50 and 75%).

30

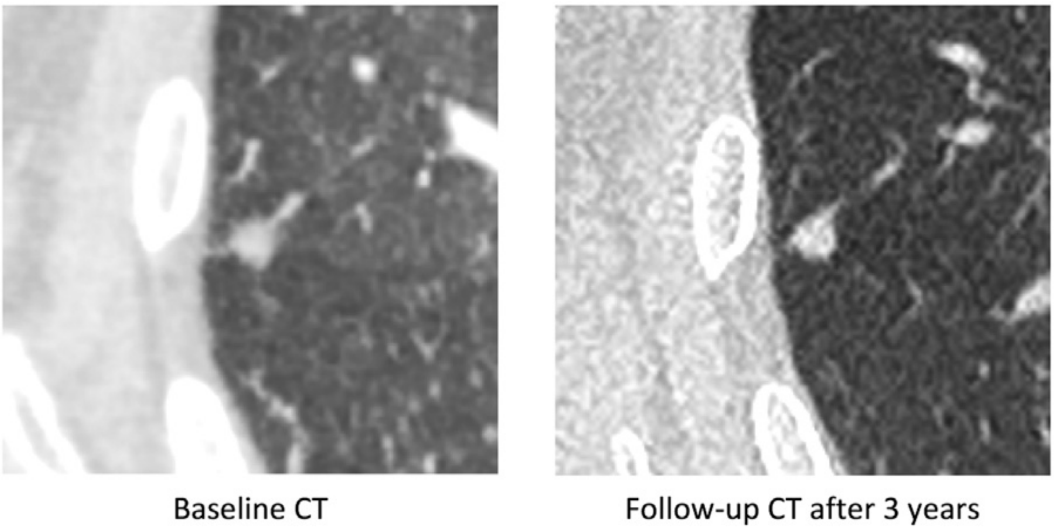

ExampleofabenignnoduleofS8mmofRLLinaxialslices,whichwassubjecttoseveralfollow-upCT(stabilityafter3years).ThenodulewasalreadycategorizedasbenignbytheAIsoftwareontheBaselinescanner(IAscore<50%).

30

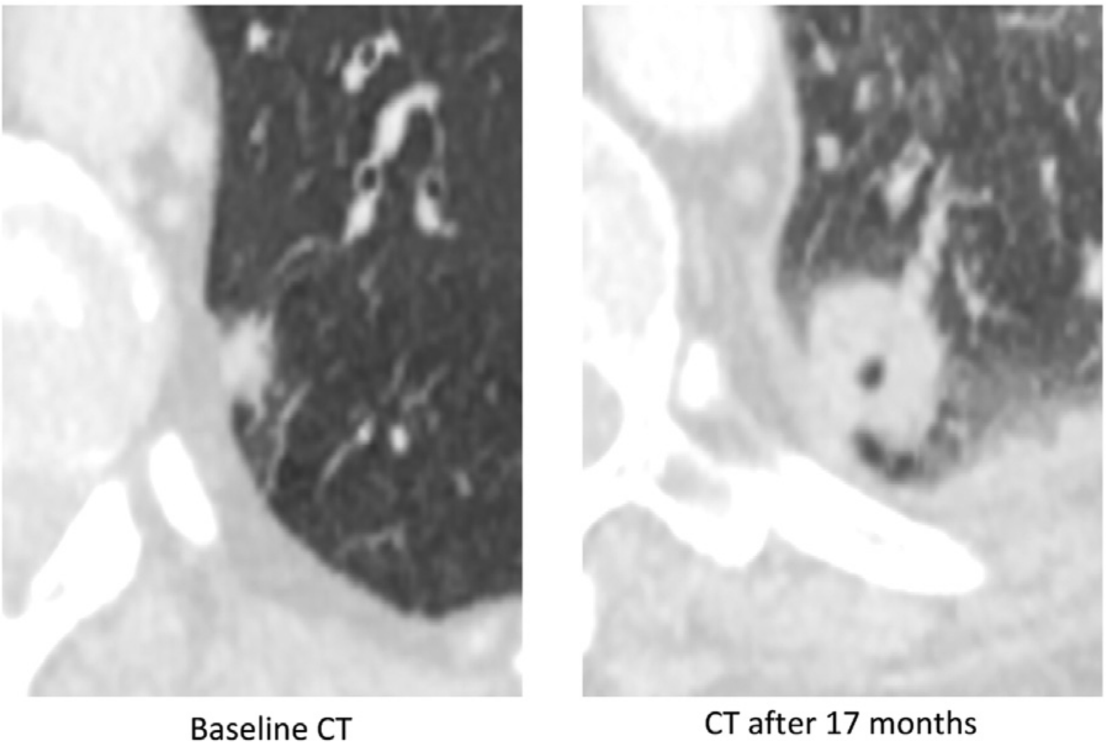

Exampleofamalignantnoduleof10mmoftheLLLinaxialslicesonthebase-linescanner.Arecommendationoffollow-upafter3monthswasmadebutwasnotimplemented.ACTscanperformed17monthslateroutofcontextforsuspectedpul-monaryembolismrevealedasignificantincreaseinthenodule,ultimatelycorrespond-ingtoanadenocarcinomaconfirmedbylungbiopsy.TheuseofAIsoftwarecouldpotentiallyhavereducedthisdiagnosticdelaybyincreas-ingtheneedforfollow-up,giventhehighAIscoreofthenoduleontheCTBaseline(IAScore=94.52)

20

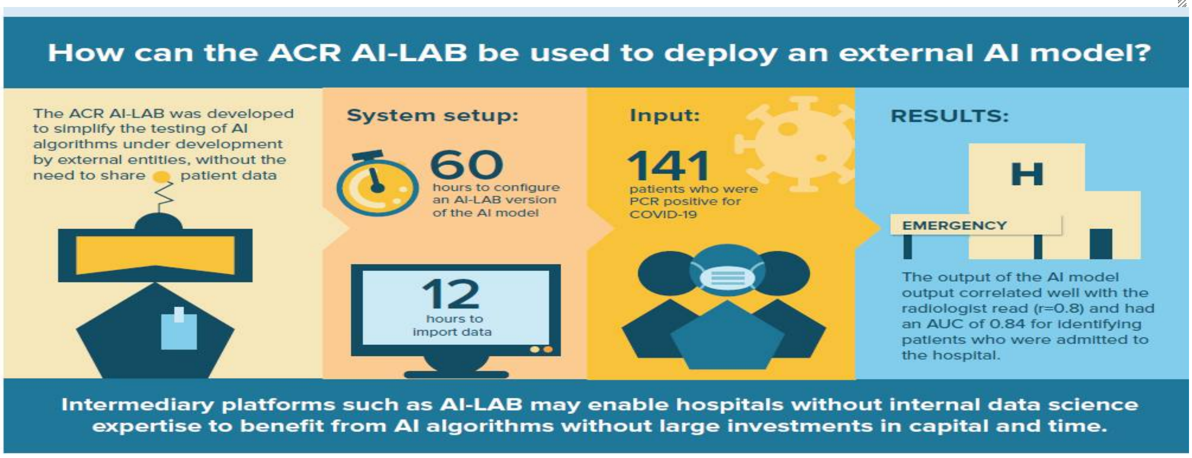

20

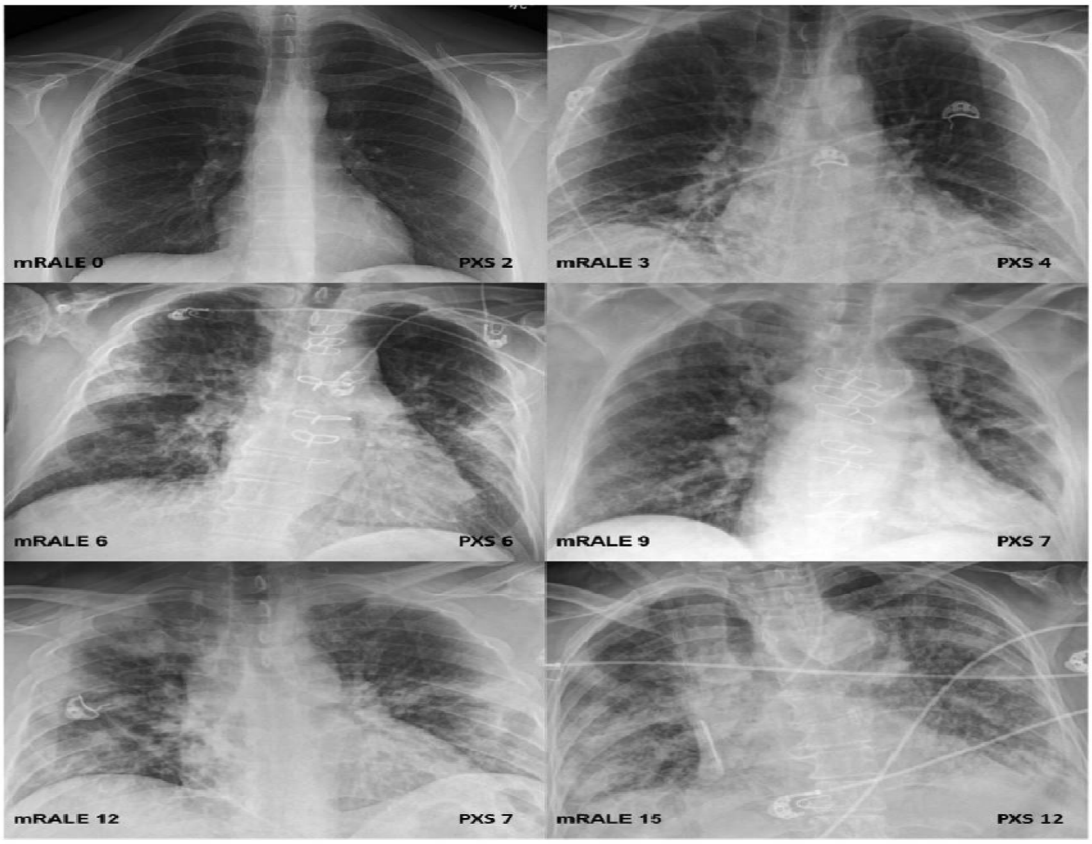

Images of modified Radiographic Assessment of Lung Edema (mRALE)
Pulmonary X-ray Severity (PXS) scores in chest radiographs of patients with COVID-19.

20

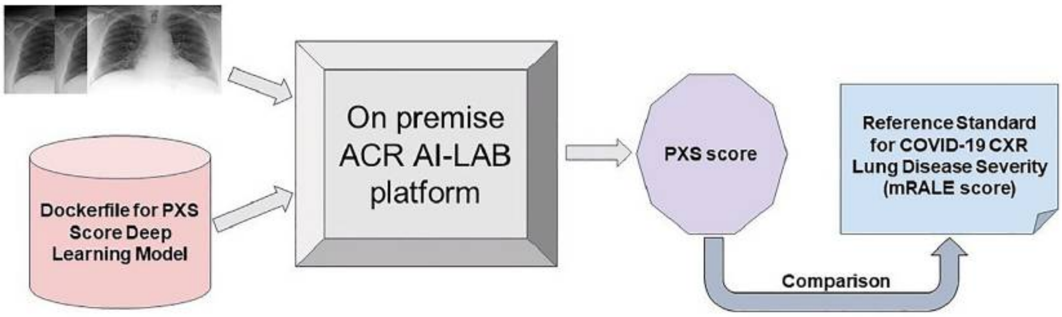

Data processing.

- CXR : Chest radiograph;
- mRALE : Modified Radiographic Assessment of Lung Edema;
- PXS : Pulmonary X-ray Severity

25

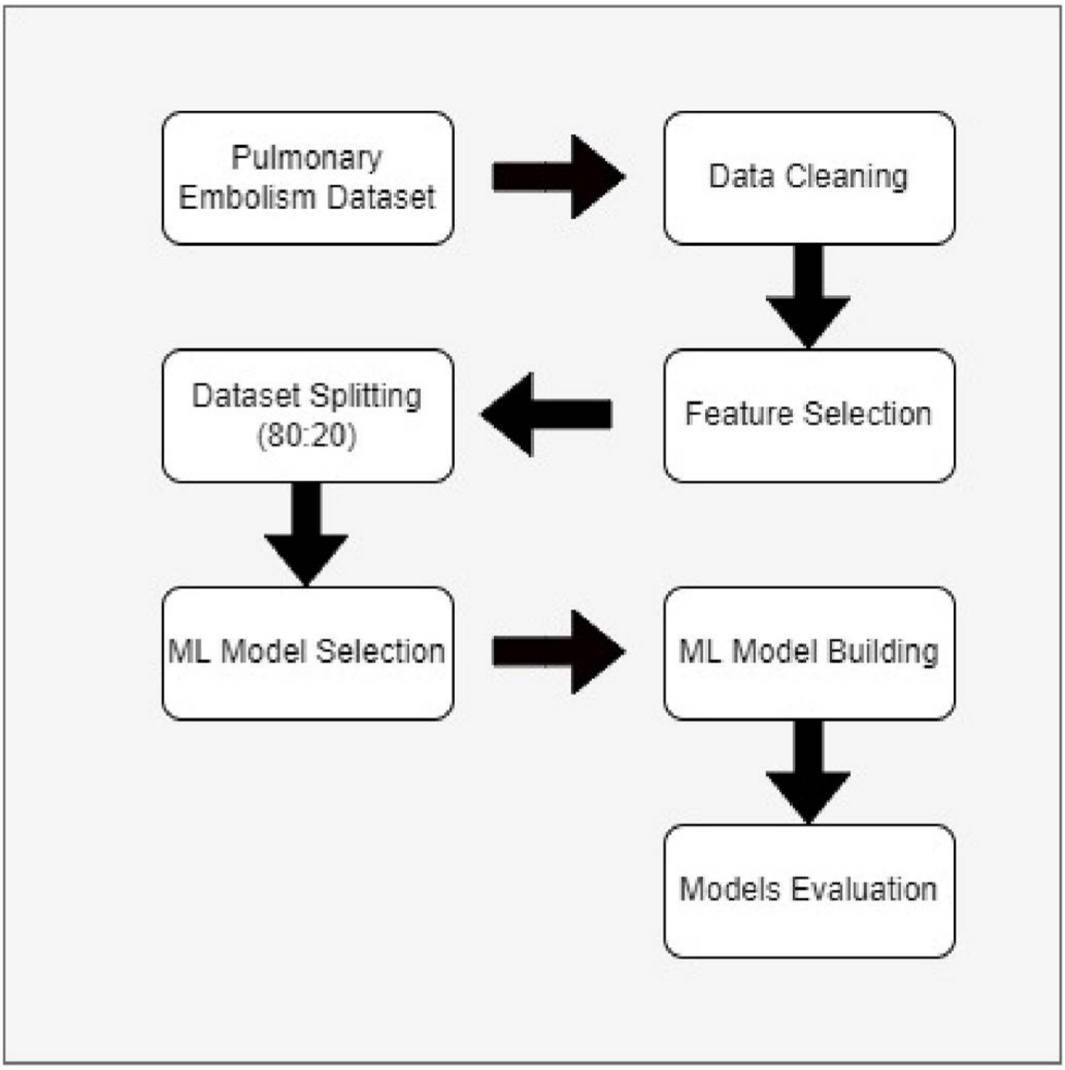

Framework of early death mortality prediction

25

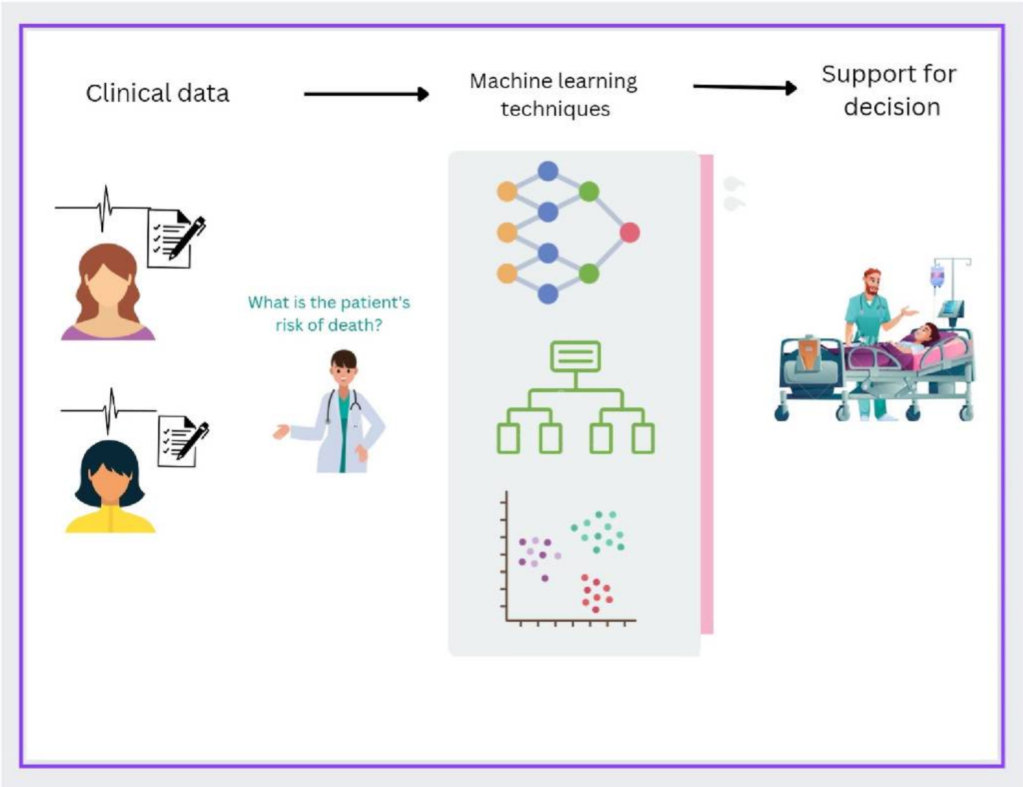

Process of converting the clinical data to decision using machinelearning.

25

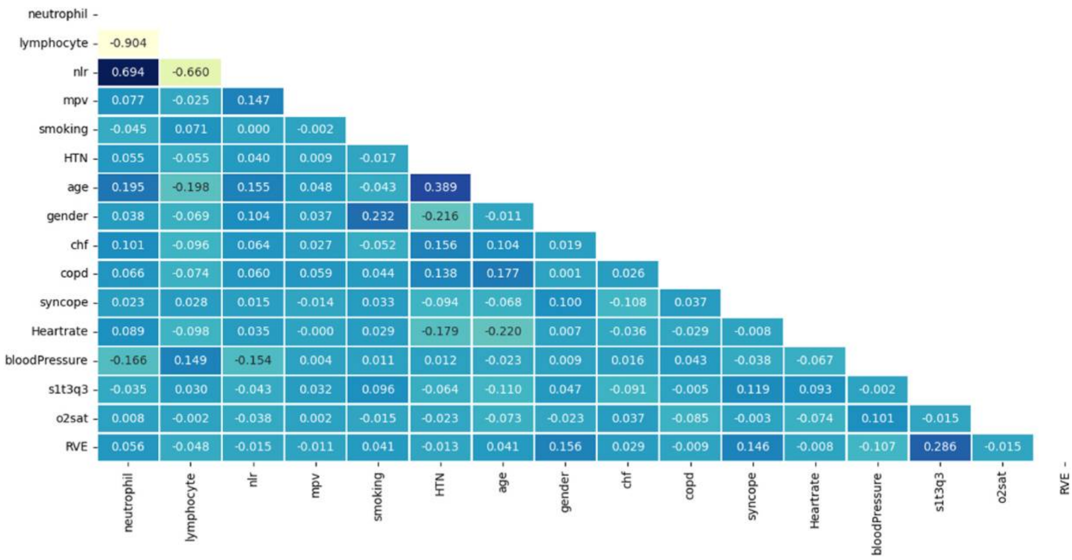

Heat-map correlation for dataset features

Pulmonary artery Hypertension

31

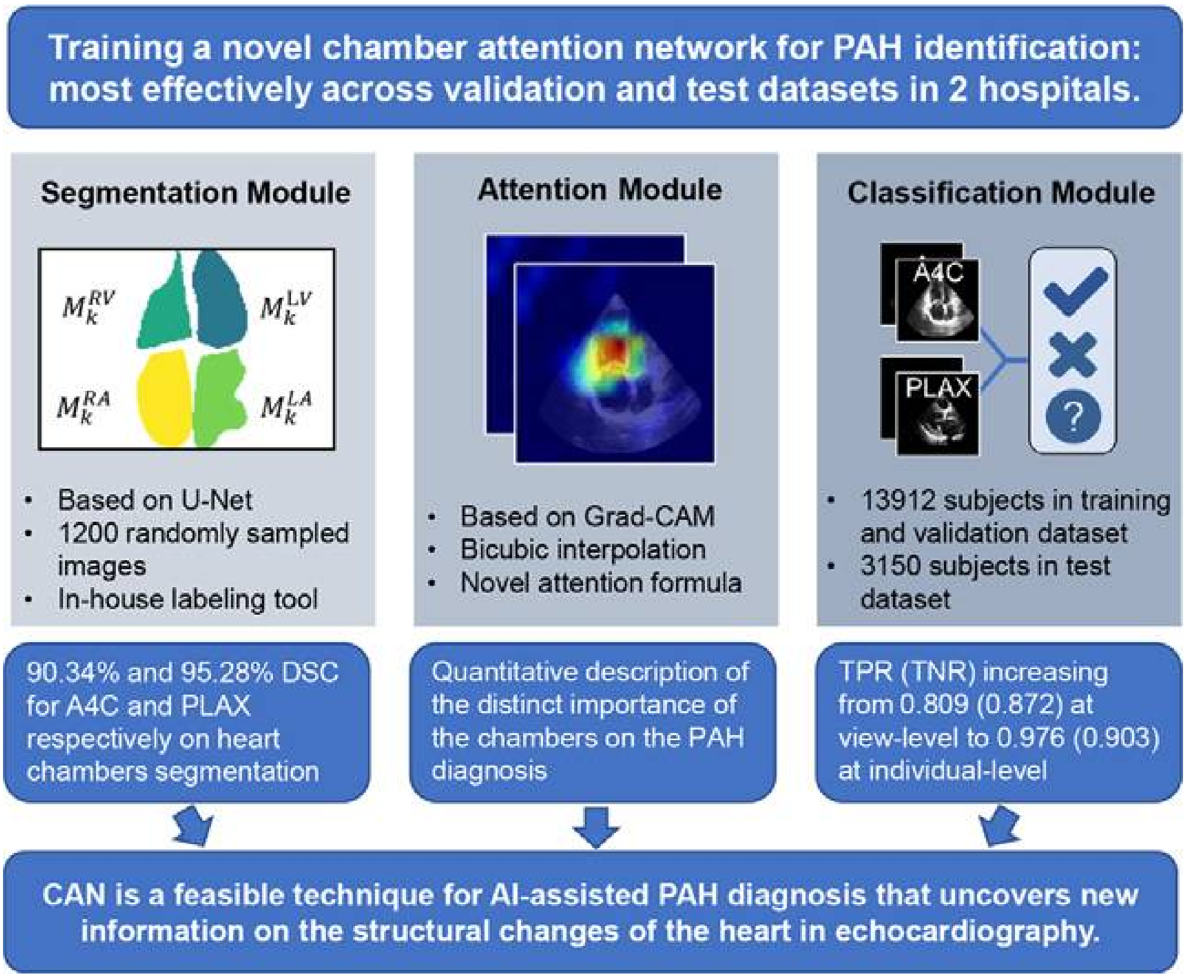

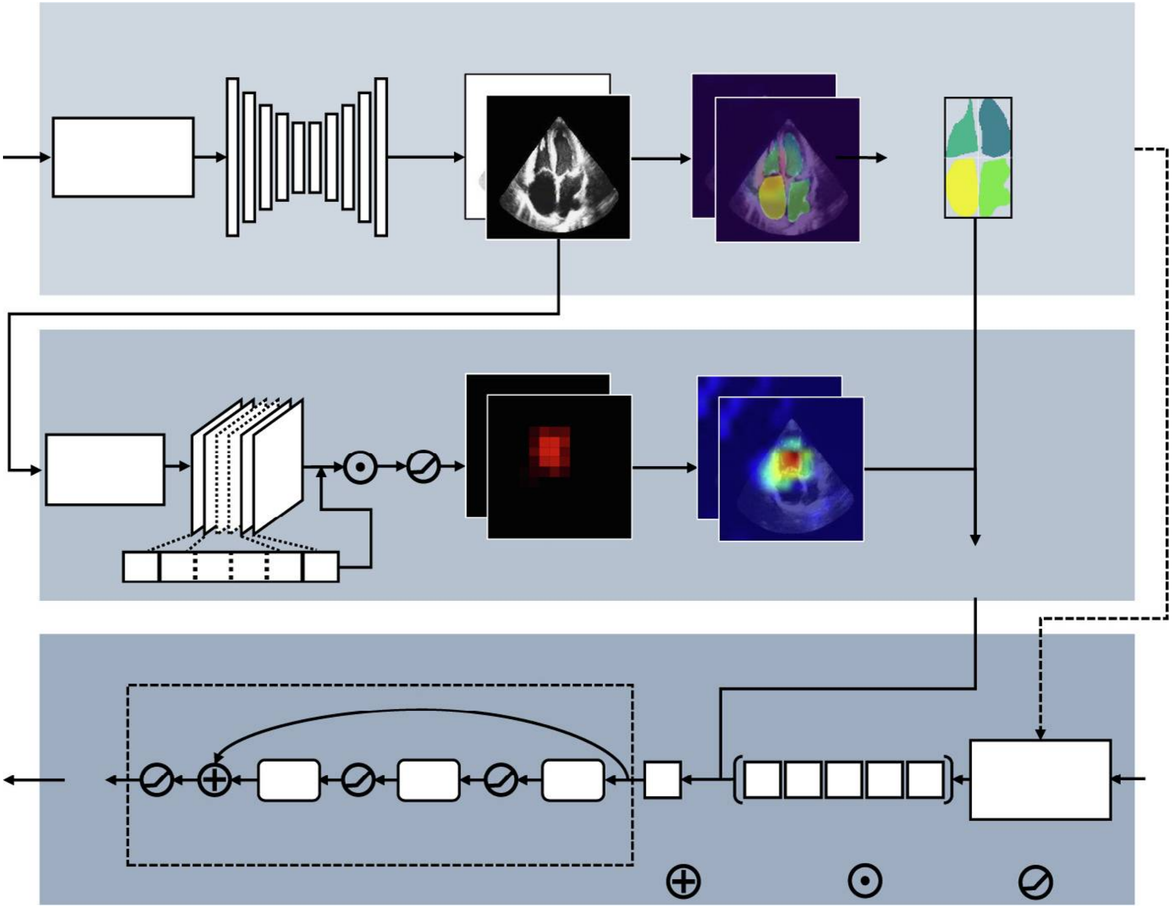

The overall framework of method

- The Segmentation Module is responsible for segmenting and positioning the cardiac chambers in the echocardiographic images.
- The Attention Module identified the key areas relevant to PAH diagnosis using Grad-CAM, which, combined with chamber locations, generates importance weights of each cardiac chamber.
- The Grad-CAM-based weights are then combined with expert scores to calculate the chamber attention vector.
- The Classification Module reconstructed the echocardiographic images based on the chamber attention vector and utilizes ResNet50 for PAH diagnosis. In the context, we denoted the k-th segmented cardiac image of a certain view as matrixeI k, with its complement matrix denoted as Ik.
  - Additionally, MRV
  - k ;MLV
  - k ;MRA
  - k and MLA
  - k represents the mask matrices of the corresponding chambers. T
- The gradient weights of the C-th channel of the last convolutional layer (layer L) of the convolutional network are denoted as wLC . The resized heatmap is denoted as Hk, and the reconstructed image is represented by Rk. The functions f 1; f 2, and f 3 correspond to Eqs. (1), (4), and the voting strategy

31

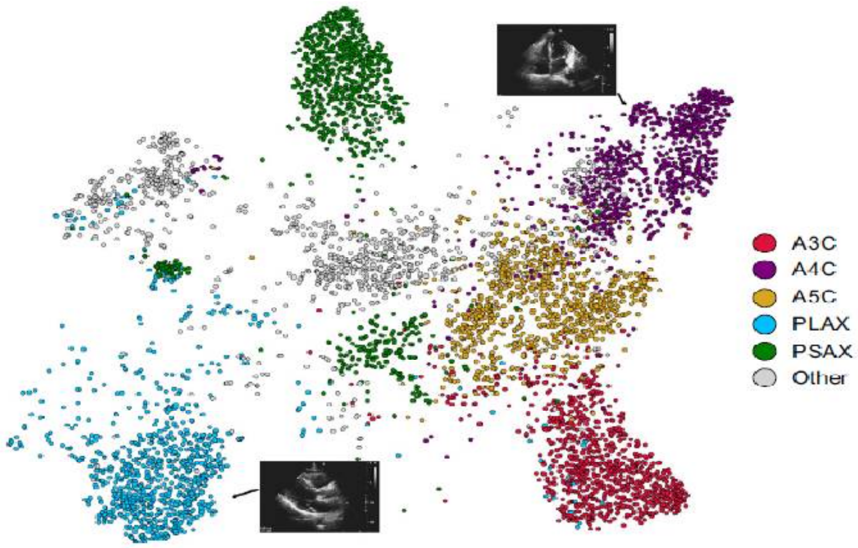

T-SNE visualization of view classification.

- ✓ Each dot in the figure represents an echocardiography image, which is the 2-dimensional space representation of the top layer features of the convolutional neural network.
- ✓ Different colors represent different viewpoint categories. It illustrates successful grouping of test images corresponding to 6 different echocardiographic views.
- ✓ Abbreviations: A4C apical 4 chamber, PLAX parasternal long axis, PSAX parasternal short axis basal, A3C apical 3 chamber, and A5C apical 5 chamber.

31

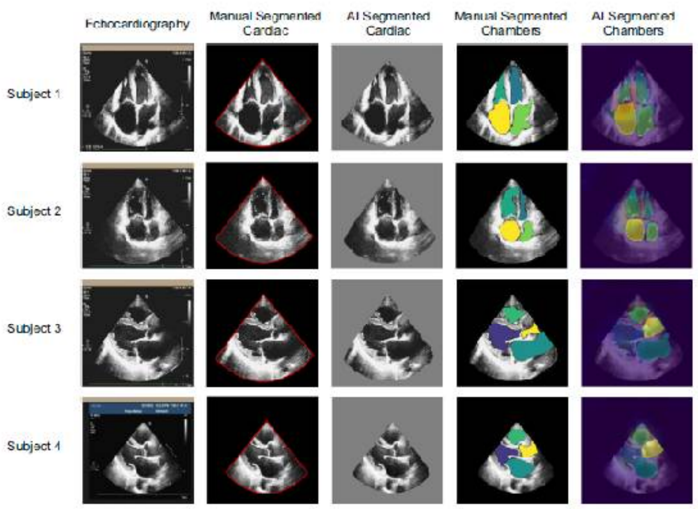

Manual and AI-based segmentation of cardiac regions and chambers in echocardiographic images of four subjects.

- ✓ The first two subjects are A4C view samples while the latter two are PLAX.
- ✓ The original echocardiographic images are showed in the first column.
- ✓ The second and third columns are the manual and AI segmented cardiac regions respectively.
- ✓ The fourth and fifth columns show the manual and AI segmented chambers

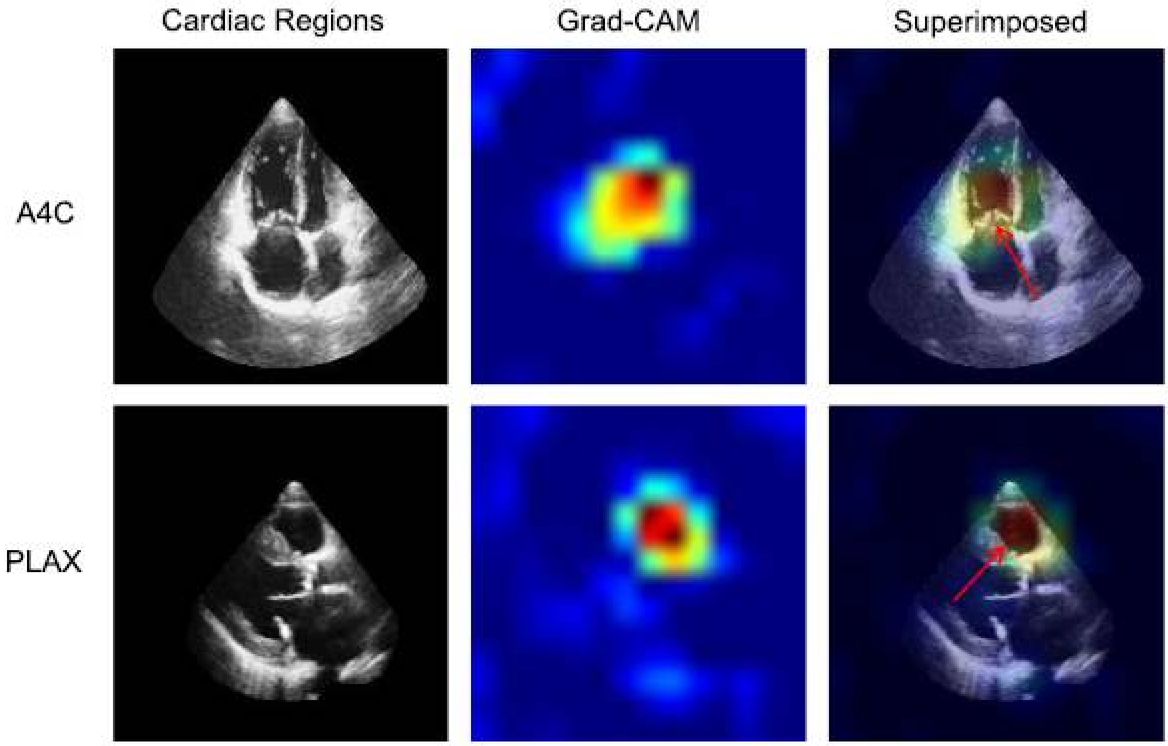

(a) Heat map

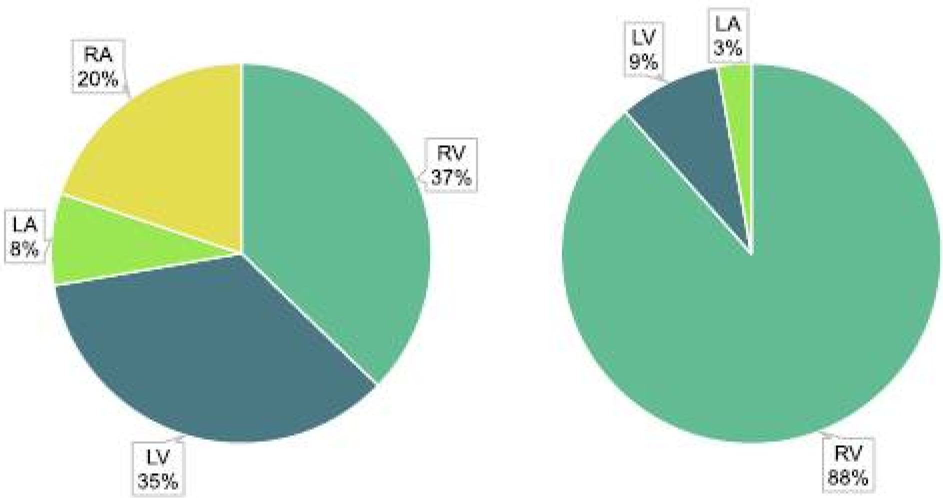

(b) A4C (c) PLAX

(a) Visualization of the attention mechanism based on Grad-CAM to differentiate PAH from normal in cardiac regions.
The highlighted areas indicated by red arrows are discriminative features for identification of PAH. The Grad-CAM of A4C and PLAX viewpoints are shown in the top and bottom of the figure.
(b) (c) The proportion of thenumber of times the cardiac chamber was covered by the Grad-CAM heat map in A4C and PLAX viewpoints. Different colors in the figure represent different chambers

31

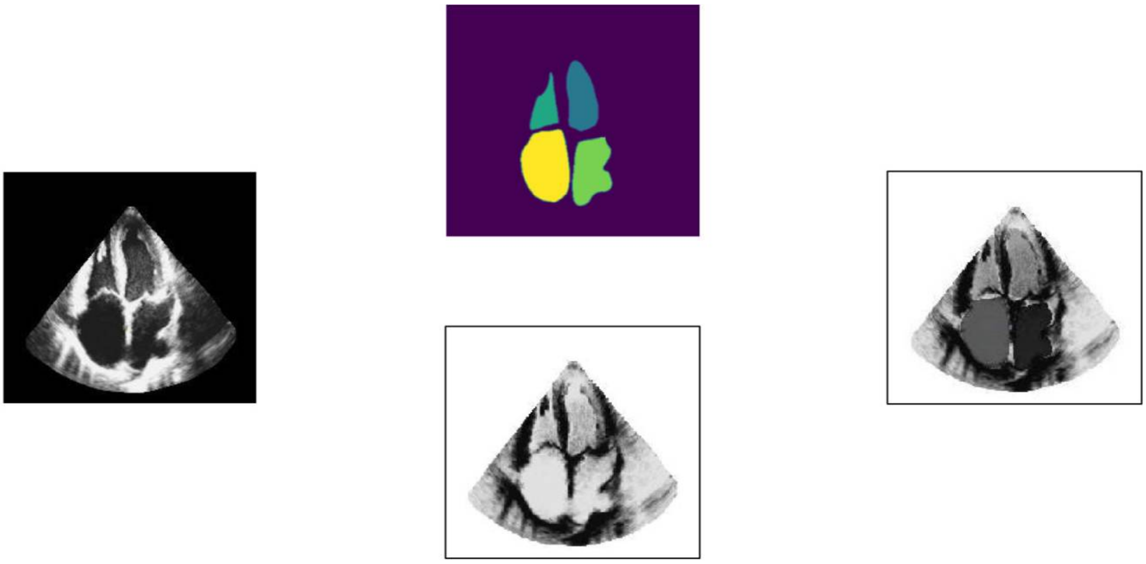

Schematic of the process for obtaining the reconstituted Rk

31

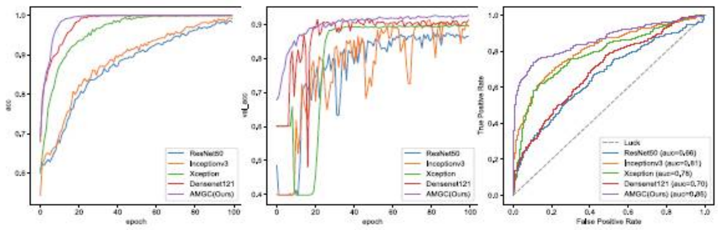

(a) Training accuracy for A4C (b) Validation accuracy for A4C (c) ROC curves for test A4C

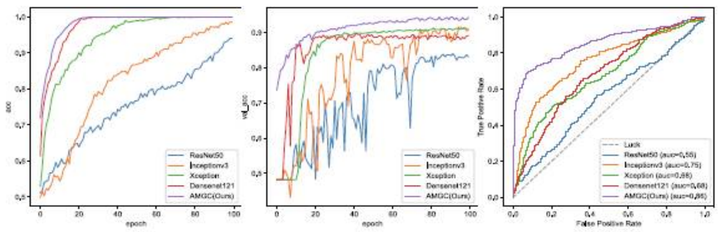

(d) Training accuracy for PLAX (e) Validation accuracy for PLAX (f) ROC curves for test PLAX

Training and testing performance of five models

- ✓ ResNet-50, Inceptionv3, Xception, DenseNet-121, and the proposed CAN
  - o for PAH identification in A4C and PLAX viewpoints separately.
- (a)(b)(d)(e) For two separate viewpoints, the training and validation accuracy of five models on the internal dataset is plotted vs number of epochs separately.
- Different models are represented by different colors.
  - ? The CAN model converges faster and
  - ? has higher accuracy than other models in both viewpoints.
- (c)(f) ROCcurves of five models in two separate viewpoints on the external dataset

18

Flow Diagram Illustrating Identification and Selection of Patients in AI HFpEF Model Development and Testing

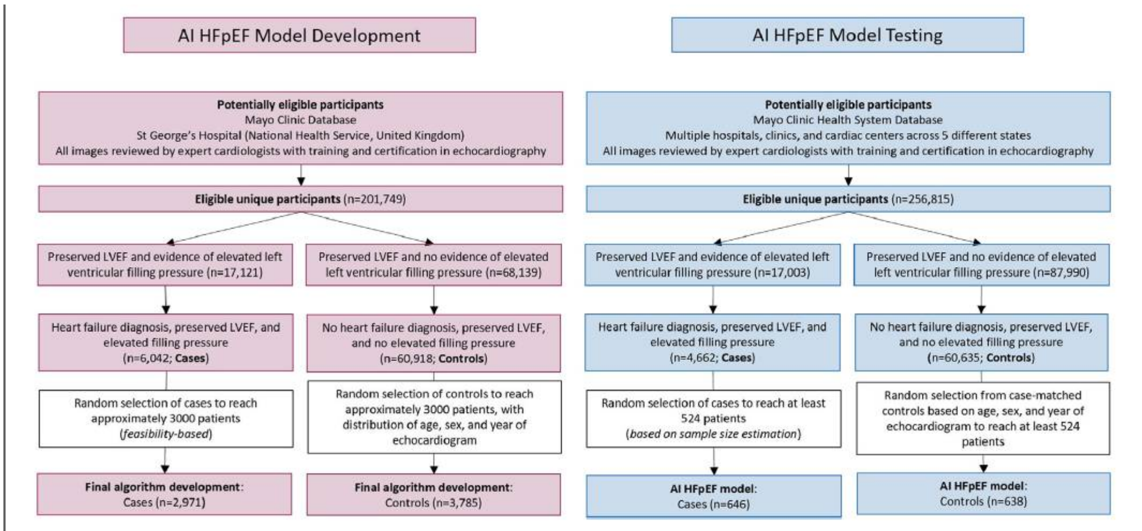

AI = artificial intelligence; HFpEF = heart failure with preserved ejection fraction; LVEF = left ventricular ejection fraction.

17

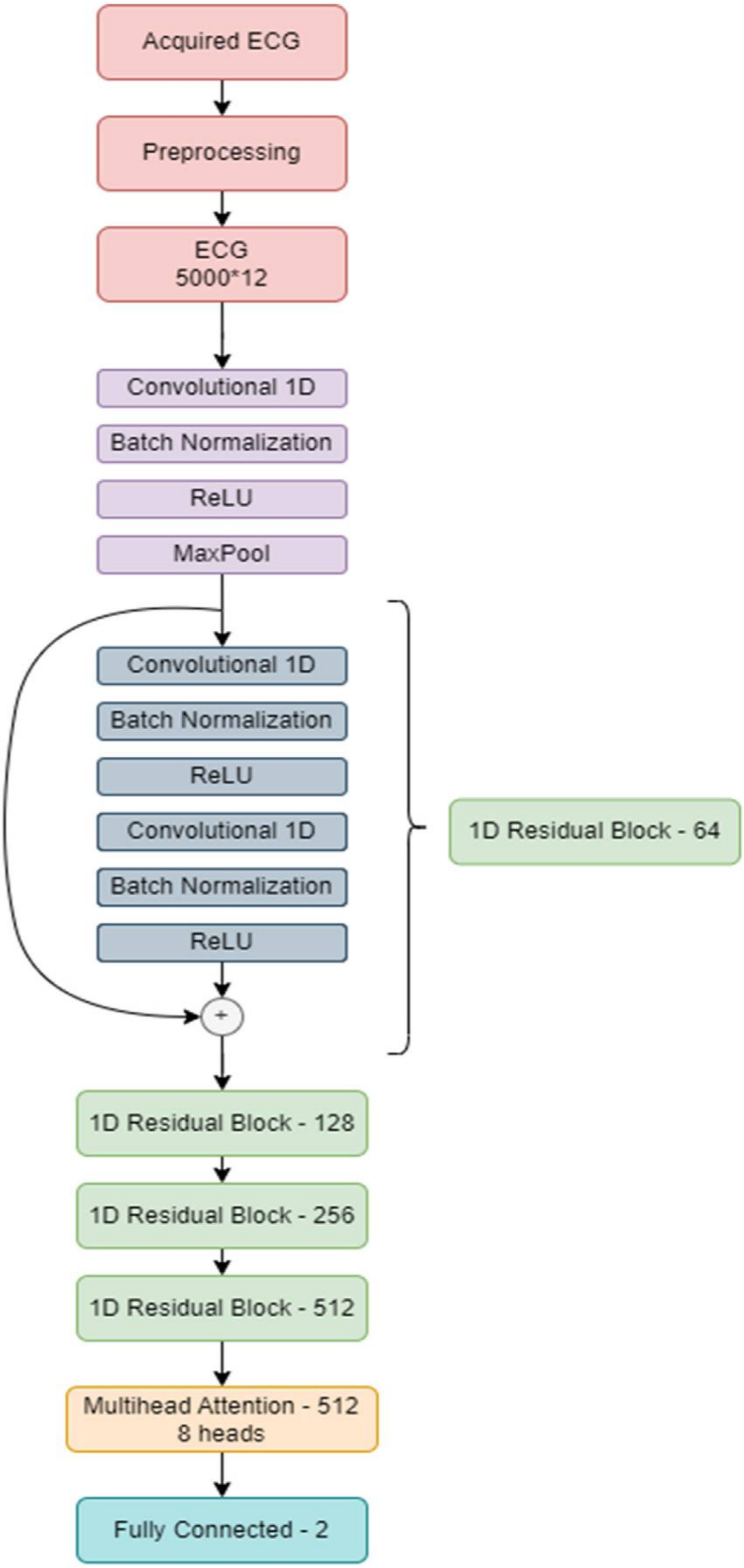

Schematic representation of the neural networkarchitecture and its different layers

8

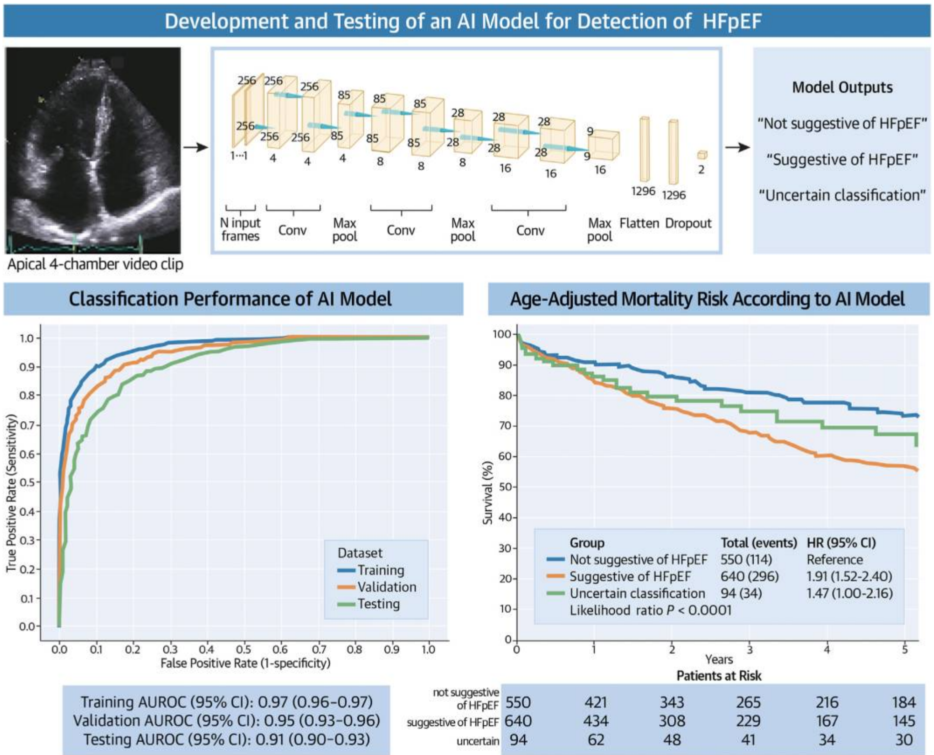

A 3-D CNN (middle) to detect heart failure with preserved ejection fraction using only apical 4-chamber video clips.

- ✓ Discrimination performance was excellent (AUROC; bottom left), and
- ✓ Age-adjusted risk of mortality was higher when patients received from the model a diagnostic output suggestive of heart failure with preserved ejection fraction compared to a diagnostic output not suggestive of heart failure with preserved ejection fraction (bottom right).
- o AI : artificial intelligence; AUROC : area under receiver-operating characteristic curve; HFpEF : heartfailure with preserved ejection fraction

18

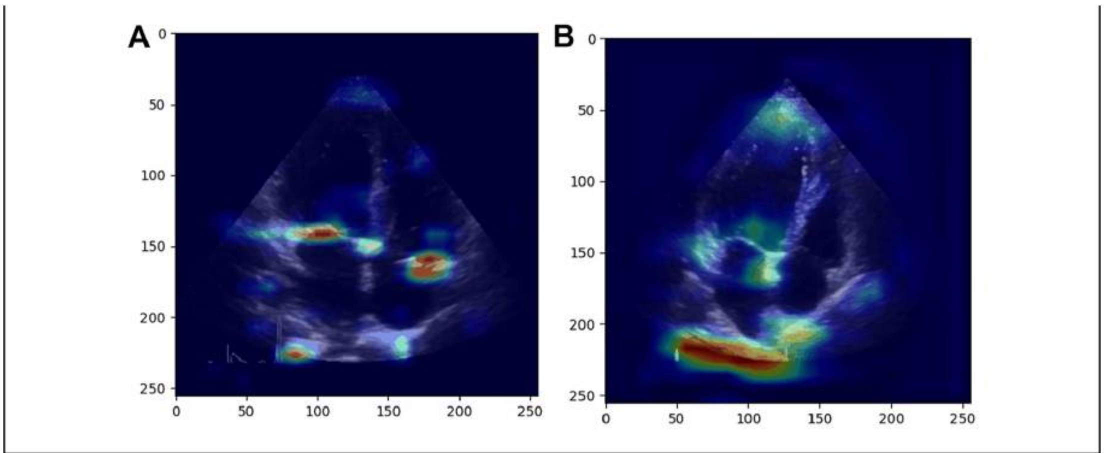

Grad-CAM for correctly **(A)** and incorrectly classified **(B)** patient. Grad-CAM = gradient-weighted class activation mapping.

Grad-CAM

18

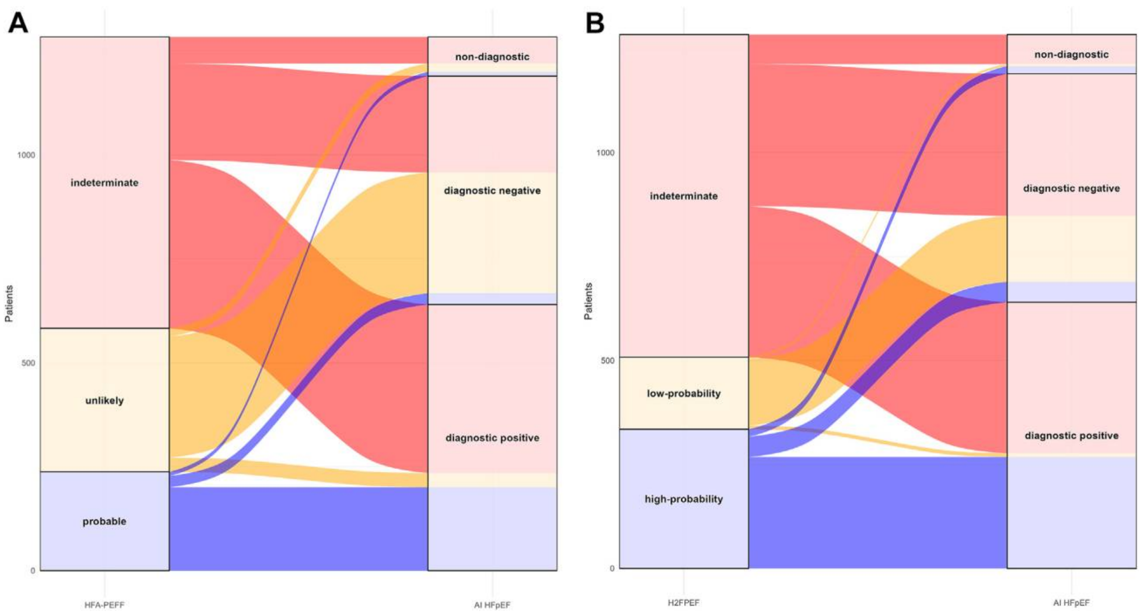

Patients in the independent testing data set

- ✓ Given a categorical score based on relevant functional and morphological echocardiographic, and biomarker parameters.
- ✓ Patients were categorized as unlikely (0 or 1), indeterminate (2-4), or probable (5-6) likelihood of heart failure with preserved ejection fraction for the Heart Failure Association-Pretest Assessment
- ✓ Echocardiographic and Natriuretic Peptide Score, Functional Testing, and Final Etiology (HFA-PEFF) score (A), and
- ✓ Lowprobability (0 or 1), indeterminate (2-5), or high-probability (6-9) of heart failure with preserved ejection fraction for the Heavy, Hypertensive, Atrial Fibrillation, Pulmonary Hypertension, Elder, and Filling Pressure (H2FPEF) score (B).
- o AI : artificial intelligence; HFpEF : heart failure with preserved ejection fraction

FIGURE 1 Flowchart of the Selection Process for the Internal Dataset

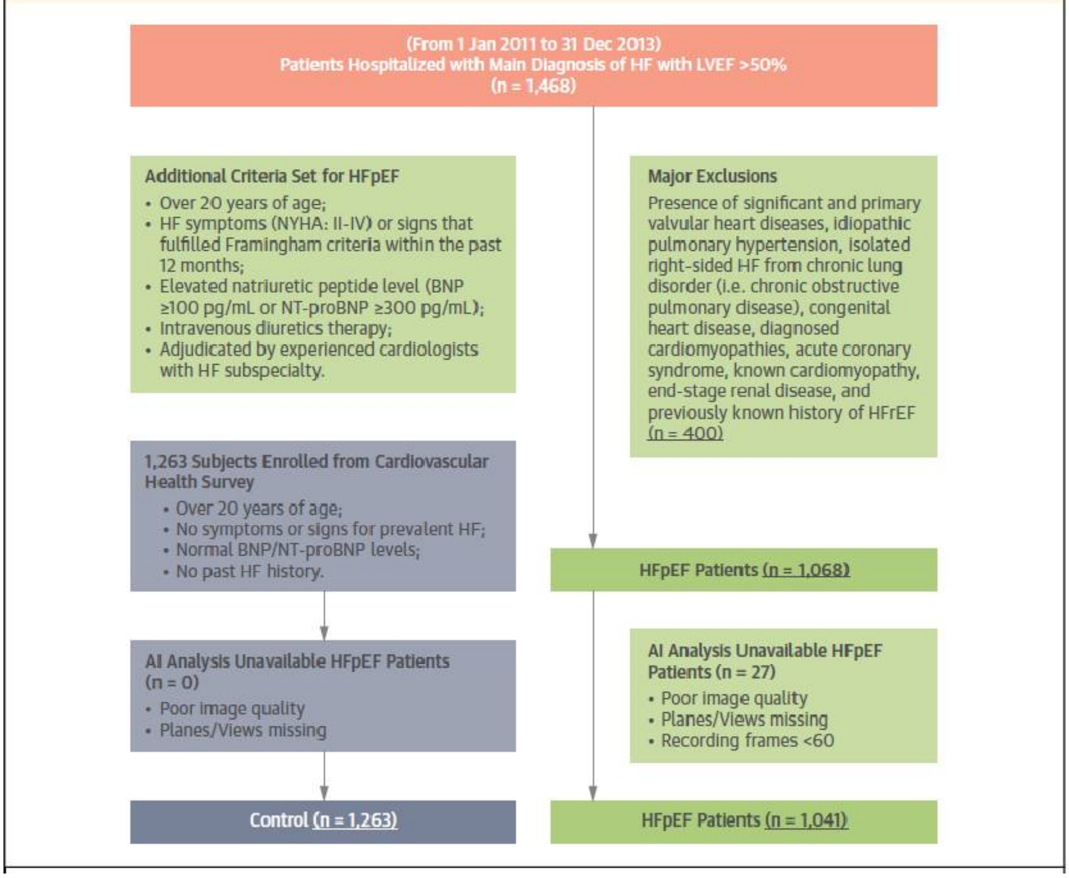

The internal data set included 1,263 asymptomatic individuals and 1,468 patients with heart failure with preserved ejection fraction (HFpEF). After data selection and exclusion, the final internal data set included 1,263 individuals without HFpEF with normal left ventricular ejection fractions (LVEFs) (>50%) as the control group and 1,041 patients with HFpEF. BNP : brain natriuretic peptide; HF : heart failure; HFrEF : heart failure with reduced ejection fraction; Nt-proBNP : N-terminal pro–brain natriuretic peptide; NYHA : New York Heart Association functional class.

34

Step-by-Step Procedures for Image Preprocessing and Segmentation, Value Extraction, and 1D CNN Model Prediction

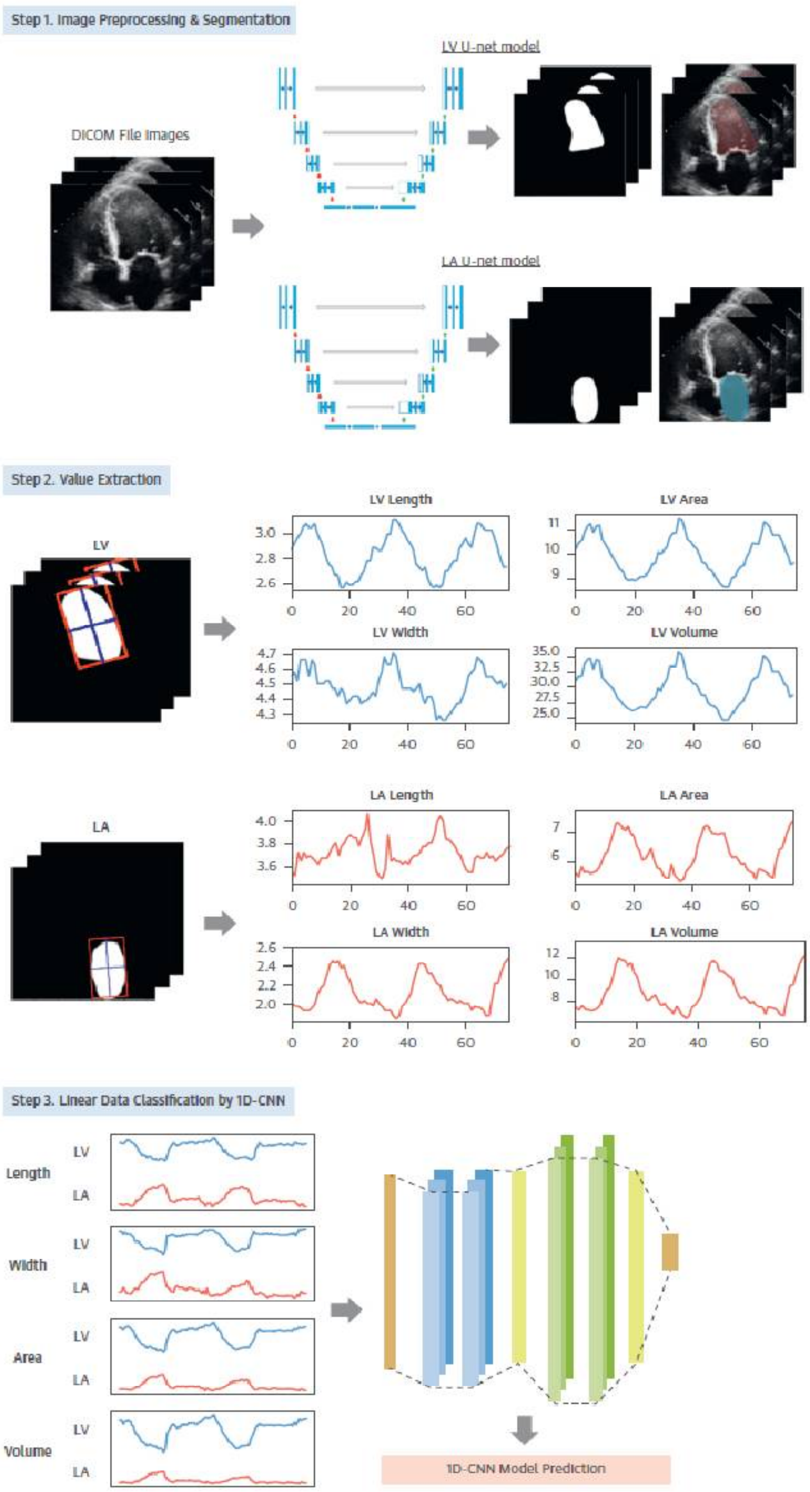

Each dynamic left ventricular (LV) and left atrial (LA) length, width, volume, and area data (60 frames) were extracted from the U-net
prediction images. These linear signals can be trained for model prediction by a 1-dimensional (1D) convolutional neural network (CNN).
DICOM : Digital Imaging and Communications in Medicine

34

Training and Testing Dataset Used for U-Net and 1D CNN Model

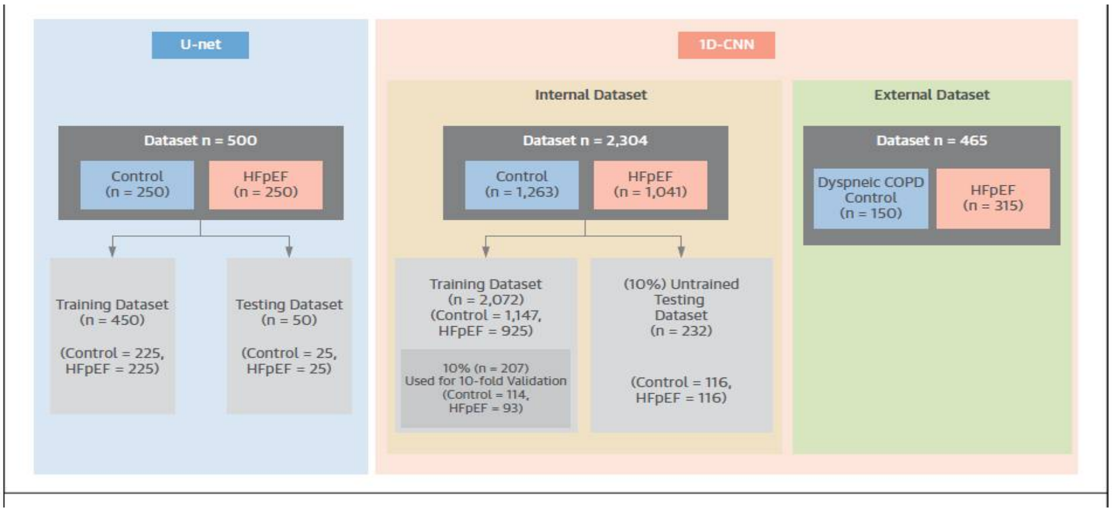

The internal data set for 1D CNN comprised patients with HFpEF and asymptomatic individuals, with the external data set further validated to distinguish patients with HFpEF from those with dyspnea and chronic obstructive pulmonary disease (COPD). Abbreviations as in Figures 1 and 2.

34

Schematic Illustration of Typical Intrabeat Dynamic LV Area Changes in Asymptomatic Control Subjects, Patients With COPD, and Patients With HFpEF

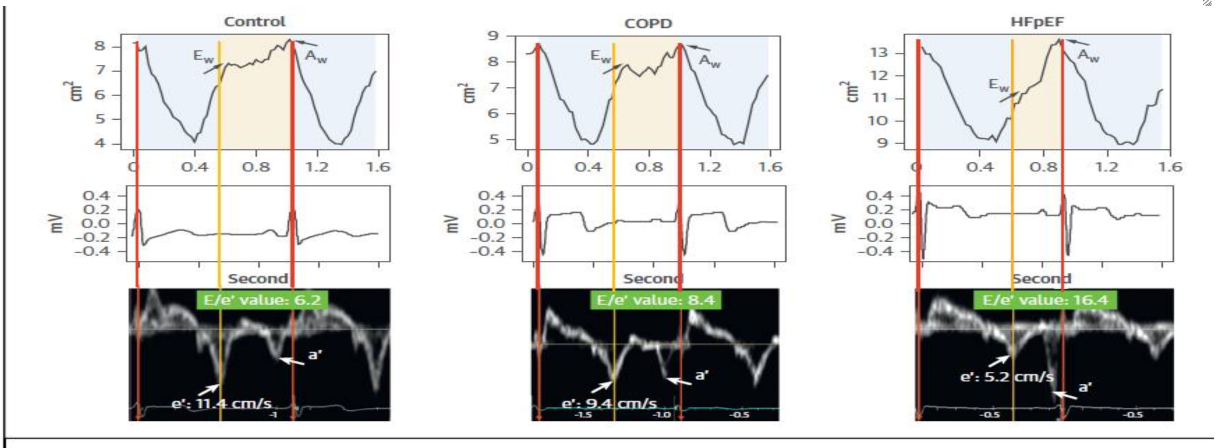

Chronologically matched cardiac phase–specific (gated using both electrocardiography and mechanical events) waveform showing impaired diastolic mechanics and delayed relaxation in HFpEF, which likely result in sharper diastolic waveform compared with control and COPD groups. Red and yellow lines indicate end-diastolic and peak e0 time point, respectively. Intrabeat dynamics Ew and Aw correspond to e0 and a0 time points, respectively. Abbreviations as in Figure 1 and 3.

34

Intrabeat Dynamic Area Changes in the Control and HFpEF Subgroups

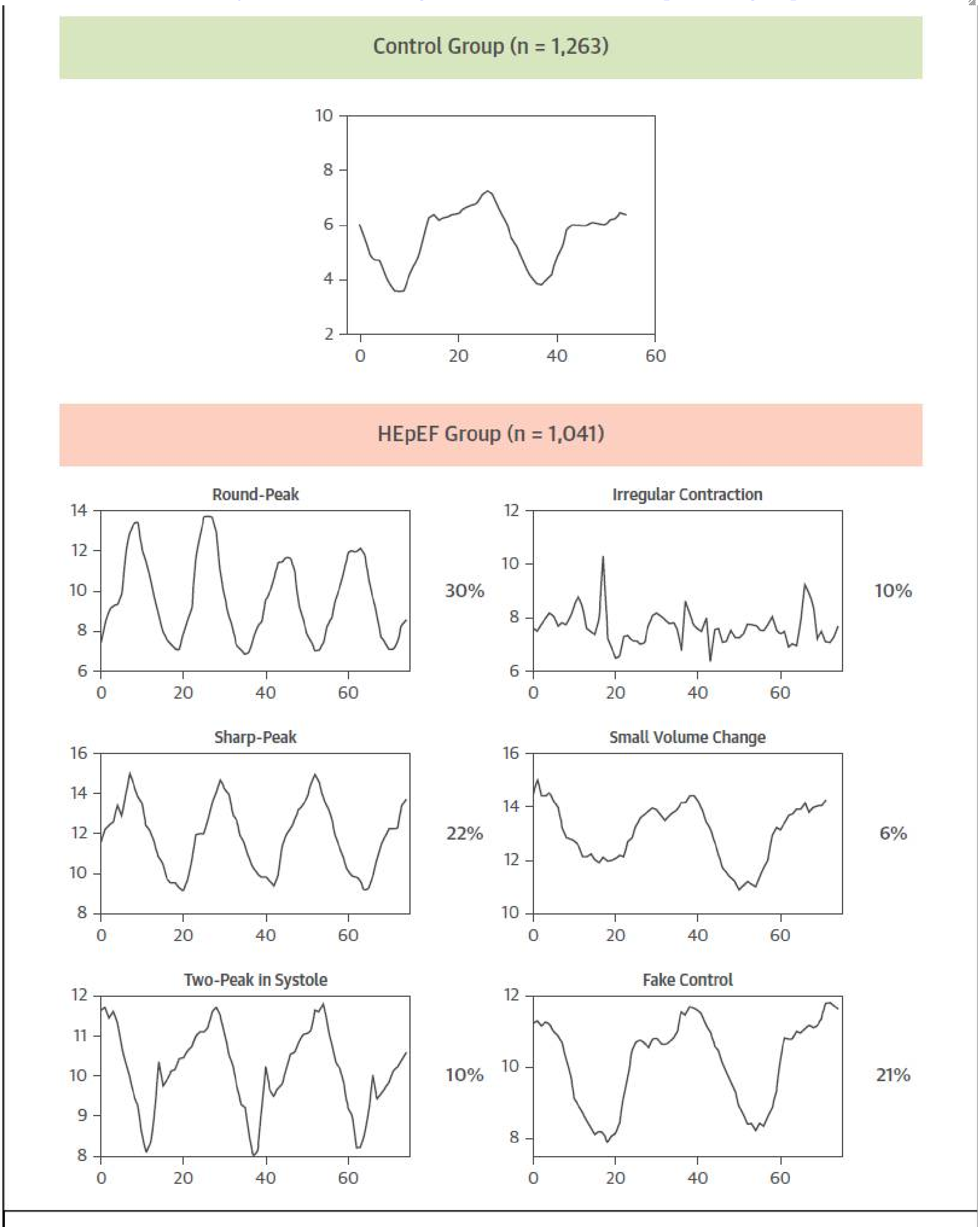

Patients with heart failure with preserved ejection fraction (HFpEF) may exhibit different types of specific dynamic left ventricular area changes during systolic-diastolic cycles

34

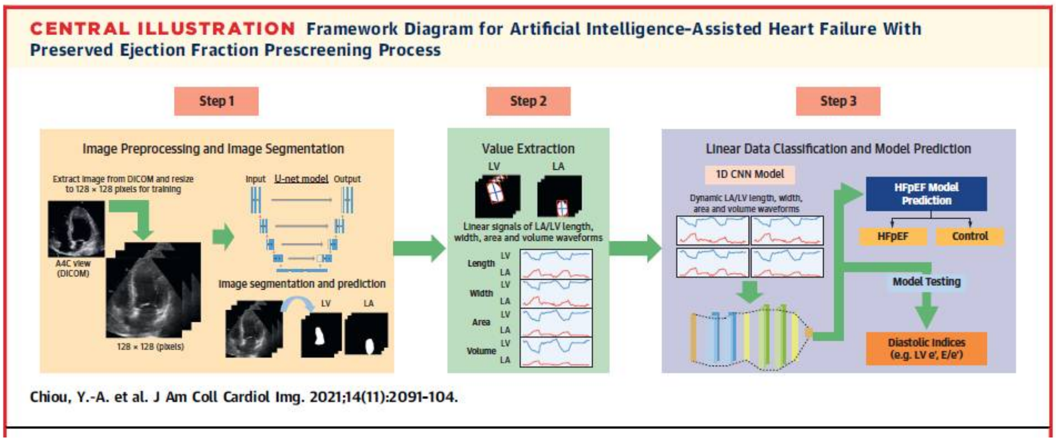

The heart failure with preserved ejection fraction prescreening procedure consisted of: 1) apical 4-chamber (A4C) image preprocessing and segmentation; 2) A4C left atrial and left ventricular chamber value extraction; and 3) dynamic intrabeat linear data classification by a one-dimensional convolutional neural network

16

Late gadolinium enhancement MRI (LGE-MRI).

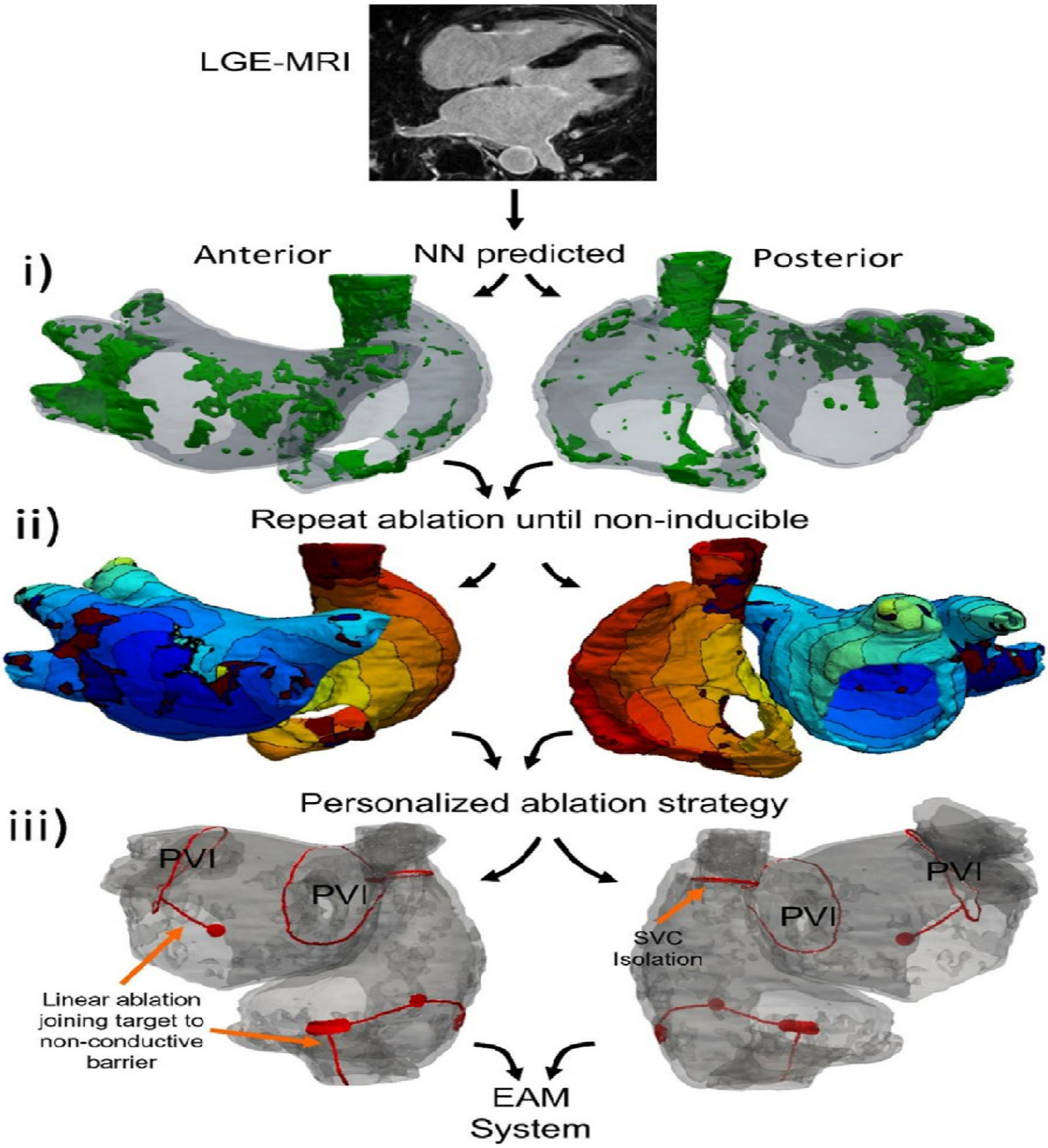

- ✓ (i) personalized bi-atrial model construction from LGE-MRI,
- ✓ ii) personalized simulation of substrate AF inducibility, and
- ✓ iii) personalized extra-PVI ablation strategy implementable in theclinical workflow.

- o Robust AI-assisted computational platform
  - for prediction of extra-PVI atrial substrate ablation targets
  - in AF patients with fibrosis,
- + enabling our FDA-approved randomized clinical trial.

52

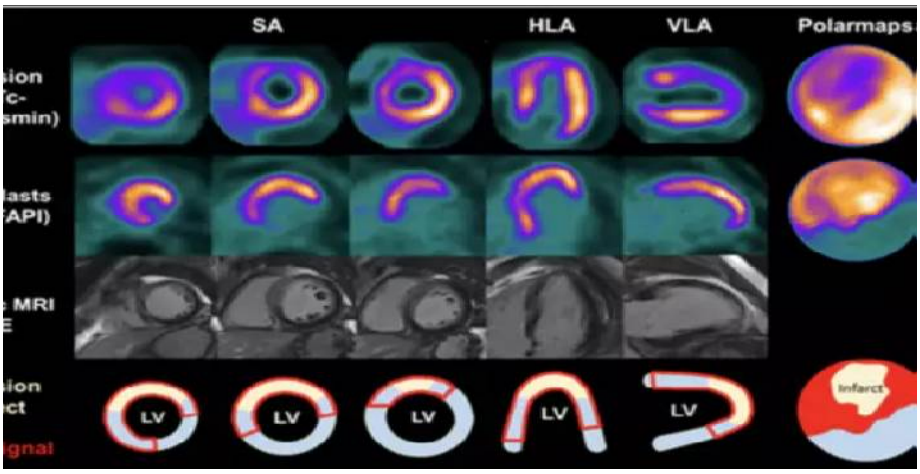

The Society of Nuclear Medicine and Molecular Imaging (SNMMI) has chosen its 2022Image of the Year, and it’s one that is sure to interest anyone in the field of cardiac imaging

54

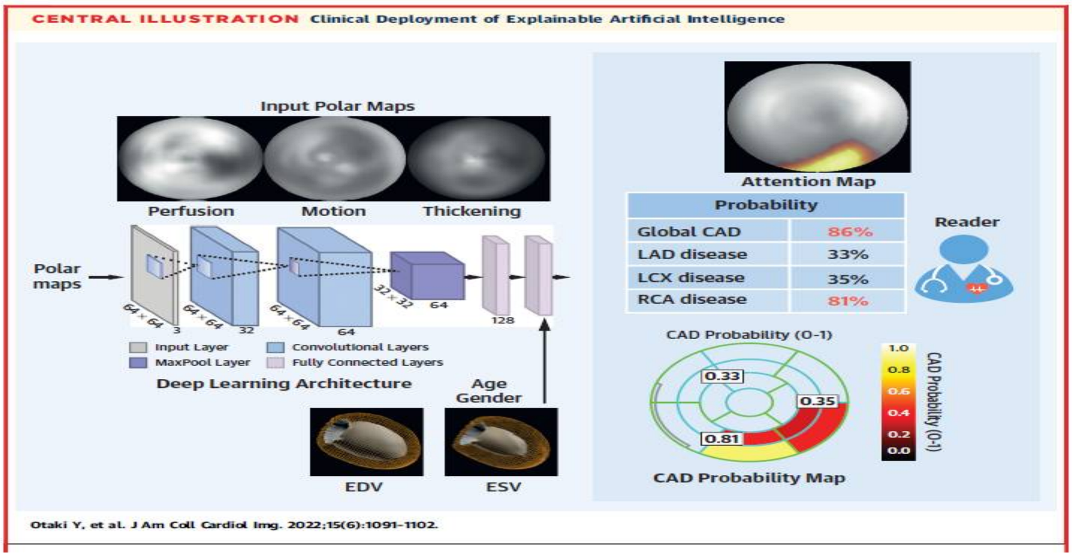

The raw myocardial perfusion, wall motion, and thickening images were input to the deep learning model “CAD-DL.” Sex, age, and cardiac volumes were added to the final fully connected layer, which Is used to estimate the per-patient and per-vessel probability. the attention maps highlight the regions and segments contributing most to the per-vessel prediction. CAD : coronary artery disease; EDV : end-diastolic volume; ESV : end-systolic volume; LAD : left anterior descending artery; LCX : left circumflex artery; RCA : right coronary

54

Diagnostic Performance of CAD-DL From Repeated 10-Fold Testing in the Overall Population

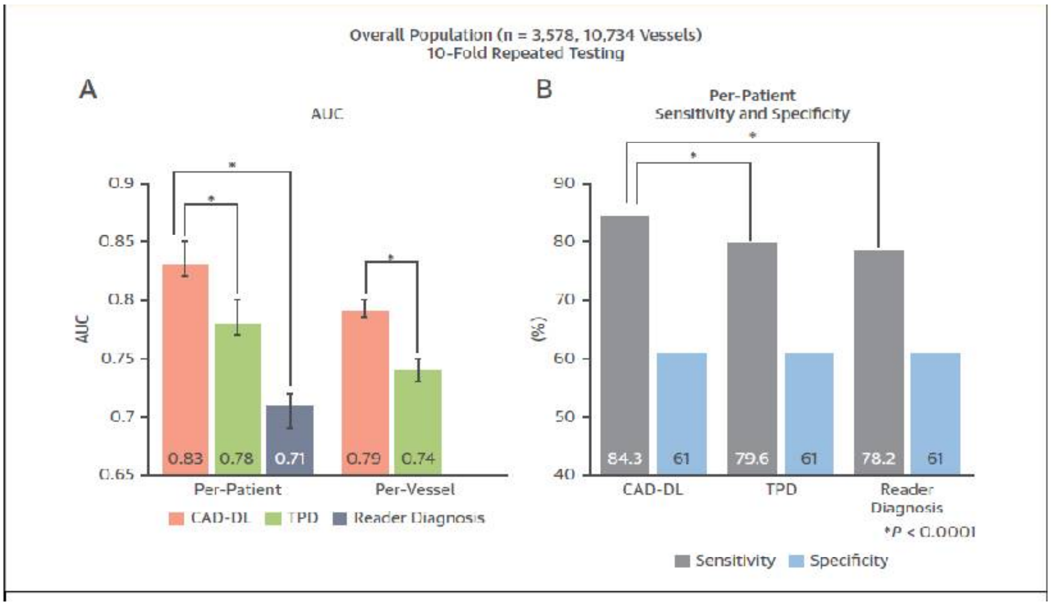

(A) Per-patient and per-vessel AUC. (B) Per-patient sensitivity. AUC : area under the receiver-operating characteristic curve;

CAD-DL : coronary artery disease–deep learning; TPD : total perfusion deficit.

54

Diagnostic Performance of CAD-DL in the Population With SSS

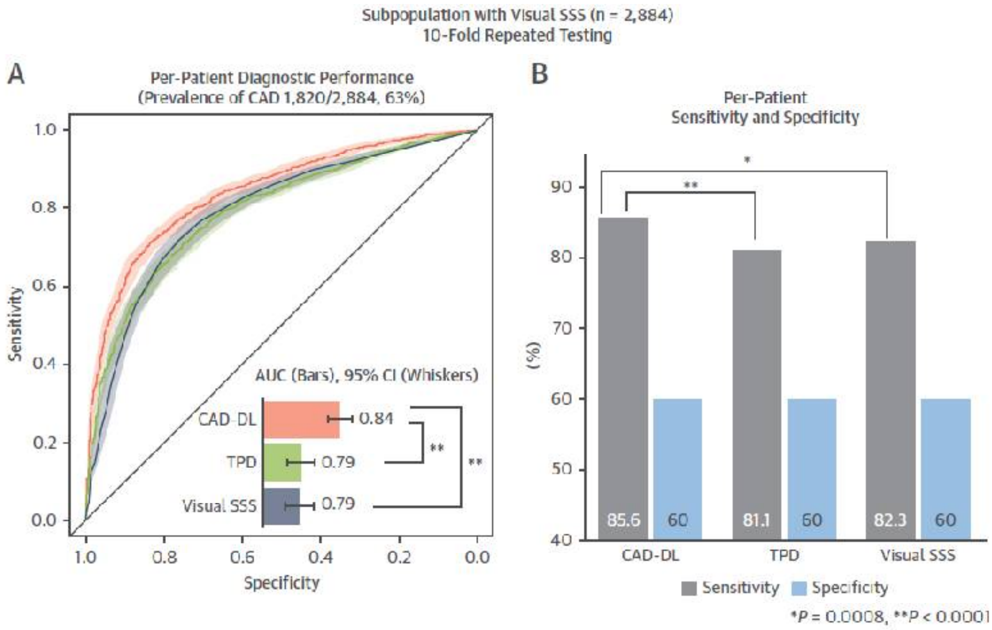

(A) Per-patient area under the receiver-operating characteristics curve (AUC). The shaded area represents 95% CI. (B) Per-patient sensitivity and specificity.

SSS : summed stress score; other abbreviations as in

54

Case Example of Solid-State SPECT-MPI

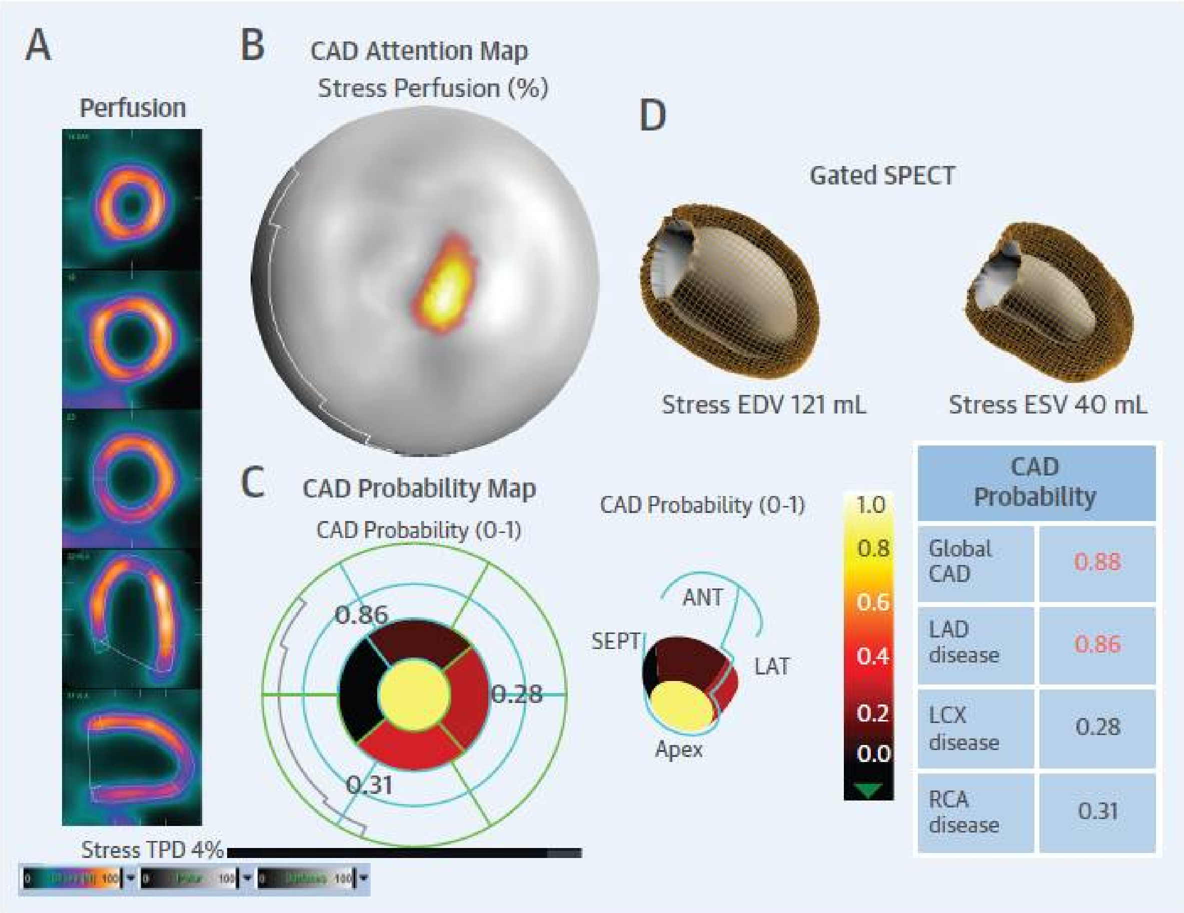

A 72-year-old male with 85% stenosis in the proximal left anterior descending artery (LAD) on coronary angiography.

(A) Visual assessmentfor stress image was interpreted as equivocal (SSS : 2).

(B) CAD attention map highlights the image regions contributing to CAD predictionoverlaid onto perfusion polar map.

(C) CAD probability map shows a high probability of CAD and specifically LAD disease with the distalanterior and apical segments contributing to the prediction.

(D) Left ventricular volumes from gated SPECT.

- ANT : anterior; LAT : lateral;
-
- EDV : end diastolic volume; ESV : end-systolic volume;
- LAD : left anterior descending artery;
- LCX : left circumflex artery;
-
- MPI : myocardial perfusion imaging;
- RCA : right coronary artery; SEPT : septal;
- SPECT : single-photon emission computed tomography;

Computed tomography pulmonary angiography

23

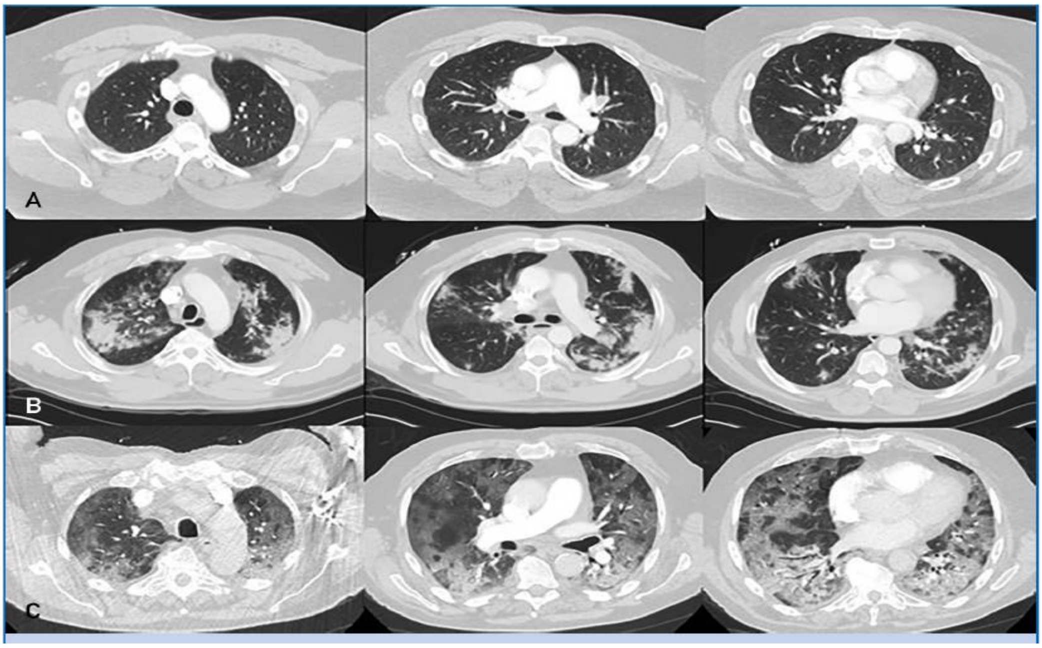

Axial computed tomography pulmonary angiogram images

- illustrating total severity scoring (TSS) semiquantitative assessment.
- TSS: 0 (mild),
- TSS: 13 (moderate), and
- (C) TSS: 25 (severe).

23

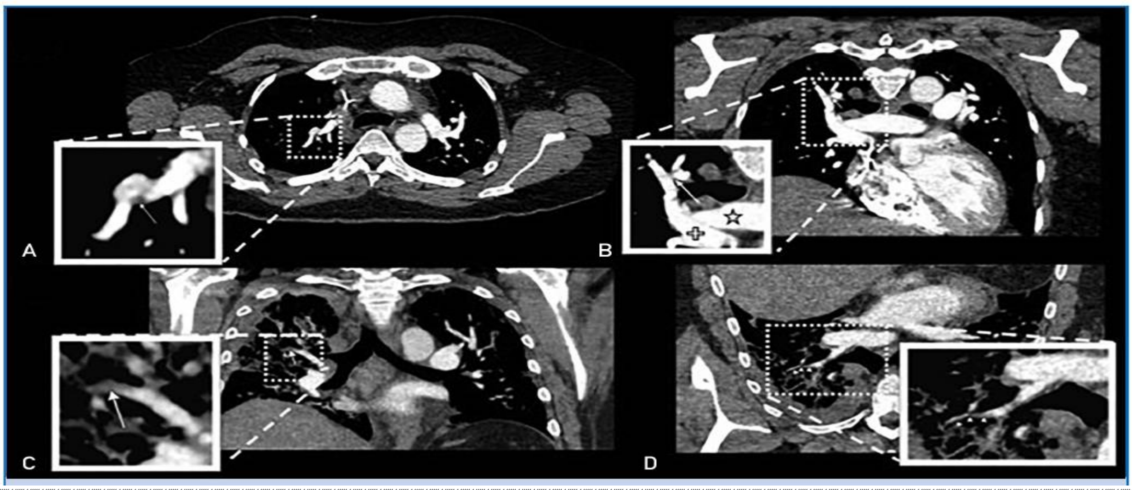

Computed tomography showing original reports of 2 false-positive studies.

(A) The axial computed tomography pulmonaryangiography (CTPA) image shows a soft tissue density misinterpreted as an eccentric filling defect (arrow).

(B) The coronalobliquemultiplanar reconstructed image shows presumed a filling defect (arrow) between the branch of the right superior pulmonaryartery (star) and one of the right superior pulmonary vein tributaries (cross).

(C) The coronal reconstructed CTPA image shows soft tissue density (arrow) misinterpreted as a filling defect within the right subsegmental upper lobar artery.

(D) The oblique-obliquemultiplanar reconstructed CTPA image shows the subsegmental branch (arrowheads) to be patent.

23

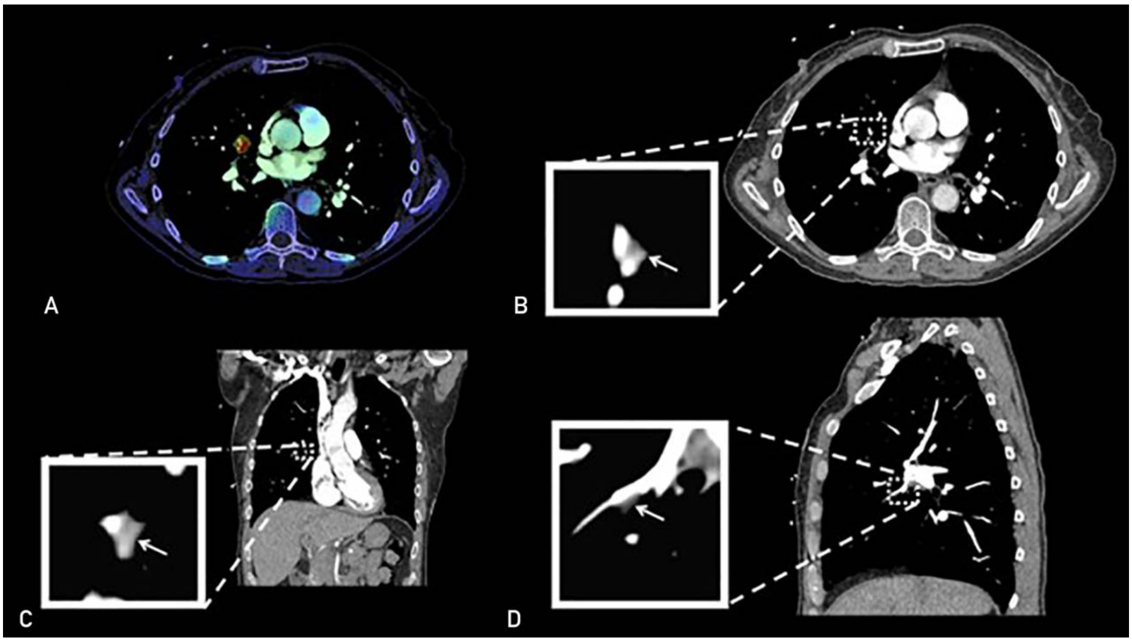

Computed tomography pulmonary angiography shows false-positive result of artificial intelligence.

(A) An artificial intelligence generated image highlighting the misinterpreted filling defect within the right middle lobar branch, also seen on

(B) thecorresponding axial computed tomography pulmonary angiography image. Note that the presumed filling defect (arrow) is seeninferior to the vessel on both

(C) the coronal and (D) sagittal reconstructed images

23

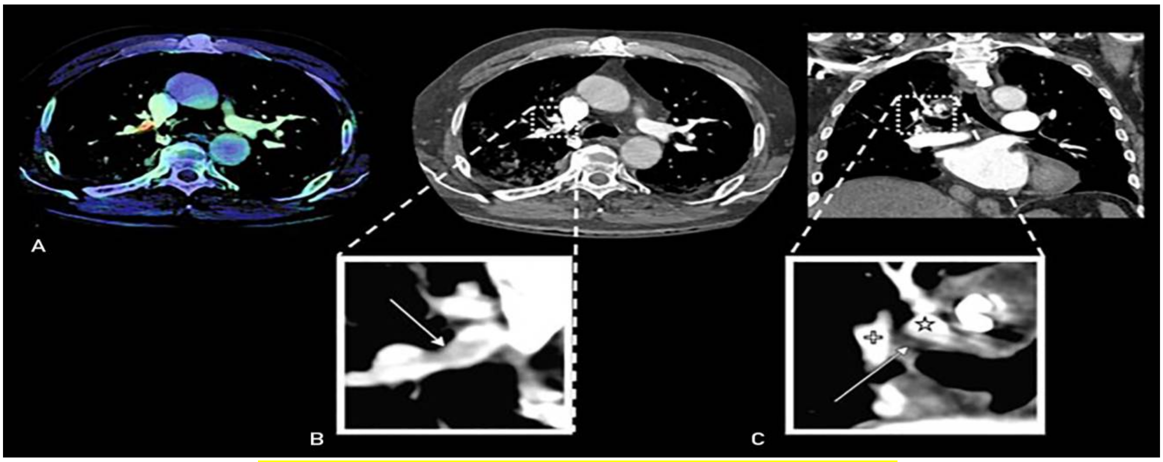

Computed tomography pulmonary angiography shows false-positive result of artificial intelligence.

(A) AI generated image highlighting the misinterpreted filling defect, also seen on
(B) corresponding axial computed tomographypulmonary angiography image. Arrow represent filling defects.
(C) A coronal reconstructed image shows the presumedfilling defect soft (arrow) between the apical branch of the right superior pulmonary artery (star) and one of the right superiorpulmonary vein tributaries (cross)

Literature survey
Medicine

19

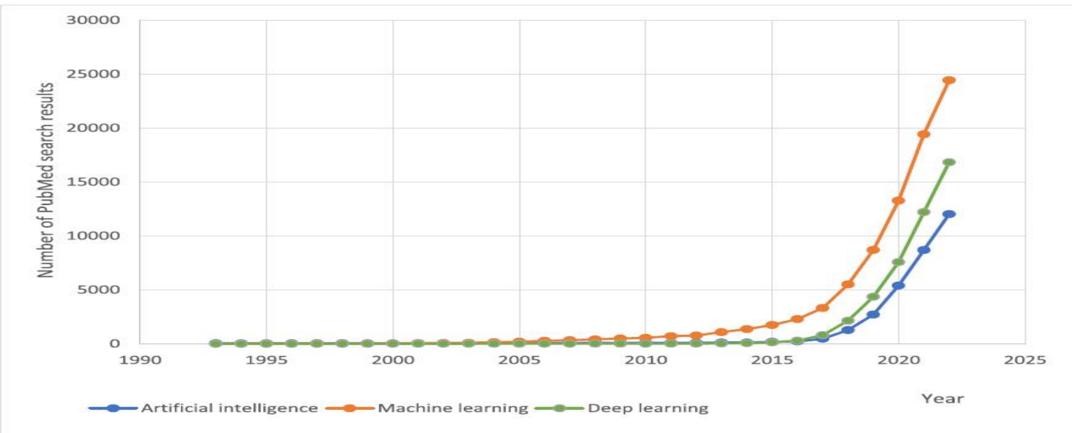

Recent trends in PubMed search results.

- Search field: Title/Abstract;
- Search terms: artificial intelligence, machine learning, deeplearning

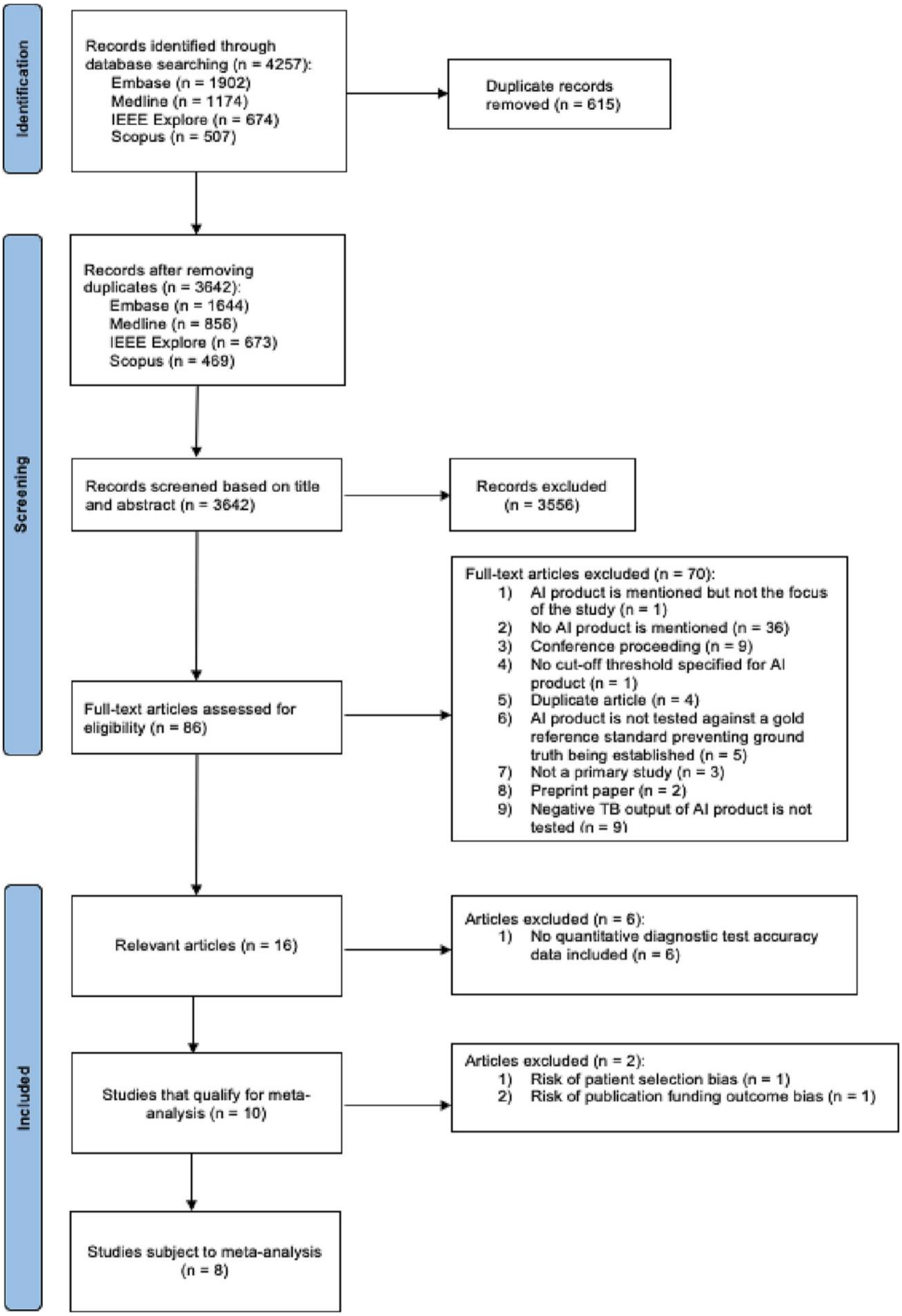

Study screening and selection flow chart

29

✓ The structure of the search strategy for all databases is based on the following string format:

- ? (Tuberculosis terms) AND (AI computer aided detection, including current certified products, terms) AND (chest X-rays terms) AND (diagnostic test accuracy/performance/validation/tuberculosis test culture terms).

#	Searches	Results
1	exp Tuberculosis/	203,273
2	Mycobacterium tuberculosis/	56,024
3	Tuberculosis.tw.	206,243
4	TB.tw.	67,343
5	Mycobacteri*.tw.	103,279
6	or/1–5	329,403
7	exp Artificial Intelligence/	156,058
8	exp cluster analysis/	71,341
9	Pattern Recognition, Automated/	26,300
10	exp neural networks, computer/	51,611
11	exp Image Processing, Computer-Assisted/	255,189
12	exp Image Interpretation, Computer-Assisted/	591,193
13	exp Signal Processing, Computer-Assisted/	68,221
14	Computational Biology/	90,165
15	Imaging Genomics/	42
16	exp Diagnosis, Computer-Assisted/	86,294
17	exp decision support techniques/	81,775
18	Data Analysis/	3934

29

Scopus

TITLE-ABS-KEY(tuberculosis OR tb OR mycobacteri*) AND TITLE-ABS-KEY("Artificial* Intel*" OR AI OR (Learning W/1 (machine OR deep OR lazy OR "multiple instance")) OR "Cluster analysis" OR ((Comput* OR Automat* OR Machine*) W/3 ("pattern recognition" OR "signal processing" OR "neural network*" OR diagnos* OR detect* OR classif*)) OR (Imag* W/2 (analy* OR processing OR interpret* OR recogni*)) OR (Comput* W/2 (cognitive OR intelligen* OR biolog* OR diagnos* OR detect* OR screening OR interpret*)) OR "Support vector machine*" OR "Feature extraction" OR (Vision W/1 (comput* OR machine*)) OR (Perception W/1 (machine OR visual OR comput*)) OR (Data W/1 (analy* OR big OR mining OR fusion)) OR (Decision* W/1 (tree* OR processing)) OR (software W/2 (diagnosis OR detection OR screening OR interpretation)) OR "Analytic hierarchy process*" OR (annalise OR cad4tb OR inferread OR Lunit OR CXR OR QXR OR genki OR radify OR JLD-02K OR JVIEWER-X OR TiSepX OR TB ChestLink OR ChestEye OR axir OR vuno OR chest Xray OR delft imaging OR envisionit deep ai OR infervision OR JLK OR oxipit OR "qure.ai" OR radisen)) AND TITLE-ABS-KEY((chest* OR lung* OR pulmonary OR respiratory) W/3 (imag* OR radiograph* OR ct OR tomograph* OR mri OR "magnetic resonance")) AND TITLE-ABS-KEY(sensitivity OR specificity OR ((pre-test OR pretest) W/1 probability) OR "post-test probability" OR "predictive value*" OR "likelihood ratio*" OR ((valid* OR reliab* OR predict*) W/3 (result* OR finding* OR screening OR diagnos*)) OR ((diagnos* OR screening) W/2 (accura* OR validat* OR correct* OR error* OR precis*)) OR "ROC curve" OR xpert OR screening OR "culture test" OR radiologist OR radiographer) AND (LIMIT-TO (PUBYEAR,2023) OR LIMIT-TO (PUBYEAR,2022) OR LIMIT-TO (PUBYEAR,2021) OR LIMIT-TO (PUBYEAR,2020) OR LIMIT-TO (PUBYEAR,2019) OR LIMIT-TO (PUBYEAR,2018) OR LIMIT-TO (PUBYEAR,2017) OR LIMIT-TO (PUBYEAR,2016) OR LIMIT-TO (PUBYEAR,2015) OR LIMIT-TO (PUBYEAR,2014) OR LIMIT-TO (PUBYEAR,2013) OR LIMIT-TO (PUBYEAR,2012) OR LIMIT-TO (PUBYEAR,2011) OR LIMIT-TO (PUBYEAR,2010) OR LIMIT-TO (PUBYEAR,2009) OR LIMIT-TO (PUBYEAR,2008) OR LIMIT-TO (PUBYEAR,2007) OR LIMIT-TO (PUBYEAR,2006) OR LIMIT-TO (PUBYEAR,2005) OR LIMIT-TO (PUBYEAR,2004)) AND (LIMIT-TO (LANGUAGE,"English")).

Future of Medical field

22

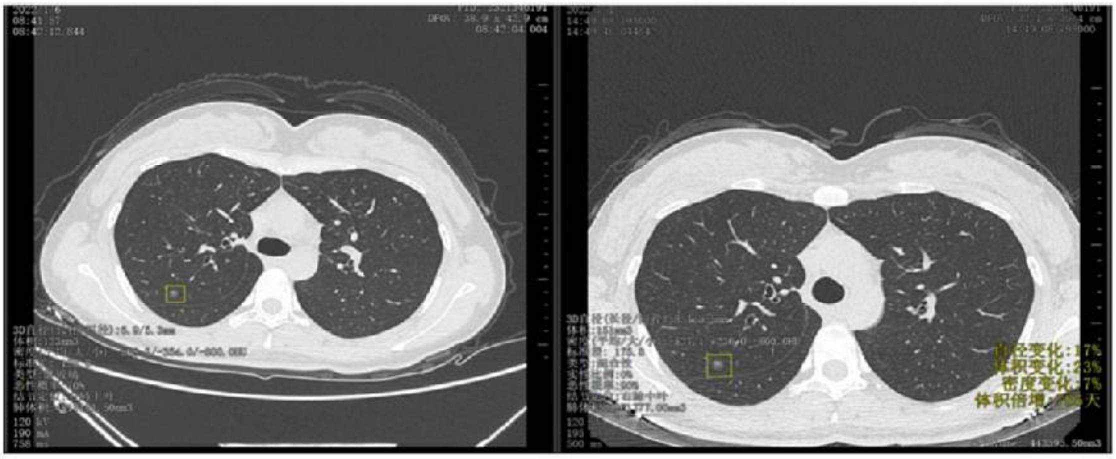

AI interprets the appearance, content and malignant risk of pulmonary nodules

22

Leading Technology - IoT integrated into metacosmic medicine

Integrate IoT sensing transmission and intelligent processing into AR/VR/XR/MR and digital people

《未来已来-我们的元宇宙医学》，上海科技出版社

Human-computer MDT clinic and meta-cosmic medicine clinic.

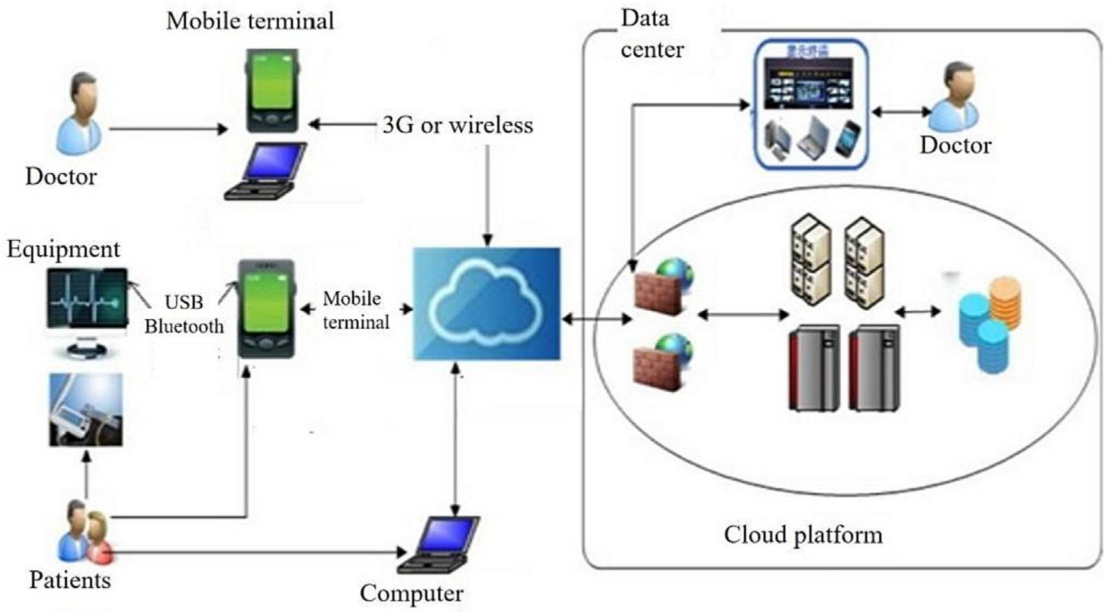

The IoT platform connecting the PNapp5A mobile terminal entrance and the background PC terminal

22

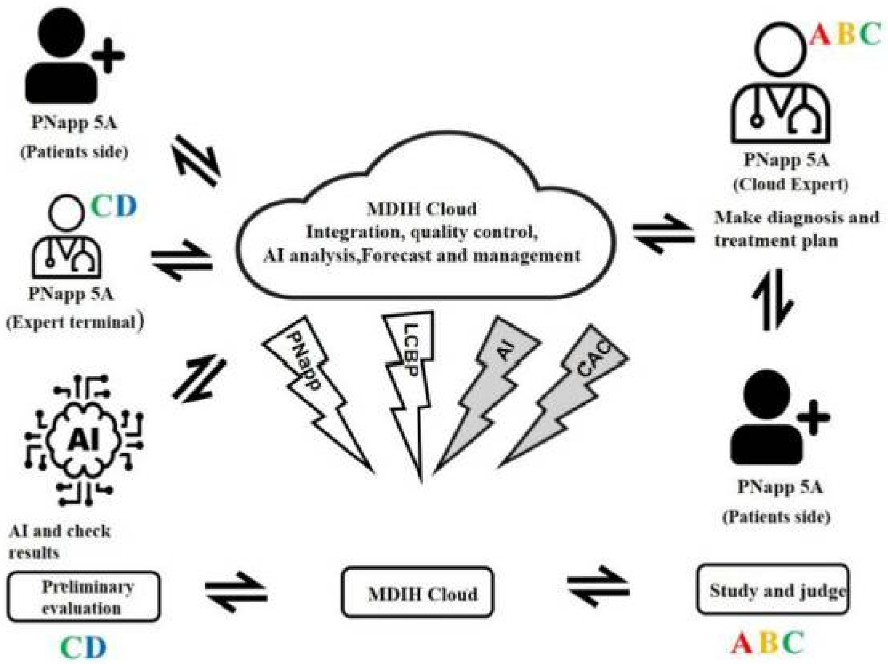

IOT-assisted assessment and management ofpulmonary nodule

- ✓ Preliminary evaluation and the second process of research and judgement.

22

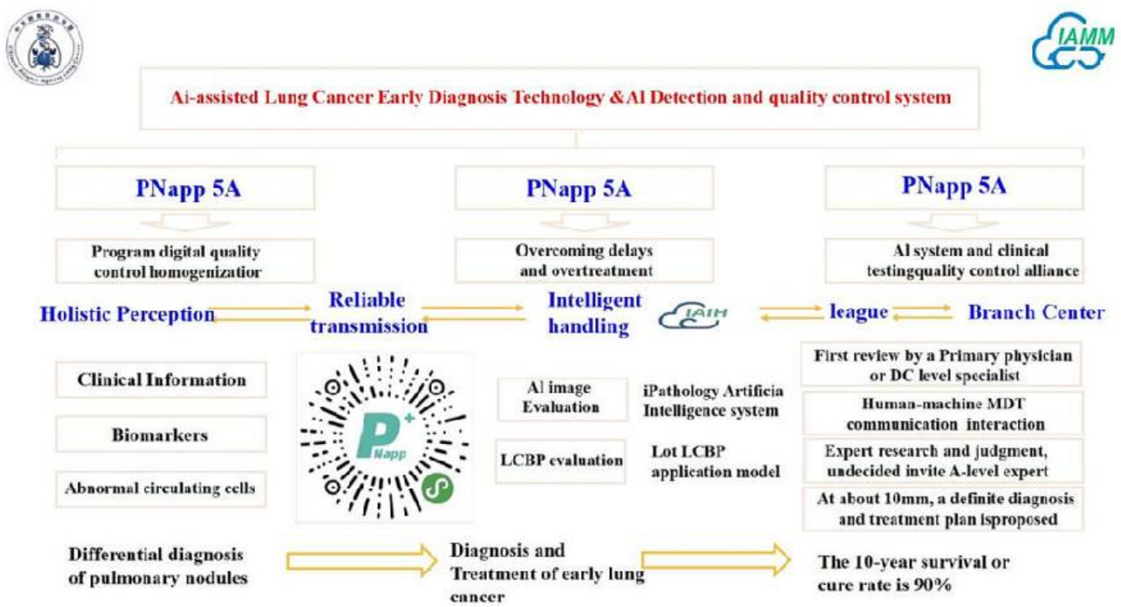

AI-assisted lung cancer early diagnosis technology & AI detection and quality control diagram

23

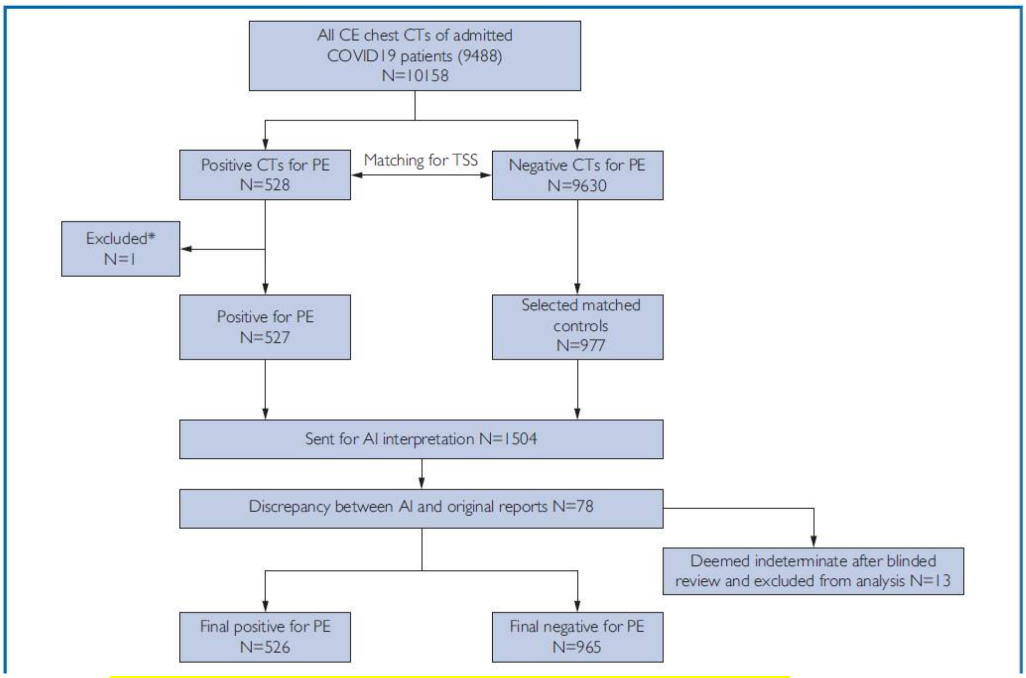

Reversed-flow diagnostic case-control design (single gate) flowchart.

*The patient was excluded because they underwentlung operation, excluding total severity score (TSS) calculation.

- AI, artificial intelligence; CE, contrast-enhanced; COVID-19, coronavirus disease 2019;
- CT, computed tomography; PE, pulmonary embolism

05

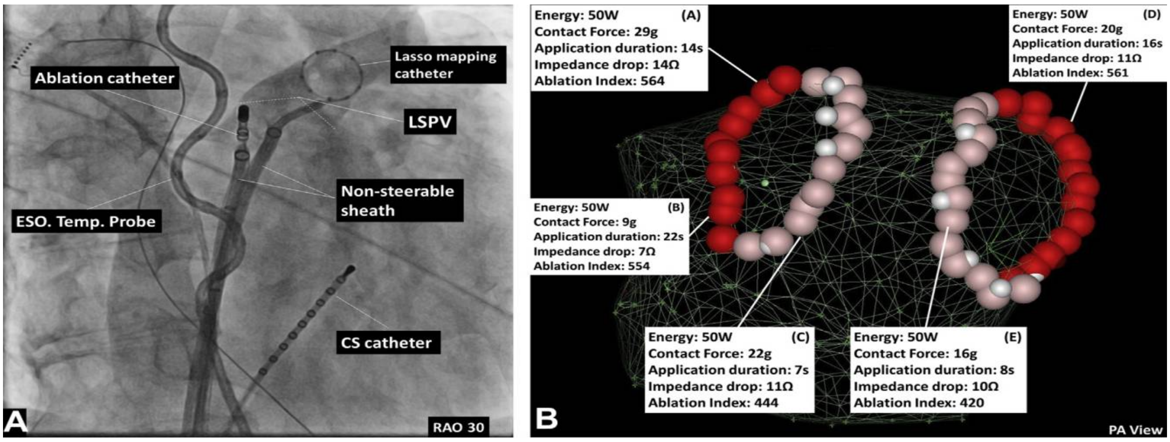

(A) A fluoroscopic example of the procedure.

(B) A representative example of a 3-dimensional left atrial map during the procedure.

- ✓ Tag (A): ablation lesion at the left anterior superior region. Tag (B): ablation lesion at the left anterior inferior region. Tag (C): ablation lesion at left posterior region. Tag (D): ablation lesion at right anterior region. Tag (E): ablation lesion at the right posterior region. The open dots indicate the marked antral-ostium of the pulmonary veins.
- o AI-HP ablation index–guided high power; CS : coronary sinus; ESO Temp esophageal temperature; LSPV : left superior pulmonary vein; PA : posteroanterior; PVI : pulmonary vein isolation; RAO : right anterior oblique

05

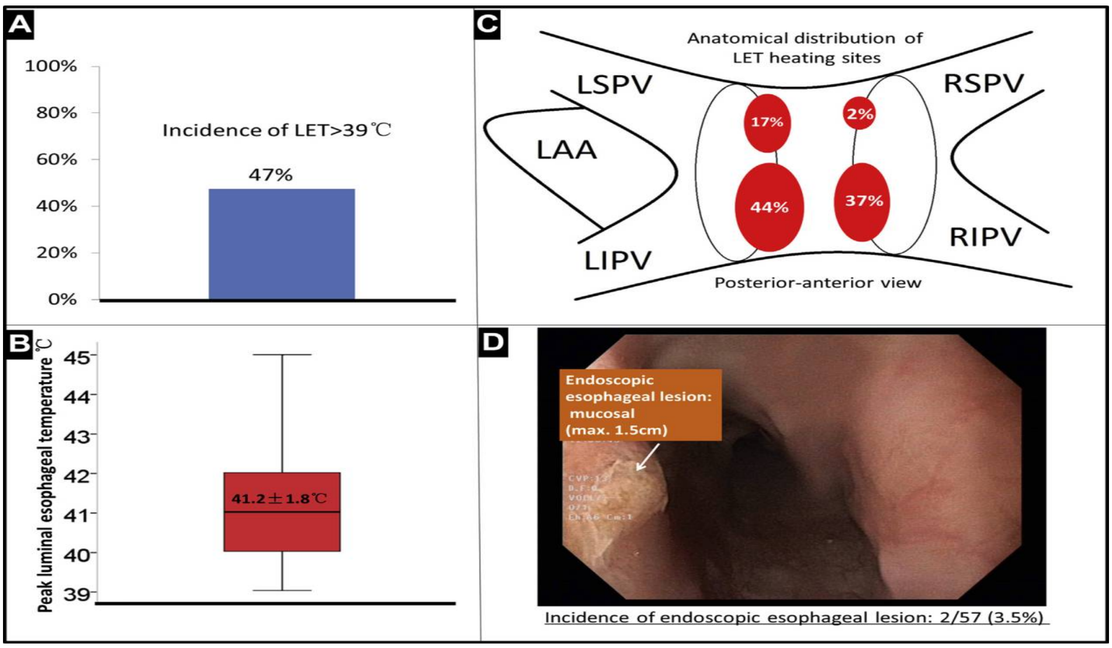

(A) The incidence of LET >39C was 47%.

(B) The mean peak LET was 41.2-- 1.8C.

(C) Anatomic distribution of LET increase, LSPV posterior(17%), LIPV posterior (44%), RSPV posterior (2%), RIPV posterior (37%).

(D) Endoscopic esophageal lesion 1 day after the ablation procedure.

LAA : left atrial appendage; LET : luminal esophageal temperature; LIPV : left inferior pulmonary vein; LSPV : left superior pulmonary vein;RIPV : right inferior pulmonary vein; RSPV : right superior pulmonary vein

05

CENTRAL ILLUSTRATION Ablation Lesion Analysis of Sites With Increased LET

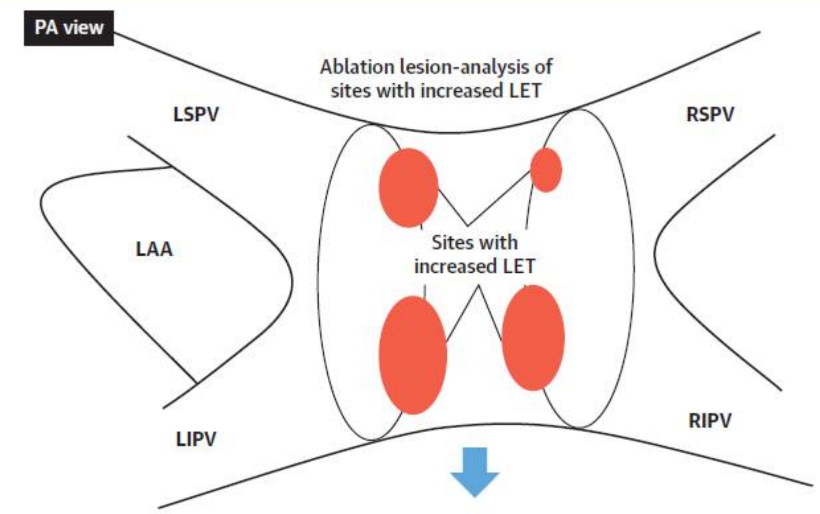

Ablation Lesion-Analysis of Sites with Increased LET (>39 °C)	*Lesion Quality*
- Mean ablation duration until LET increased, s	*7 ± 2.4*
- Mean impedance drop until LET increased, Ω	*9.4 ± 4.6*
- Mean contact force until LET increased, g	*22.1 ± 8.9*
- Mean AI value until LET increased	*419 ± 44.6*

Chen, S. et al. J Am Coll Cardiol EP. 2020;6(10):1253-61.

The ablation lesion analysis of the sites with LET >39C:

- mean ablation duration (7 -- 2.4 s), mean impedance drop (9.4 --4.6 U), mean
- contact force (22.1 -- 8.9 g), mean AI value (419 --44.6).
- AI : ablation index; LAA : left atrial appendage; LET : luminal esophagealtemperature; LIPV : left inferior pulmonary vein; LSPV : left superior pulmonary vein; RIPV : right inferior pulmonary vein; RSPV : rightsuperior pulmonary vein.

AI software in comparison with pulmonologist

39

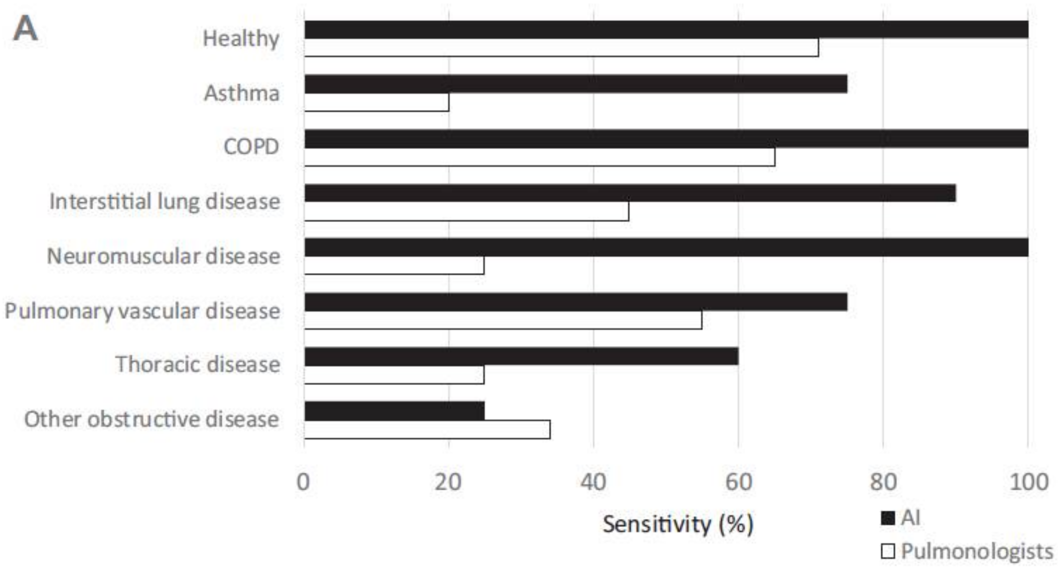

39

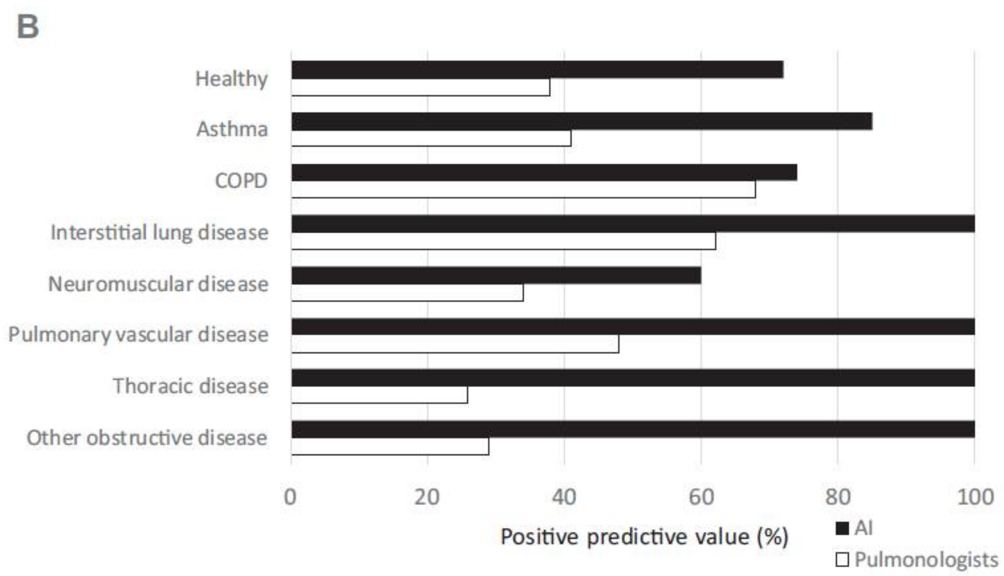

Performance of pulmonologists in comparison with the AI software for allocation to each disease category.
A, Sensitivity (ie,true positive/[true positive þ false negative]) shows how many relevant subjects (from a specific group) were correctly identified.
B,Positive predictive value (i.e, true positive/[true positive þ false positive]) shows how many labeled subjects rightly belonged to thespecific group. Data from Topalovic et al

39

May 2018	X-ray wrist fracture diagnosis (Imagen) Transcranial Doppler probe positioning (NeuralBot) Motion capture for the elderly (MindMotionGO)
June 2018	Managing type I diabetes (DreaMed) Blood glucose monitoring system (POGO)
July 2018	Coronary artery calcification algorithm (Zebra Medical Vision) Quantification of liver iron concentration (FerriSmart)
August 2018	Breast density via mammography (iCAD) Triage and diagnosis of time-sensitive patients (Aidoc) Detection of atrial fibrillation (PhysiQ Heart Rhythm Module)
September 2018	Detection of atrial fibrillation (Apple) Identifying visual tracking impairment (RightEye Vision System)
November 2018	Acute intracranial hemorrhage triage algorithm (MaxQ) Decision support for mammograms (ScreenPoint Medical)
December 2018	Detection and diagnosis of suspicious lesions (ProFound AI) Adjuvant treatment for substance abuse disorder (ReSET-O)
January 2019	ECG feature of the Study Watch (Verly)
March 2019	Clinical grading in pathology (Paige.AI) Breast cancer detection in mammograms (CureMetrix)
May 2019	Six-lead smartphone ECG (AliveCor) Chest X-ray analysis (Zebra Medical Vision) Identifying pulmonary embolism (Aidoc)

TABLE I. *(Continued)*

Date	AI-based algorithm
June 2019	Decision support in breast cancer (Canon Medical)
July 2019	CT noise reduction (Koios Medical)

ADHD, Attention deficit/hyperactivity disorder; *ECG*, electrocardiogram; *MRI*, magnetic resonance imaging.

AI (1956-2024)

19

a.

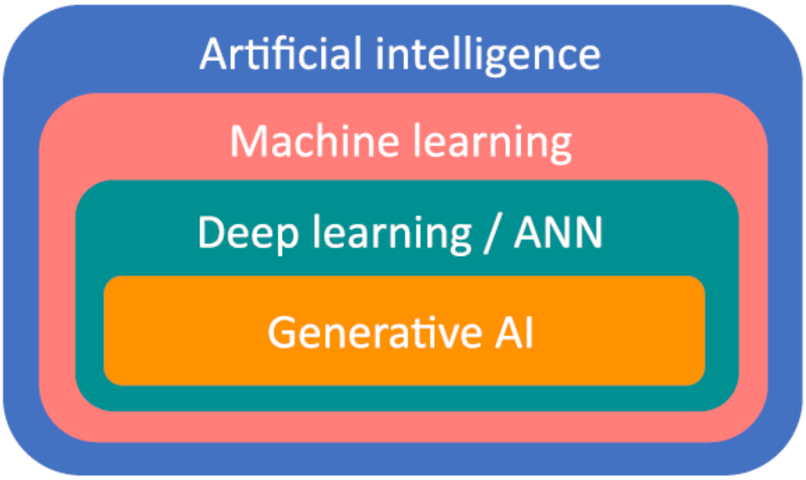

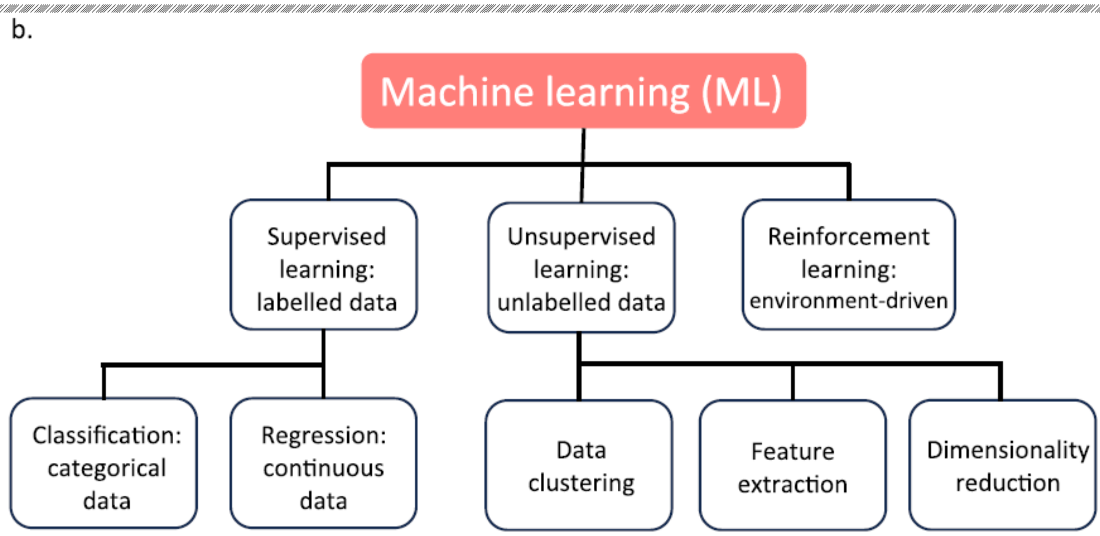

Relationship between artificial intelligence (AI), machine learning (ML), deep learning/artificial neural networks (ANN), and generative AI (a); subdivisions and applications of ML (b).

19

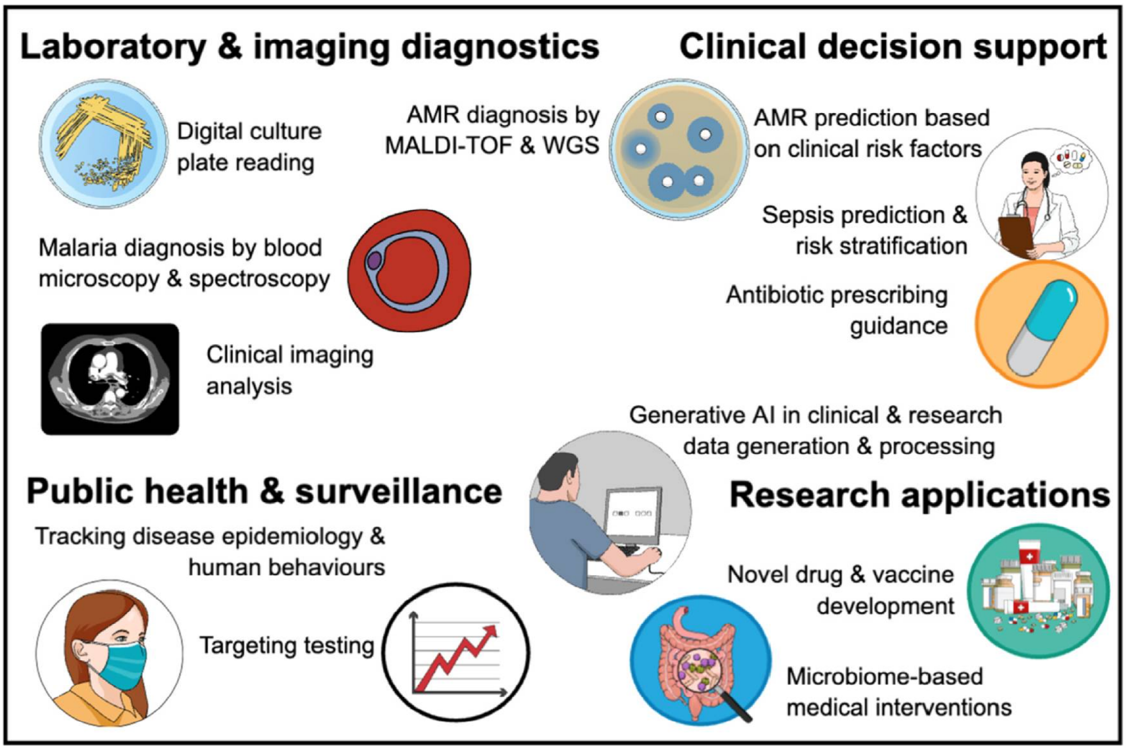

Examples of artificial intelligence (AI) applications in research and management of human infections.

- ✓ AMR: antimicrobial resistance;
- ✓ MALDI-TOF: matrix-assisted laser desorption/ionisation–time of flight mass spectrometry;
- ✓ WGS: whole genome sequencing

xAI
Saliency maps

28

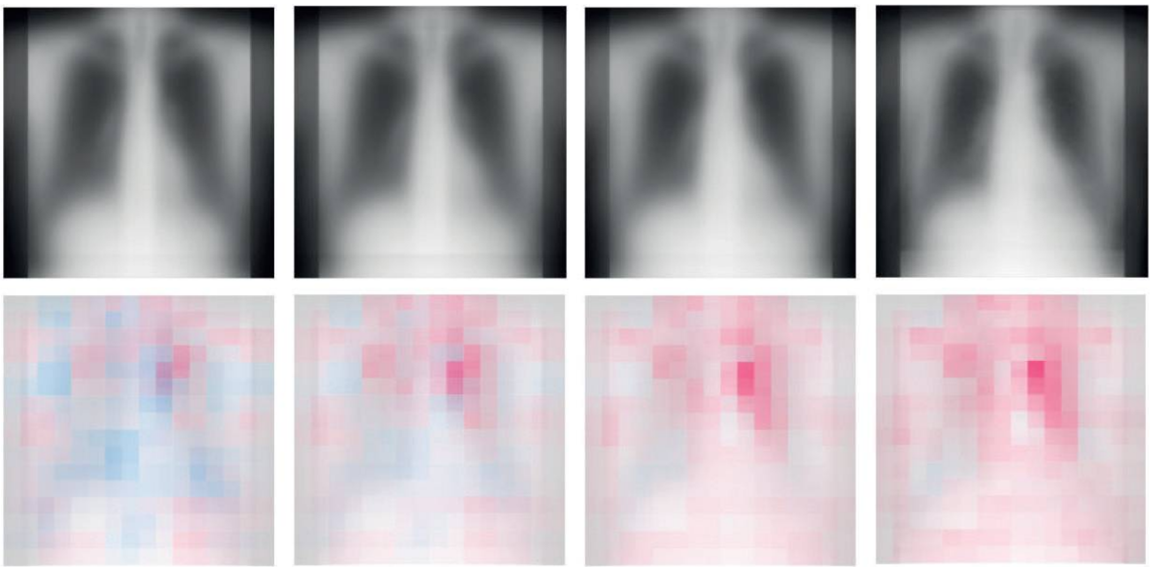

Saliency maps from the external test dataset

- ✓ Average saliency images of each 20-year chronological age group in the external test dataset
- ✓ The top panels show averaged chest radiographs for all participants in the group and the bottom panels show averaged saliency maps.
- Hot areas in the saliency maps indicate characteristics of increasing age in chest radiographs; cold areas indicate characteristics of decreasing age

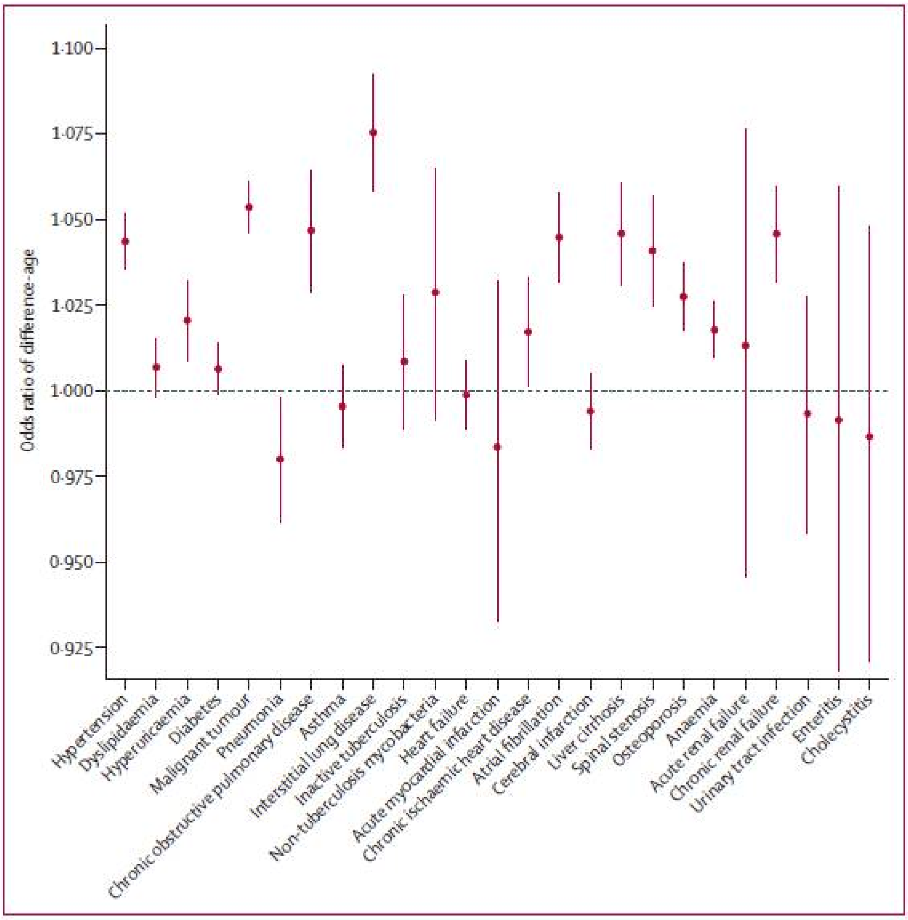

Correlation between difference-age and each disease

- ✓ Odds ratio of difference-age of each disease in the external datasets from institutions D and E. Circles representmeans and lines represent 99% CIs.